Geophys. J. Int. (2003) **154,** 300–354

The theory of non-linear transresonant wave phenomena and an examination of Charles Darwin's earthquake reports

Sh. U. Galiev

Department of Mechanical Engineering, The University of Auckland, Private Bag 92019, Auckland 1, *New Zealand. E-mail: s.galiyev@auckland.ac.nz*

Accepted 2003 January 20. Received 2002 November 4; in original form 2000 June 6

SUMMARY

A non-linear theory of transresonant wave phenomena based on consideration of perturbed wave equations is presented. In particular, the waves in a surface layer of a porous compressible viscoelastoplastic material are considered. For such layers the 3-D equations of deformable media are reduced to 1-D or 2-D perturbed wave equations. A set of approximate, closed-form, general solutions of these equations are presented, which take into account non-linear, dissipative, dispersive, topographic and boundary effects. Then resonant, site and liquefaction effects are analysed. Resonance is considered as a global parameter. Transresonant evolution of the equations is studied. Within the resonant band, $u_{tt} \approx a_0^2 \nabla^2 u$ and the perturbed wave equations transform into non-linear diffusion equations, either to a basic highly non-linear ordinary differential equation or to the basic algebraic equation for travelling waves. Resonances can destroy predictability and wave reversibility. Surface topography (valleys, islands, etc.) is considered as a series of earthquake-induced resonators. A non-linear transresonant evolution of smooth seismic waves into shock-, jet- and mushroom-like waves and vortices is studied. The amplitude of the resonant waves may be of the order of the square or cube root of the exciting amplitude. Therefore, seismic waves with a moderate amplitude can be amplified very strongly in natural resonators, whereas strong seismic waves can be attenuated. Reports of the 1835 February 20 Chilean earthquake given by Charles Darwin are qualitatively examined using the non-linear theory. The theory qualitatively describes the 'shivering' of islands and ridges, volcano spouts and generation of tsunami-like waves and supports Darwin's opinion that these events were part of a single phenomenon. Same-day earthquake/eruption events and catastrophic amplification of seismic waves near the edge of sediment layers are discussed. At the same time the theory can account for recent counterintuitive results of experiments with water, liquified matter and granular materials.

Key words: analytical solutions, chaos, earthquake-induced eruption, perturbation method, resonance, strong ground motion.

1 INTRODUCTION

Wave non-linearity is an important element of Nature. This non-linearity is often focused near and at critical points where greatly different natural and artificial (for example, the Bose–Einstein condensate) systems exhibit a strong similarity. These points have been called 'resonances' (Galiev & Galiev 2001). In the resonant band, non-linear effects can increase strongly and first-order linear effects drop to zero. In particular, harmonic waves can be transformed into anomalous waves and wave structures (breakers, mushroom-like waves, jets, vortices and so on). The evolution of governing equations, generation of singularities of wave fronts, a complex competition of non-linear, dissipative, dispersive and spatial effects occur. The traditional methods of non-linear physics fail within transresonant bands because of the evolution, the singularities, a problem of small divisors, the competition of various effects and the diffusion effect (Poincaré 1892; Sagdeev *et al.* 1988; Arnold 1990; Prigogine 1997). Therefore, a development of the theory is required to describe non-linear transresonant waves.

Resonance is a classical problem of great practical impact. This phenomenon is usually described by one or a few second-order non-linear differential equations (for example, the pendulum equation). However, sometimes, wave properties must be taken into account (Sagdeev *et al.* 1988; Nayfeh & Mook 1995; Ilgamov *et al.* 1996; Nayfeh 2000; Ibrahim *et al.* 2001). It was found (Chester 1964; Van Wijngaarden 1968; Galiev *et al.* 1970; Mortell & Varley 1970; Galiev 1972, 1988; Mortell & Seymour 1981; Galiev & Galiev 1994; Ilgamov *et al.* 1996; Galiev 1999b) that strongly non-linear waves and shock waves may be excited in 1-D resonators (tubes, spheres and layers) within the resonant bands. Following Galiev & Galiev (2001) we develop the theory of non-linear transresonant waves based on

consideration of perturbed wave equations. These equations are derived for a layer of a weakly cohesive medium. Media such as granular materials, sediments and some soils, transform into a liquified state during strong ground motion and maintain this state for up to a day (Aguirre & Irikura 1997; O'Rourke & Pease 1997; Pease & O'Rourke 1997). For these media we generalize the well-known theory of non-linear shallow water waves (Airy 1845; Boussinesq 1872; Lamb 1932; Stoker 1957; Whitham 1974; Dean & Dalrymple 1991; Debnath 1994; Kirby 1997). It is known that the transresonant evolution of water waves in a horizontally oscillating container is very complex (Verhagen & Van Wijngaarden 1965; Chester & Bones 1968; Ockendon *et al.* 1985; Cox & Mortell 1986; Galiev & Galiev 1998). Here we solve the equations of continuum mechanics for layers, whereas the classical water wave problem consists of solving the Euler equations in the presence of a free surface. Effects of the vertical acceleration of particles, compressibility, shear strains and stresses, and high-order non-linearity are all taken into account.

The influence of non-linearity on strong ground motion has begun to be analysed in recent years. Laboratory studies (Johnson *et al.* 1996) reveal that the linear approximation can break down and resonant non-linear waves can be formed if the amplitude of forced oscillations is sufficiently large. It is more difficult to observe non-linear effects in the field. However, Singh *et al.* (1988), Aki (1993), Field *et al.* (1997, 1998), Su *et al.* (1998) and Fukushima *et al.* (2000) demonstrated a non-linear relationship between peak ground motion and site response. Porosity, surface geology, the free surface and relief may induce non-linear effects. In particular, the seismic wave amplitude is greater in a low-density, low-velocity soil than in a high-density, high-velocity rock. Sediments amplify ground motion relative to bedrock (Reiter 1990). Therefore, non-linearity is more important for upper-lying sedimentary layers than for underlying material (Aki 1993). If the wave amplitude increases beyond some threshold level, the linear predictions break down. The influence of non-linearity increases and causes changes in both the amplitude and the form of seismic waves. In particular, seismic waves may be trapped by the upper layer or topography and then begin to reverberate. Resonance occurs if the reverberating waves are in phase with each other. If dissipative effects are small, non-linearity is the most important mechanism that limits the resonant amplification of the trapped seismic waves. Thus resonance, which is usually observed in upper sediments, is sometimes a non-linear phenomenon. Resonant amplification of about 75, with respect to coastal sites at similar distances, was produced in the Mexico City sediments during the 1985 September 19 and 21 Michoacan earthquakes (Singh *et al.* 1988). However, non-linear effects may also influence seismic body waves. In particular, the effects may be important for porous materials saturated by gas (or a gas/oil mixture).

I suggest that studying non-linear effects can give a new understanding of some aspects of earthquake behaviour. In particular, the linear elastic model predicts extreme amplification of seismic waves at resonance. According to this model, the resonant singularity in amplitude exists for weak, moderate and strong seismic waves. However, according to the non-linear theory, the resonant amplitude is bounded and may be of the order of the square or cube root of the exciting amplitude (Galiev 1997b, 1999a). Thus, the greater the amplitude of an incident seismic wave, the smaller the amplification. Indeed, the amplification of strong motions is often significantly smaller than that observed for moderate motions (Field *et al.* 1997, 1998). The width of the resonant frequency band is very small for weak seismic waves. Therefore, they are not amplified in the natural resonators according to the non-linear theory. Strong seismic waves are attenuated within the resonant band. The non-linear theory also predicts that strong resonant ground motion may be more dependent upon the ground properties at a site than on the proximity or intensity of the earthquake sources (Galiev 1999a). Thus, the non-linear theory can give us insight into a phenomena of particular importance to earthquake engineering.

Non-linear seismic effects have previously been widely discussed (Singh *et al.* 1988; Aki 1993; Su *et al.* 1998). In particular, equations for non-linear seismic waves have been derived (Biot 1973; Beresnev & Wen 1996a; Johnson *et al.* 1996; Nikolaevskiy 1996). However, surface effects are not generally taken into account. Indeed, when considering waves in surface layers we need to take into account relevant boundary conditions.

In considering a non-linear problem, we should first determine the sources of non-linearities. There are four. The first source is the equation of continuity, the equations of motion and energy, written in terms of stresses. The second source is the constitutive equations relating stresses and displacements. The third source is the equation of state relating pressure p and density ρ (or p, ρ and temperature). This source is very important for porous and highly compressible materials. The last (but sometimes the most important) source is the boundaries of the layer. Indeed, the non-linear waves considered herein are formed due to the boundary surfaces. The contributions of these sources to the total effect of the non-linearities vary. For example, sometimes liquified weakly cohesive media have high linear elastic thresholds (Singh *et al.* 1988). The effect of non-linearity of the stress–strain relationship can drop to zero during the earthquake-forced transformation of the solid into a liquid-like state (Pease & O'Rourke 1997).

The influence of non-linearities is important only when the wave amplitude is sufficiently large. In this paper we focus on two causes of amplification: resonant and topographic effects. There are two natural timescales associated with earthquake-induced natural resonators: the time for a wave to travel the length of the natural resonators, and the time over which non-linear effects become significant. In considering the resonant oscillations of topographies we shall assume that the latter scale is much smaller then the former. The above non-linear waves are treated far from the earthquake source. We shall not consider here strongly non-linear effects in and near this source (fracture, etc.).

The paper is organized as follows. In Section 2, equations of deformable media for surface waves in weakly cohesive porous materials are developed. Weakly compressible materials and highly non-linear problems are considered in Section 3. In particular, the 2-D equations of deformable media are reduced to a 1-D perturbed wave equation and an approximate general solution of this equation is constructed. The 2-D results presented in Section 4 are the generalization of the 1-D case. Thus, in Sections 2–4 we derive equations and obtain solutions describing the evolution and propagation of non-linear seismic waves in surface layers. These solutions make it possible to analyse non-linear effects due to strong ground motion. Sections 5–7 are devoted to applications of the general theory. The boundary problems of topography (valleys,

islands, volcanoes, ridges and coastline) are considered. Charles Darwin's (1839) reports of shivering of islands, anomalous earthquake/volcano interaction, violent crest amplification and vortices are qualitatively examined. Scenarios of transresonant evolution of seismic waves into breakers and tsunami-like waves, surface wave patterns and field data are treated. In Section 8 some novel and important aspects of the theory are discussed and a summary may be found.

2 MAIN ASSUMPTIONS AND GENERAL 3-D EQUATIONS OF THE THEORY

In this section we develop and analyse 3-D equations for a layer. We use a rectangular coordinate system. Let coordinates x_1 and x_2 be located on the bottom surface of the layer, and the coordinate x_3 be drawn vertically upwards. The motion of the layer is determined by the displacement vector components $u_i (i = 1, 2, 3)$ directed along x_i.

The material of the layer is considered as a compound of condensed (solid or solid+liquid) phase and gas. Let us assume that the exchange of the mass, momentum and energy between the gas and the condensed phase is negligible. The above assumption allows us to describe the behaviour of the material using space-averaged values for variables. The properties of the material, as a multiphase medium, will be described with the help of the equation of state.

The dynamic boundary conditions on the upper surface are

$$p_{33} = p_{\rm a} \quad p_{31} = \tau_{31}^{+} \quad p_{32} = \tau_{32}^{+} \quad \text{at} \quad x_3 = x_3^{+}. \tag{1}$$

Here $p_{\rm a}$ is the known pressure (in the case of the free surface $p_{\rm a}$ is the atmospheric pressure), p_{31} and p_{32} are the shear stresses (p_{ij} are the stress tensor components), x_3^{+} specifies the position of the upper surface. The values τ_{31}^{+} and τ_{32}^{+} are the surface shear stresses. We assume that

$$u_3 = \eta + \eta^{+} \quad \text{at} \quad x_3 = x_3^{+}. \tag{2}$$

The vertical displacement u_3 on the surface $x_3 = x_3^{+}$ is the sum of an unknown vertical displacement (dynamic elevation) of the surface η and an initial known vertical displacement of the surface η^{+}. For example, η^{+} might be the surface wave generated by an earthquake source, while η takes into account the strong amplification of the wave due to site (topographic or resonant) effects. We assume that η^{+} is much smaller than η. The vertical displacement η is determined by the equations of deformable media. The kinematic and dynamic boundary conditions on the bottom surface of the layer ($x_3 = x_3^{-}$) are

$$u_3 = \eta^{-}, \quad p_{31} = \tau_{31}^{-}; \quad p_{32} = \tau_{32}^{-} \quad (x_3 = x_3^{-}). \tag{3}$$

Here an incident wave η^{-} is much smaller than η. For example, the earthquake-induced hard rock (base) oscillations η^{-} may be amplified to η on the upper surface of the sediment layer. The thickness of the layer is $h = x_3^{+} - x_3^{-}$.

2.1 Model of the material

We assume a viscoelastoplastic model of a compressible material. Under the assumption of small plastic deformations, the viscoelastic (ε_{ij}^{*}, $j = 1, 2, 3$) and plastic ($\sum_{n=1}^{N} \Delta_n \varepsilon_{ij}^{p}$) strain components may be separated:

$$\varepsilon_{ij} = \varepsilon_{ij}^{*} + \sum_{n=1}^{N} \Delta_n \varepsilon_{ij}^{p}. \tag{4}$$

The viscoelastic components can be found from eq. (4). They are related to the deviatoric stress tensor components s_{ij}^{*} according to the following equations for a linear viscoelastic material (Nowacki 1963):

$$s_{ij}^{*} = 2G\left(\varepsilon_{ij}^{*} - \varepsilon_{ll}^{*}\delta_{ij}/3\right). \tag{5}$$

Here δ_{ij} is the Kronecker symbol, $l = 1, 2, 3$. In eq. (5) G is an operator which takes into account both the elastic and viscous properties of the material. It is assumed that the elastic and viscous effects are independent, and the total deformation is the sum of the elastic and viscous components. These components depend on the mean porosity ϕ_0 of the material (Rabotnov 1969). For materials with porosity ϕ we assume $G = \nu(1 - \alpha_s\phi_0) + \eta^{*}(1 - \alpha_\nu\phi_0)\partial(\cdots)/\partial t$, where ν and η^{*} are the elastic shear modulus and an effective viscosity, respectively. Coefficients α_s and α_ν are experimentally determined constants. The values of $\alpha_s\phi_0$ and $\alpha_\nu\phi_0$ lie between 0 and 1. According to the model, if $\alpha_s\phi_0 \to 1$, the material transforms into a liquified state (Galiev 1999a). This mechanism can take place for the vertical excitation of a layer (Umbanhowar *et al.* 1996; Wassgren *et al.* 1996; Cerda *et al.* 1997; Galiev 1999a). Under horizontal excitation the porosity can decrease. As a result, in saturated materials the water pressure increases due to lack of drainage. The material loses its shear strength and behaves like a liquid (Seed *et al.* 1976). In this case $G = \nu\alpha_s\phi_0 + \eta^{*}\alpha_\nu\phi_0\partial(\cdots)\partial t$.

The stress tensor components p_{ij} are defined by the pressure p and s_{ij}^{*} (Nowacki 1963; Mendelson 1968):

$$p_{ij} = s_{ij}^{*} - p\delta_{ij}. \tag{6}$$

Here $p = -(p_{11} + p_{22} + p_{33})/3 = -p_{ll}/3$. Now we can find from eqs (4)–(6) that

$$p_{ij} = 2G(\varepsilon_{ij} - \varepsilon_{ll}\delta_{ij}/3) + s_{ij} - p\delta_{ij}. \tag{7}$$

Here terms $s_{ij} = -2\nu(1 - \alpha_s\phi_0)\sum_{n=1}^{N} \Delta_n \varepsilon_{ij}^{p}$ take into account the accumulated plastic strains and $\sum_{n=1}^{N} \Delta_n \varepsilon_{ij}^{p} = 0$. The terms s_{ij} can be found using the criterion for plasticity and the Prandtl–Reuss constitutive equations (Mendelson 1968). The criterion for the material transfer into the plastic state can be written in the form (Shima & Oyane 1976)

$$\sigma_{\rm e}^2 + C^{*}\phi p^2 = C_{*}(\phi)\sigma_Y^2, \tag{8}$$

where $\sigma_e^2 = 1.5 s_{ij} s_{ij}$, σ_Y is the yield stress, and C^* and $C_*(\phi)$ are an experimentally defined constant and a function of the porosity, respectively. Note that $\sigma_e^2 = 3J_2$, where J_2 is the second invariant of the deviatoric stress tensor: $J_2 = s_{ij}s_{ij}/2$.

Expression (8) can be determined experimentally. For example, it was found (Shima & Oyane 1976) that $C^* = 6.25$ and $C_*(\phi) = (1-\phi)^5$ for a porous metal. However, expression (8) does not provide the relation between individual stress and strain components. Therefore, the Prandtl–Reuss constitutive equations must be used to determine σ_{ij} and ε_{ij}:

$$\Delta_n \varepsilon_{ij}^p = 1.5 \Delta_n \varepsilon_e^p S_{ij} \big/ \sigma_e, \tag{9}$$

where $\Delta_n \varepsilon_e^p = (2\ \Delta_n \varepsilon_e^p / \sigma_e\ \Delta_n \varepsilon_{ij}^p / 3)^{1/2}$.

The equations are sufficient to study the elastic, weakly viscous and plastic strains in the material. They contain both finite and infinitesimal quantities, and are valid for small plastic segments of the stress–strain curve. Therefore, a step-by-step algorithm should be used to solve the plastic problem (Galiev 1981, 1997a).

Let us consider the equations of motion, continuity and state for weakly cohesive media, assuming that the viscous and plastic effects are very small.

2.2 The Lagrangian equations

Let x_1, x_2 and x_3 be the initial coordinates of any particle of the material, and x, y and z be its coordinates at time t. There is the following relation between these values: $x = x_1 + u_1$, $y = x_2 + u_2$ and $z = x_3 + u_3$ (Lamb 1932). Considering the motion of the mass of the material and following Novozhilov (1961) we find that

$$\rho(u_{1,tt} - X) = p_{11,x} + p_{21,y} + p_{31,z}, \tag{10}$$

$$\rho(u_{2,tt} - Y) = p_{12,x} + p_{22,y} + p_{32,z}, \tag{11}$$

$$\rho(u_{3,tt} + g) = p_{13,x} + p_{32,y} + p_{33,z}. \tag{12}$$

Here X, Y and $g = g_0 + g_d$ are the components of the external forces per unit mass, where g_0 is the acceleration due to gravity and $g_d = g_d(t)$ is the excited acceleration. The subscripts t, x, y and z indicate derivatives with respect to time and coordinate. These equations contain differential coefficients with respect to x, y and z, whereas our independent variables are x_1, x_2, x_3 and t. To eliminate these differential coefficients, we multiply the above equations by $\partial x/\partial x_1$, $\partial y/\partial x_1$ and $\partial z/\partial x_1$, respectively, and add; then by $\partial x/\partial x_2$, $\partial y/\partial x_2$ and $\partial z/\partial x_2$, and add; and again a third time by $\partial x/\partial x_3$, $\partial y/\partial x_3$ and $\partial z/\partial x_3$ and add. Then we neglect the non-linear terms in the right-hand side of the equations. For this case, it follows that

$$\rho[(u_{1,tt} - X)(1 + u_{1,1}) + (u_{2,tt} - Y)u_{2,1} + (u_{3,tt} + g)u_{3,1}] + p_1 = s^*_{11,1} + p_{21,2} + p_{31,3}, \tag{13}$$

$$\rho[(u_{1,tt} - X)u_{1,2} + (u_{2,tt} - Y)(1 + u_{2,2}) + (u_{3,tt} + g)u_{3,1}] + p_2 = p_{12,1} + s^*_{22,2} + p_{32,3}, \tag{14}$$

$$\rho[(u_{1,tt} - X)u_{1,3} + (u_{2,tt} - Y)u_{2,3} + (u_{3,tt} + g)(1 + u_{3,3})] = p_{13,1} + p_{32,2} + p_{33,3}, \tag{15}$$

where $s^*_{ij,l} = \partial s^*_{ij}/\partial x_l$, $p_i = \partial p/\partial x_i$ and eqs (6) are used. We emphasize that soft and liquified layers are considered. Therefore, we presented the equations so that the left-hand sides of (13) and (14) coincide with the 'Lagrangian' form of the hydrodynamic equations (Lamb 1932, p. 13). The right-hand side terms take into account the stresses. Thus, the left-hand side of eqs (13)–(15) describe the motion of the media as an inviscid liquid. The right-hand side stress terms correct the motion taking into account solid-like properties of the media. These terms can drop to zero during the earthquake-forced transformation of the material into the liquified state. For example, the effective shear modulus can reduce from 9000 kPa to 20 kPa because of liquefaction (Pease & O'Rourke 1997). Many shallow-water seabeds are characterized by sediments of low rigidity. Thus, the right-hand side terms in eqs (13)–(15) are small for the layers considered. For rock and stiff soils the stress terms in eqs (13)–(15) are larger but the non-linear effects are smaller (Aki 1993; Beresnev & Wen 1996b). Therefore, for hard materials we can use linearized versions of eqs (13)–(15). For a plate-like layer we assume that u_1, u_2 and ρ are nearly independent of x_3. Therefore, in eqs (13)–(15) we have

$$u_{1,3} = \partial u_1/\partial x_3 \approx 0, \quad u_{2,3} = \partial u_2/\partial x_3 \approx 0 \quad \text{and} \quad \rho_3 = \partial \rho/\partial x_3 \approx 0. \tag{16}$$

The deformations are expressed in terms of u_i according to the following formula:

$$\varepsilon_{ij} = 0.5(u_{i,j} + u_{j,i} + u_{l,i}u_{l,j}), \tag{17}$$

where $\partial u_i/\partial x_j = u_{i,j}$. From eqs (17) and (7) we have

$$p_{ij} = G(u_{i,j} + u_{j,i} - 2u_{l,l}\delta_{ij}/3) + s_{ij} + p^N_{ij} - p\delta_{ij}, \tag{18}$$

where $p^N_{ij} = Gu_{l,i}u_{l,j} - G(u^2_{l,1} + u^2_{l,2} + u^2_{l,3})\ \delta_{ij}/3$. It follows from eqs (6) and (18) that

$$s^*_{ij} = G(u_{i,j} + u_{j,i} - 2u_{l,l}\delta_{ij}/3) + s_{ij} + p^N_{ij}. \tag{19}$$

The equation of continuity (Lamb 1932) is written using eq. (25):

$$\rho_0 = \rho\big(1 + nh^{-n}x_3^{n-1}\eta\big)(1 + u_{1,1} + u_{2,2} + u_{1,1}u_{2,2} - u_{1,2}u_{2,1}). \tag{20}$$

Here n is a positive constant.

2.3 Equations of state for the material

Following Galiev (1988, 1997a, 1999a) we use the following approximate equation of state for the multiphase material:

$$\rho = \rho_0\{(1-\phi_0)[1-\lambda(p-p_0)]+\phi\}^{-1}, \tag{21}$$

where λ is the compressibility of the condensed phase. The wave velocity $(\partial p/\partial\rho)$ depends strongly on porosity ϕ (Van der Grinten *et al.* 1987; Nakoryakov *et al.* 1989; Carcione & Poletto 2000). For example, in very soft muddy sediments, gassy and liquified soils the velocity is of the order of 10 m s^{-1} (see eq. 216). Gas oscillations will be considered as isothermal. Therefore, we have the following relation:

$$p = p_0\phi_0\phi^{-1}. \tag{22}$$

For a weakly compressible material, eqs (21) and (22) approximate to

$$\rho^{-1} \approx \rho_0^{-1}\big\{1-\big[\lambda(1-\phi_0)+\phi_0 p_0^{-1}\big](p-p_0)+\phi_0 p_0^{-2}(p-p_0)^2-\phi_0 p_0^{-3}(p-p_0)^3+\cdots\big\}. \tag{23}$$

We assume that ρ_0 is a weakly varying function of the coordinates: $\rho_{0,1}\approx 0$ and $\rho_{0,2}\approx 0$. The components s^*_{ij} in eqs (13)–(15) are functions of u_i. Thus, we have six equations (13)–(15), (20), (23) and (25) for six unknown values: η, u_i, p and ρ.

2.4 Pressure and the thickness-averaged equations

Pressure may be determined from the linearized equation of vertical motion. Using eqs (16) and (19), and neglecting small and non-linear terms, we find from eq. (15) that

$$u_{3,tt} = -g+\rho_0^{-1}G(u_{3,22}+u_{3,11}+u_{2,32}+u_{1,31})+\rho_0^{-1}p_{33,3}, \tag{24}$$

where ρ_0 is the undisturbed density. We determine the terms $u_{3,22}$ and $u_{3,11}$ using the following assumption:

$$u_3 = x_3^n h^{-n}(\eta-\eta^+)+\eta^-. \tag{25}$$

We assume that $(x_3^-)^n h^{-n}\approx 0$ and $\eta^+ \gg \eta^-$, so kinematic conditions (2) and (3) are satisfied. Eq. (25) yields Boussinesq's approximation (Boussinesq 1872) if $\eta^+=0$, $\eta^-=0$ and $n=1$. Then eq. (24) is integrated from the upper surface $(x_3=x_3^+)$ to an arbitrary surface x_3. Taking into account boundary conditions (1) and (25), we find the stress p_{33} at depth x_3:

$$p_{33} = p_a - g\rho_0\big[(2n+1)(n+1)^{-1}\eta+h-x_3\big]-h^{-n}(n+1)^{-1}\big(h^{n+1}-x_3^{n+1}\big)\big(\rho_0\eta_{tt}-G\nabla^2\eta\big)+\rho_0 C_*, \tag{26}$$

where $C_* = C_*(x_1,x_2,t)$ is an arbitrary function. It was assumed that the thickness of the layer changes very slowly ($h_1\approx 0$, $h_2\approx 0$) and $h-h_0 \ll h_0$, where h_0 is the average thickness. Now integrating the equations between x^+ and x^- we can reduce the problem to a 2-D formulation. Since $\eta \ll h$ we shall integrate the equations between h and 0. For example, the thickness-averaged pressure and the displacements are introduced as

$$P = h^{-1}\int_0^h p\,dx_3, \quad u_{i*} = h^{-1}\int_0^h u_i\,dx_3, \tag{27}$$

where the subscript * denotes the averaged value and will be dropped for these values in the rest of the paper. Taking into account eqs (18) and (27) we have from eq. (26),

$$P-P_0 = g\rho_0[(2n+1)\eta/(n+1)+h-h_0]-\frac{2}{3}G(u_{1,1}+u_{2,2})+\frac{4}{3}Gh^{-1}\eta+h(n+2)^{-1}\big(\rho_0\eta_{tt}-G\nabla^2\eta\big), \tag{28}$$

where $P_0 = p_a+g_0\rho_0 h_0/2$, and we have assumed that $g=g_0+g_d$ and $C_* = g_d h_0/2$. Here P_0 is the average static pressure.

Now we rewrite eqs (13) and (14) using the averaged values (27), boundary conditions (1) and (3), and expressions (19) and (25),

$$\begin{aligned}&(u_{1,tt}-X)(1+u_{1,1})+(u_{2,tt}-Y)u_{2,1}+(2n+1)^{-1}\eta_{tt}\eta_1+g(n+1)^{-1}\big(\eta_1-\eta_1^+\big)+g\eta_1^-\\&\quad=-\rho^{-1}P_1+\rho^{-1}G\left(\frac{4}{3}u_{1,11}+\frac{1}{3}u_{2,12}+u_{1,22}-\frac{2}{3}h^{-1}\eta_1\right)+\rho^{-1}X_N^p+\rho^{-1}h^{-1}\tau_{31},\end{aligned} \tag{29}$$

$$\begin{aligned}&(u_{2,tt}-Y)(1+u_{2,2})+(u_{1,tt}-X)u_{1,2}+(2n+1)^{-1}\eta_{tt}\eta_2+g(n+1)^{-1}\big(\eta_2-\eta_2^+\big)+g\eta_2^-\\&\quad=-\rho^{-1}P_2+\rho^{-1}G\left(\frac{4}{3}u_{2,22}+\frac{1}{3}u_{1,12}+u_{2,11}-\frac{2}{3}h^{-1}\eta_2\right)+\rho^{-1}Y_N^p+\rho^{-1}h^{-1}\tau_{32},\end{aligned} \tag{30}$$

where $X_N^p = s_{11,1}+s_{21,2}+p_{11,1}^N+p_{21,2}^N$, $Y_N^p = s_{12,1}+s_{22,2}+p_{12,1}^N+p_{22,2}^N$, $P_i = \partial P/\partial x_i$, $\eta_i = \partial\eta/\partial x_i (i=1,2)$ and

$$\tau_{31} = p_{31}\big(x_1,x_2,x_3=x_3^+,t\big) = p_{31}\big(x_1,x_2,x_3=x_3^-,t\big). \tag{31}$$

The expression for τ_{32} is similar to eq. (31). Eq. (20) yields

$$\rho_0 = \rho(1+h^{-1}\eta)(1+u_{1,1}+u_{2,2}+u_{1,1}u_{2,2}-u_{1,2}u_{2,1}). \tag{32}$$

The approximate equation (23) is valid for the averaged values too. Thus, eqs (20), (23), (28), (29), (30) and (32) are derived for weakly 3-D waves. These equations describe the generation and the evolution of non-linear seismic waves when liquefaction of the layer occurs. We used assumptions (16), (25) and assumed that the effects of plasticity and of the boundary stresses are very small.

According to the equations presented, the surface waves may depend on n, the vertical acceleration of particles of media and the geometric non-linearity, eq. (17). We shall take into account the geometric non-linearity in Section 7. In Sections 3–6 the linearized eq. (17) is used and we also assume that $n = 1$ and $(2n+1)^{-1}\eta_{tt}\eta_1 + g(n+1)^{-1}(\eta_1 + \eta_1^+) + g\eta_1^- \approx 0$, $(2n+1)^{-1}\eta_{tt}\eta_2 + g(n+1)^{-1}(\eta_2 + \eta_2^+) + g\eta_2^- \approx 0$, and $gu_{3,3} \approx 0$ in eqs (29), (30) and (15), respectively. In particular, for this case eq. (15) yields

$$P - P_0 = g\rho_0(\eta + h - h_0) - \frac{2}{3}G(u_{1,1} + u_{2,2}) + \frac{4}{3}Gh_0^{-1}\eta + \frac{1}{3}h\big(\rho_0\eta_{tt} - G\nabla^2\eta\big), \tag{33}$$

instead of eq. (28).

Remark. The equations presented describe a wide spectrum of wave phenomena in different media. For example, if $G = 0$ and the vertical acceleration is small, we have the classical expression for the pressure of long water waves $P - P_0 = g\rho_0(\eta + h - h_0)$ from eq. (33) (Lamb 1932). If $\eta = \eta^+ = \eta^- = 0$ and $\tau_{31} = \tau_{32} = 0$ then the equations are valid for 2-D body waves propagating in porous geomaterials, weakly cohesive soils, bubbly liquids and so on (see also Section 8.1). Thus, eqs (23), (28), (29), (30) and (32) describe 2-D body waves when $h \to \infty$ and $\eta \to 0$, $\eta^+ \to 0$, $\eta^- \to 0$, $\tau_{31} \to 0$, $\tau_{32} \to 0$.

3 1-D HIGHLY NONLINEAR THEORY FOR SLIGHTLY COMPRESSIBLE MATERIALS

The equation of continuity (32) and the linearized equation (23) yield

$$-hb(P - P_0) - hu_{1,1} = \eta(1 + u_{1,1}), \tag{34}$$

where $b = \lambda(1 - \phi_0) + \phi_0 P_0^{-1}$. Expression (33) reduces to the following form:

$$P - P_0 = g\rho_0(h - h_0) - \frac{2}{3}Gu_{1,1} + \left(\frac{4}{3}Gh^{-1} + g\rho_0\right)\eta + h(\rho_0\eta_{tt} - G\eta_{11})/3. \tag{35}$$

Now using the equation of continuity (33), we rewrite eq. (29) so that

$$u_{1,tt} = \rho_0^{-1}(1 + \eta h^{-1})\left[-P_1 + \frac{2}{3}G\big(2u_{1,11} - h^{-1}\eta_1\big)\right] + X + \rho_0^{-1}X_N^p + \rho_0^{-1}h^{-1}\tau_{31} + g\big(0.5\eta_1^+ - \eta_1^-\big). \tag{36}$$

Eqs (34)–(36) define the 1-D problem completely. Let us reduce these equations to one equation neglecting the sixth-order non-linear terms.

Eqs (34) and (35) yield approximately

$$\eta = -Ah\left(1 - \frac{2}{3}bG\right)\big(1 - Au_{1,1} + A^2u_{1,1}^2 - A^3u_{1,1}^3 + A^4u_{1,1}^4\big)\,u_{1,1}, \tag{37}$$

where $A = 1/(1 + hbg\rho_0 + \frac{4}{3}bG)$. The dispersive terms were eliminated in eq. (37). Using eq. (37), we rewrite expression (35) so that

$$\begin{aligned} P - P_0 = {} & -\frac{2}{3}Gu_{1,1} - Ah\left(1 - \frac{2}{3}bG\right)\left(g\rho_0 + \frac{4}{3}h^{-1}G\right)\big(1 - Au_{1,1} + A^2u_{1,1}^2 - A^3u_{1,1}^3 + A^4u_{1,1}^4\big)u_{1,1} \\ & -\frac{1}{3}A\rho_0h^2\left(1 - \frac{2}{3}bG\right)\big(u_{1,1tt} - \rho_0^{-1}Gu_{1,111}\big) + g\rho_0(h - h_0). \end{aligned} \tag{38}$$

Thus η and P are determined with the help of u_1. Now, after some algebra, the equation for u_1 may be derived from eq. (36) using eqs (37) and (38):

$$\begin{aligned} u_{1,tt} - a_0^2u_{1,11} = {} & X - gh_1 + \big(\beta u_{1,1} + \beta_1u_{1,1}^2 + \beta_2u_{1,1}^3 + \beta_3u_{1,1}^4\big)\,u_{1,11} + \mu u_{1,1t} \\ & + \frac{1}{3}A_*h^2\left(1 - \frac{2}{3}bG_*\right)\big(u_{1,11tt} - a_s^2u_{1,1111}\big) + \rho_0^{-1}X_N^p + \rho_0^{-1}h^{-1}\tau_{31} + g\big(0.5\eta_1^+ - \eta_1^-\big), \end{aligned} \tag{39}$$

here $G_* = \nu(1 - \alpha_s\phi_0)$, $A_* = (1 + gbh\rho_0 + \frac{4}{3}bG_*)^{-1}$, $\mu \approx 2\eta^*\rho_0^{-1}(1 - \alpha_s\phi_0)$, $a_s^2 = \rho_0^{-1}G_*$ and

$$a_0^2 = A_*\left(1 - \frac{2}{3}bG_*\right)\big(gh + 2\rho_0^{-1}G_*\big) + 2\rho_0^{-1}G_*, \tag{40}$$

$$\beta = A_*\left(\frac{2}{3}bG_* - 1\right)\left[2\rho_0^{-1}G_* + A_*\big(gh + 2\rho_0^{-1}G_*\big)\left(3 - \frac{2}{3}bG_*\right)\right], \tag{41}$$

$$\beta_1 = A_*\left(1 - \frac{2}{3}bG_*\right)A_*^2\left[2\rho_0^{-1}G_* + 3A_*\big(gh + 2\rho_0^{-1}G_*\big)\left(2 - \frac{2}{3}bG_*\right)\right], \tag{42}$$

$$\beta_2 = \left(\frac{2}{3}bG_* - 1\right)A_*^3\left[2\rho_0^{-1}G_* + A_*\big(gh + 2\rho_0^{-1}G_*\big)(10 - 4bG_*)\right], \tag{43}$$

$$\beta_3 = \left(1 - \frac{2}{3}bG_*\right)A_*^4\left[2\rho_0^{-1}G_* + 5A_*\big(gh + 2\rho_0^{-1}G_*\big)\left(3 - \frac{4}{3}bG_*\right)\right]. \tag{44}$$

We note that the expression for μ was very long and here the main part of the expression was retained. The second term in the right-hand side of eq. (39) takes into account the topographic effect (Galiev 1997b, 1998, 1999a; Galiev & Galiev 1998). Then there are quadratic, cubic, fourth and fifth-order terms with regard to u_1. The dissipative and dispersive terms in eq. (39) follow the non-linear terms. The term $\rho_0^{-1}X_N^p$ takes into account plastic and geometric non-linear properties of the layer material. The term $\rho_0^{-1}h^{-1}\tau_{31}$ is determined by the boundary friction. The final term takes into account the initial waves propagating on the upper and lower surfaces. It is assumed that the thickness of the layer changes very slowly and the linear and non-linear terms containing partial derivatives of h (for example, $gh_1u_{1,1}$) are negligible. Moreover, non-linear terms containing the viscosity coefficient η^* are neglected. These assumptions simplify the analysis of the influence of non-linearity, the topographic, dispersive and dissipative effects on the surface waves. From the linearized equation (39) it follows that $u_{1,tt11} \approx a_0^2 u_{1,1111}$. Using this equation, we rewrite eq. (39) so that

$$u_{1,tt} - a_0^2 u_{1,11} = X - gh_1 + \left(\beta u_{1,1} + \beta_1 u_{1,1}^2 + \beta_2 u_{1,1}^3 + \beta_3 u_{1,1}^4\right)u_{1,11} + \mu u_{1,11t} + k u_{1,1111} + \rho_0^{-1}X_N^p + \rho_0^{-1}h^{-1}\tau_{31} + g\left(0.5\eta_1^+ - \eta_1^-\right), \tag{45}$$

where $k = A_* h^2(1 - \frac{2}{3}bG_*)(a_0^2 - a_s^2)/3$. We emphasize that eq. (45) takes into account the strength and the viscous properties of the medium. In particular, in eq. (45) the dispersive term depends on the strength and h^2. The vertical displacement is determined by eq. (37). Boundary friction effects might be introduced in eq. (45) in several ways (Stoker 1957; Chester 1968; Ockendon *et al.* 1986; Galiev & Galiyev 2001). Cox & Mortell (1986) assumed that this friction is proportional to $u_{1,t}$. In Sections 5.1 and 5.2 we shall assume that the boundary friction term in eq. (45) is proportional to $u_{1,11t}(\tau_{31} = \mu_f u_{1,11t})$.

3.1 Limiting expressions for a_0

The local speed, eq. (40), depends on the mean porosity, the shear wave speed, the compressibility of the matrix material, the thickness of the layer and the vertical acceleration. In particular, the mean porosity of the material and the shear wave speed can vary during the earthquake. Thus, a_0 is a complex function of the coordinates and time. However, there are cases when expression (40) may be reduced to well-known expressions. Let $h \to \infty$; then we have $a_0^2 = \rho_0^{-1}[\lambda(1-\phi_0) + \phi_0 P_0^{-1}]^{-1} + \frac{4}{3}\nu\rho_0^{-1}(1 - \alpha_s\phi_0)$. If $\phi_0 \to 0$, then this expression determines the speed of elastic body waves in an infinite space: $a_0 = (\rho_0^{-1}\lambda^{-1} + \frac{4}{3}\nu\rho_0^{-1})^{1/2}$.

The thickness of the liquifiable layer has been found to be a significant parameter affecting the magnitude of lateral spreading (O'Rourke & Pease 1997). This also follows from the theory presented. If $\alpha_s\phi_0 \to 1$ (liquified state or bubbly liquid) then $a_0^2 = \{1/gh + \rho_0[\lambda(1-\phi_0) + \phi_0 P_0^{-1}]\}^{-1}$. Thus, the wave speed in the liquified layer is a function of the porosity, the thickness, the vertical acceleration and may be very small ($a_0^2 < gh$). If the compressibility of the solid phase is zero, $\lambda = 0$, then $a_0^2 = (1/gh + \rho_0\phi_0 P_0^{-1})^{-1}$. Let $1/gh \gg \rho_0\phi_0 P_0^{-1}$; then we have $a_0^2 \approx gh$. Furthermore, if $h \to \infty$ and $\phi_0 = 1$, then we have the relation for the speed of sound in gas (the isothermal approximation): $a_0^2 = P_0\rho_0^{-1}$.

3.2 The Airy model and equation

For a thin water layer, eq. (45) yields

$$u_{1,tt} - ghu_{1,11} = gh\left(-3u_{1,1} + 6u_{1,1}^2 - 10u_{1,1}^3 + 15u_{1,1}^4\right)u_{1,11}. \tag{46}$$

This equation may be considered as the generalization of Airy's theory (Airy 1845). Airy considered water waves propagating in a uniform canal. For this case $gh = g_0h_0$ in eq. (46) and we have the Airy equation (Lamb 1932, p. 260) written for weakly non-linear waves. Airy predicted that a non-linear wave could not propagate without a change of form: it steepens and eventually breaks. On the other hand, eq. (46) is similar to eq. (3) from Lamb (1932, p. 481) which determines the generation of wave singularities in gas. Therefore, we can expect seismic surface waves propagating in inviscid and non-dispersive media also to steepen and break. On the other hand, there are dissipative and dispersive terms in eq. (45). These terms can modify the results of non-linear effects. Thus, anomalous waves having complex forms are described by eqs (45) and (46). We will study these waves in Sections 3.5 and 5–7.

Here the dynamic model of the layer presented in Section 2 was reduced to Airy's model (Airy 1845) of shallow water waves. As will be seen, the 2-D equation (43) from Beji & Nadaoka (1997) for shallow water waves also follows from the theory as a particular case (see Section 4.2.2). Thus, our theory may be considered as the generalization of shallow surface water wave theory to solid deformable layers.

3.3 Perturbation method and general solution

Eq. (45) is now rewritten in terms of new variables:

$$r = a(t) - x_1, \quad s = a(t) + x_1, \tag{47}$$

where $a(t)$ is an unknown function that will be determined later. It is found that

$$\begin{aligned} &u_{1,1} = u_{1,s} - u_{1,r},\ u_{1,t} = a_t(u_{1,s} + u_{1,r}),\ u_{1,11} = u_{1,rr} - 2u_{1,rs} + u_{1,ss},\\ &u_{1,tt} = a_t^2(u_{1,rr} + 2u_{1,rs} + u_{1,ss}) + a_{tt}(u_{1,r} + u_{1,s}),\\ &u_{1,1111} = u_{1,rrrr} - 2u_{1,rrss} + u_{1,ssss},\ u_{1,11t} = a_t(u_{1,rrr} - u_{1,rss} - u_{1,rrs} + u_{1,sss}). \end{aligned} \tag{48}$$

Here $a = a(t)$ and the subscripts r and s refer to partial derivatives with respect to r and s, respectively. Then, using eq. (48) we rewrite eq. (45) so that

$$\begin{aligned}
&\left(a_t^2 - a_0^2\right)(u_{1,rr} + u_{1,ss}) + 2\left(a_t^2 + a_0^2\right)u_{1,rs} + a_{tt}^2(u_{1,r} + u_{1,s}) = g(h_r - h_s)\\
&\quad + \left[\beta - \beta_1(u_{1,r} - u_{1,s}) + \beta_2(u_{1,r} - u_{1,s})^2 - \beta_3(u_{1,r} - u_{1,s})^3\right](u_{1,s} - u_{1,r})(u_{1,rr} - 2u_{1,rs} + u_{1,ss})\\
&\quad + \mu a_t(u_{1,rrr} - u_{1,rss} - u_{1,rrs} + u_{1,sss}) + k(u_{1,rrrr} - 2u_{1,rrss} + u_{1,ssss}) + X\\
&\quad + \rho_0^{-1}X_N^p + \rho_0^{-1}h^{-1}\tau_{31} + g\left(0.5\eta_1^+ - \eta_1^-\right).
\end{aligned} \tag{49}$$

It is seen that eq. (49) yields the non-linear diffusion equation if $u_{1,rs} \approx 0$.

We assume site resonant conditions

$$|R_e| \ll 1, \quad |a_{tt}| \ll 1, \quad u_{1,rs} \approx 0, \tag{50}$$

where a transresonant parameter $R_e = a_t^2 - a_0^2$ depends weakly on x_1 and t: $(R_e)_1 \approx 0$ and $(R_e)_t \approx 0$. At the exact site resonance $a_t^2 = a_0^2$. We assumed that a_0 and a_t are functions of t. This situation may occur as the result of the acoustic fluidization of the material (Melosh 1996; Sornette & Sornette 2000) due to earthquake-induced vibrations or the earthquake-induced vertical acceleration. We can assume that $a(t)$ is proportional to t^α, where $\alpha < 2$. Therefore, $a_{tt} \to 0$, if $t \to \infty$. When a_0 and a_t are functions of t, the solution (57) resembles the d'Alembert-type solution, but the velocity of waves $J(a - x)$ and $j(a + x)$ can vary and depends on t (Galiev 1999a, 2000a).

Below we shall consider the case where βa_t^{-2}, $\beta_1 a_t^{-2}$, $\beta_2 a_t^{-2}$, $\beta_3 a_t^{-2}$, μa_t^{-1} and $k a_t^{-2}$ are approximately constant in eq. (49). In particular, they are constants for water, liquefiable soft soils and suspensions. For water we have $\beta a_t^{-2} = -3$, $\beta_1 a_t^{-2} = 6$, $\beta_2 a_t^{-2} = -10$, $\beta_3 a_t^{-2} = 15$, $\mu a_t^{-1} \approx$ constant and $k a_t^{-2} = \frac{1}{3}h^2$. On the other hand, they are constant for solid layers if $\frac{4}{3}\nu\rho_0^{-1}(1 - \alpha_s\phi_0) \gg gh$.

The solution of eq. (49) is sought using the perturbation method:

$$u_1 = u_1^{(1)} + u_1^{(2)} + u_1^{(3)} + u_1^{(4)} + u_1^{(5)} + \cdots, \tag{51}$$

where $u_1^{(1)} \gg u_1^{(2)} \gg u_1^{(3)} \gg u_1^{(4)} \gg u_1^{(5)}$. Expansion (51) is used widely in non-linear physics (Koch & Sangani 1999; Kouznetsov & Garcia-Valenzuela 1999). We assume that at the resonance the amplitude of the waves becomes significantly larger than the amplitude of the forcing oscillations. Substituting the sum (51) into eq. (49) and equating terms of the same order, we obtain the following inhomogeneous linear differential equations:

$$u_{1,rs}^{(1)} = 0, \tag{52}$$

$$4a_0^2 u_{1,rs}^{(2)} = -R_e\left[u_{1,r}^{(1)} + 2u_{1,rs}^{(1)} + u_{1,ss}^{(1)}\right] - a_{tt}\left[u_{1,r}^{(1)} + u_{1,s}^{(1)}\right] + \beta\left[u_{1,s}^{(1)} - u_{1,r}^{(1)}\right]\left[u_{1,rr}^{(1)} - 2u_{1,rs}^{(1)} + u_{1,ss}^{(1)}\right], \tag{53}$$

$$\begin{aligned}
4a_0^2 u_{1,rs}^{(3)} &= -R_e\left[u_{1,rr}^{(2)} + 2u_{1,rs}^{(2)} + u_{1,ss}^{(2)}\right] - a_{tt}\left[u_{1,r}^{(2)} + u_{1,s}^{(2)}\right] + \beta\left[u_{1,s}^{(2)} - u_{1,r}^{(2)}\right]\left[u_{1,rr}^{(1)} - 2u_{1,rs}^{(1)} + u_{1,ss}^{(1)}\right]\\
&\quad + \beta\left[u_{1,s}^{(1)} - u_{1,r}^{(1)}\right]\left[u_{1,rr}^{(2)} - 2u_{1,rs}^{(2)} + u_{1,ss}^{(2)}\right] + \beta_1\left[u_{1,s}^{(1)} - u_{1,r}^{(1)}\right]^2\left[u_{1,rr}^{(1)} - 2u_{1,rs}^{(1)} + u_{1,ss}^{(1)}\right],
\end{aligned} \tag{54}$$

$$4a_0^2 u_{1,rs}^{(4)} = \beta_2\left[u_{1,s}^{(1)} - u_{1,r}^{(1)}\right]^3\left[u_{1,rr}^{(1)} - 2u_{1,rs}^{(1)} + u_{1,ss}^{(1)}\right], \tag{55}$$

$$\begin{aligned}
4a_0^2 u_{1,rs}^{(5)} &= \beta_3\left[u_{1,s}^{(1)} - u_{1,r}^{(1)}\right]^4\left[u_{1,rr}^{(1)} - 2u_{1,rs}^{(1)} + u_{1,ss}^{(1)}\right] + \mu a_0\left[u_{1,rrr}^{(1)} - u_{1,rss}^{(1)} - u_{1,rrs}^{(1)} + u_{1,sss}^{(1)}\right]\\
&\quad + k\left[u_{1,rrrr}^{(1)} - 2u_{1,rrss}^{(1)} + u_{1,ssss}^{(1)}\right] + \rho_0^{-1}h^{-1}\tau_{31} + \rho_0^{-1}X_N^p + g(h_r - h_s) + X + g\left(0.5\eta_1^+ - \eta_1^-\right).
\end{aligned} \tag{56}$$

The equations for $u_1^{(4)}$ and $u_1^{(5)}$ following from eq. (49) are very long and complex. We retain only a few terms in eqs (55) and (56) to simplify the problem. These simplified equations will allow us to evaluate qualitatively the influence of high non-linearity on the waves.

The solution of eq. (52) is

$$u_1^{(1)} = J(r) + j(s). \tag{57}$$

Now we shall correct solution (57) taking into account $u_1^{(2)}$, and then $u_1^{(i)} (i = 3, 4, 5)$. We assume that $R_e \approx$ constant , $a_{tt} \approx$ constant. Substituting eq. (57) into eq. (53) and integrating, one can find that

$$u_1^{(2)} = J_2(r) + j_2(s) - \frac{1}{4}a_0^{-2}\left[s(R_eJ' + a_{tt}J) + r(R_ej' + a_{tt}j)\right] + \beta a_0^{-2}[r(j')^2 - s(J')^2 + 2jJ' - 2j'J]/8 + x_1 d + d_1, \tag{58}$$

where $J_2(r)$ and $j_2(s)$ are functions of integration, and d and d_1 are constants of integration. In eq. (58), $J = J(r)$ and $j = j(s)$, and the prime denotes differentiation with respect to the appropriate variables r or s. The influence of d and d_1 on the high-order values will not be considered. Using eqs (57) and (58), we can rewrite eq. (54) in the following form:

$$u^{(3)}_{1,rs} = -0.25a_0^{-2}\left\{R_{\rm e}\left[u^{(2)}_{1,rr} + 2u^{(2)}_{1,rs} + u^{(2)}_{1,ss}\right] + a_{tt}\left[u^{(2)}_{1,r} + u^{(2)}_{1,s}\right]\right\}$$
$$+ \beta^2 a_0^{-4}\left\{\frac{1}{2}(j^2)'J''' + \frac{1}{2}(J^2)'j''' - Jj'j''' - jJ'J''' - \frac{5}{6}[(j')^3]' - \frac{5}{6}[(J')^3]' - JJ''j'' - jj''J'' - \frac{7}{2}(j')^2J'' - \frac{7}{2}(J')^2j''\right.$$
$$\left. + \frac{7}{2}[(J')^2]'j' + \frac{7}{2}[(j')^2]'J' - j(J'')^2 - J(j'')^2\right\}\Big/16$$
$$- \frac{1}{32}\beta^2 a_0^{-4}s\left\{j'[(J')^2]'' - j''[(J')^2]' - \frac{2}{3}[(J')^3]''\right\}$$
$$+ \frac{1}{32}\beta^2 a_0^{-4}r\left\{-J'[(j')^2]'' + J''[(j')^2]' + \frac{2}{3}[(j')^3]''\right\} + \frac{1}{4}\beta_1 a_0^{-2}[J''(j')^2 - 2J'j'J'' + J''(J')^2 + j''(j')^2 - 2J'j'j'' + j''(J')^2]$$
$$+ \frac{1}{4}\beta a_0^{-2}[(J_2'' + j_2'')(j' - J') - (J_2' - j_2')(J'' + j'')]. \tag{59}$$

Here $J_2 = J_2(r)$ and $j_2 = j_2(s)$. Eq. (59) yields

$$u^{(3)}_1 = J_3(r) + j_3(s) - 0.25a_0^{-2}\iint\left\{R_{\rm e}\left[u^{(2)}_{1,rr} + u^{(2)}_{1,ss}\right] + a_{tt}\left[u^{(2)}_{1,r} + u^{(2)}_{1,s}\right]\right\}dr\,ds - 0.5a_0^{-2}R_{\rm e}u^{(2)}_1$$
$$+ \frac{1}{32}\beta^2 a_0^{-4}\left\{j^2J'' + J^2j'' + 7(J')^2j + 7(j')^2J - 5r(j')^3/3 - 5s(J')^3/3\right.$$
$$\left. - 2\iint[Jj'j''' + jJ'J''' + j(J'')^2 + J(j'')^2]\,dr\,ds - J'\int[7(j')^2 + 2jj'']\,ds - j'\int[7(J')^2 + 2JJ'']\,dr\right\}$$
$$- \frac{1}{32}\beta^2 a_0^{-4}\int s\{j'[(J')^2]' - j''(J')^2\}\,ds + \frac{1}{96}\beta^2 a_0^{-4}s^2[(J')^3]'$$
$$+ \frac{1}{32}\beta^2 a_0^{-4}\int r\{-J'[(j')^2]' + J''(j')^2\}\,ds + \frac{1}{96}\beta^2 a_0^{-4}r^2[(j')^3]'$$
$$+ 0.25\beta_1 a_0^{-2}\left[J'\int(j')^2\,ds + j'\int(J')^2\,dr + s(J')^3/3 + r(j')^3/3 - j(J')^2 - J(j')^2\right]$$
$$+ 0.25\beta a_0^{-2}(J_2'j - j_2'J + j_2J' - J_2j' + rj_2'j' - sJ_2'J'). \tag{60}$$

After some algebra, u_3 is determined from eq. (60) as

$$u^{(3)}_1 = J_3(r) + j_3(s) - 0.25a_0^{-2}\iint\left\{R_{\rm e}\left[u^{(2)}_{1,rr} + u^{(2)}_{1,ss}\right] + a_{tt}\left[u^{(2)}_{1,r} + u^{(2)}_{1,s}\right]\right\}drds - 0.5a_0^{-2}R_{\rm e}u^{(2)}_1$$
$$+ \beta^2 a_0^{-4}[J''j^2 + j''J^2 - 2j'J'J - 2j'J'j - 2sjJ'J'' + sj'(J')^2 - 2rJj'j''$$
$$+ rJ'(j')^2 + s^2(J')^2J'' + r^2(j')^2j'']/32 - \left(\beta_1 a_0^{-2}/4 - 3\beta^2 a_0^{-4}/16\right)[j(J')^2 + J(j')^2]$$
$$+ \left(\beta_1 a_0^{-2}/4 - 5\beta^2 a_0^{-4}/32\right)\left[j'\int(J')^2\,dr + J'\int(j')^2ds + s(J')^3/3 + r(j')^3/3\right]$$
$$+ 0.25\beta a_0^{-2}(J_2'j - j_2'J + j_2J' - J_2j' + rj_2'j' - sJ_2'J'). \tag{61}$$

Now we can approximately take into account highly non-linear effects. With the help of eq. (57), eqs (55) and (56) can be rewritten as

$$4a_0^2u^{(4)}_{1,rs} = \beta_2(j' - J')^3(j'' + J''), \tag{62}$$

$$4a_0^2u^{(5)}_{1,rs} = \beta_3(j' - J')^4(j'' + J'') + \mu a_0(j'''' + J'''') + k(j'''' + J'''') + \rho_0^{-1}h^{-1}\tau_{31} + \rho_0^{-1}X_N^p + g(h_r - h_s) + X - g\left(0.5\eta_1^+ + \eta_1^-\right). \tag{63}$$

We shall neglect the interaction of the waves J' and j' in eqs (62) and (63). In this case, the previous equations yield

$$u^{(4)}_1 = J_4(r) + j_4(s) + \beta_2 a_0^{-2}[r(j')^4 - s(J')^4]/16, \tag{64}$$

$$u^{(5)}_1 = J_5(r) + j_5(s) + 0.05\beta_3 a_0^{-2}[r(j')^5 - s(J')^5] + 0.25\mu a_0^{-1}(rj'' + sJ'')$$
$$+ 0.25ka_0^{-2}(rj'''' + sJ'''') + 0.25\iint a_0^{-2}\left[X + \rho_0^{-1}h^{-1}\tau_{31} + \rho_0^{-1}X_N^p + g(h_r - h_s) - g\left(0.5\eta_1^+ + \eta_1^-\right)\right]dr\,ds. \tag{65}$$

The approximate general solution of eq. (45) is the sum (51):

$$
\begin{aligned}
u_1 &= J + j + \big(1 - 0.5a_0^{-2}R_e\big)\{J_2 + j_2 + x_1 d + d_1 - 0.25a_0^{-2}R_e(sJ' + rj') \\
&\quad + 0.125\beta a_0^{-2}[r(j')^2 - s(J')^2 + 2jJ' - 2j'J]\} + J_3(r) + j_3(s) \\
&\quad - 0.25a_0^{-2}\iint \big[R_e\big(u^{(2)}_{1,rr} + u^{(2)}_{1,ss}\big) + a_{tt}(u^{(2)}_{1,r} + u^{(2)}_{1,s})\big]\,dr\,ds \\
&\quad + \beta^2 a_0^{-4}[J''j^2 + j''J^2 - 2j'J'J - 2j'J'j - 2sjJ'J'' + sj'(J')^2 \\
&\quad - 2rJj'j'' + rJ'(j')^2 + s^2(J')^2J'' + r^2(j')^2j'']/32 - \big(\beta_1 a_0^{-2}/4 - 3\beta^2 a_0^{-4}/16\big)[j(J')^2 + J(j')^2] \\
&\quad + \big(\beta_1 a_0^{-2}/4 - 5\beta^2 a_0^{-4}/32\big)\left[j'\int (J')^2\,dr + J'\int (j')^2\,ds + s(J')^3/3 + r(j')^3/3\right] \\
&\quad + 0.25\beta a_0^{-2}(J_2'j - j_2'J + j_2J' - J_2j' + rj_2'j' - sJ_2'J') + \beta_2 a_0^{-2}[r(j')^4 - s(J')^4]/16 \\
&\quad + J_4(r) + j_4(s) + J_5(r) + j_5(s) + 0.05\beta_3 a_0^{-2}[r(j')^5 - s(J')^5] + 0.25\mu a_0^{-1}(rj'' + sJ'') \\
&\quad + \frac{1}{8}ka_0^{-2}(rj''' + sJ''') + \frac{1}{8}\iint a_0^{-2}\big[X + \rho_0^{-1}h^{-1}\tau_{31} + \rho_0^{-1}X_N^p + g(h_r - h_s) + g\big(0.5\eta_1^+ - \eta_1^-\big)\big]\,dr\,ds.
\end{aligned}
\tag{66}
$$

Expression (66) is the approximate solution of the 2-D equations of deformable media under conditions (1)–(3) on the upper and lower surfaces of the layer. The coefficients in eq. (66) explicitly depend on t because of the fact that in eqs (53)–(56) some right-hand 'driving' terms are in *resonance* with the intrinsic oscillator frequency (Poincaré 1892; Tabor 1989). The infamous problem of resonances (or *small divisors,* Poincaré 1892) has been studied over the past hundred years (Poincaré 1892; Sagdeev *et al.* 1988; Prigogine 1997; Nayfeh 2000). We consider this fundamental problem below.

3.3.1 Bounded solution of eq. (45)

Expression (66) may be modified to exclude the secular terms. First we modify expression (58). There the secular terms will be eliminated if

$$
\begin{aligned}
J_2(r) &= 0.25a_0^{-2}r(R_eJ' + a_{tt}J) + \beta a_0^{-2}r(J')^2/8 + \Psi_2(r), \\
j_2(s) &= 0.25a_0^{-2}s(R_ej' + a_{tt}j) - \beta a_0^{-2}s(j')^2/8 + \psi_2(s).
\end{aligned}
\tag{67}
$$

As a result, we have

$$
u_1^{(2)} = \Psi_2(r) + \psi_2(s) - 0.5a_0^{-2}x_1[R_e(J' - j') + a_{tt}(J - j)] + \beta a_0^{-2}[(r - s)(j')^2 - (s - r)(J')^2 + 2jJ' - 2j'J]/8 + x_1\,d + d_1. \tag{68}
$$

Using eqs (57) and (68), we rewrite eq. (54) and obtain a variation of eq. (59). Then, following Section 3.3, we find $u_1^{(3)}$:

$$
\begin{aligned}
u_1^{(3)} &= J_3(r) + j_3(s) + \frac{1}{12}\beta^2 a_0^{-4}\left\{j^2J'' + J^2j'' + 7(J')^2j + 7(j')^2J - 5r(j')^3/3 - 5s(J')^3/3\right. \\
&\quad \left. - 2\iint [Jj'j''' + jJ'J''' + j(J'')^2 + J(j'')^2]\,dr\,ds - J'\int [7(j')^2 + 2jj'']\,ds - j'\int [7(J')^2 + 2JJ'']\,dr\right\} \\
&\quad - \frac{1}{32}\beta^2 a_0^{-4}\iint (s - r)\left\{j'[(J')^2]'' - J'[(j')^2]'' + J''[(j')^2]' - j''[(J')^2]' + \frac{2}{3}[(j')^3]'' - \frac{2}{3}[(J')^3]''\right\}dr\,ds \\
&\quad + 0.25\beta_1 a_0^{-2}\left[J'\int (j')^2\,ds + j'\int (J')^2\,dr + s(J')^3/3 + r(j')^3/3 - j(J')^2 - J(j')^2\right] \\
&\quad + 0.25\beta a_0^{-2}(\Psi_2'j - \psi_2'J + \psi_2J' - \Psi_2j' + r\psi_2'j' - s\Psi_2'J').
\end{aligned}
\tag{69}
$$

Here $\Psi_2 = \Psi_2(r)$ and $\psi_2 = \psi_2(s)$. For simplicity we assumed $R_e \approx 0$ and $a_{tt} \approx 0$ in eq. (69). We have

$$
\iint (s - r)[(j')^3]''\,dr\,ds = 1.5(sr - 0.5r^2)j'[(j')^2]' - r(j')^3. \tag{70}
$$

Now, after some algebra, u_3 is determined from eq. (69) as

$$
\begin{aligned}
u_1^{(3)} &= J_3(r) + j_3(s) + \beta^2 a_0^{-4}(J''j^2 + j''J^2 - 2j'J'J - 2j'J'j)/32 \\
&\quad - \big(\beta_1 a_0^{-2}/4 - 5\beta^2 a_0^{-4}/32\big)\big[j(J')^2 + J(j')^2\big] + \big(\beta_1 a_0^{-2}/4 - \beta^2 a_0^{-4}/8\big)\left[j'\int (J')^2\,dr + J'\int (j')^2 ds\right] \\
&\quad + \big(\beta_1 a_0^{-2}/12 - \beta^2 a_0^{-4}/32\big)\big[s(J')^3 + r(j')^3\big] + \beta^2 a_0^{-4}\big\{(r - s)[2jJ'J'' - 2Jj'j'' \\
&\quad + J'(j')^2 - j'(J')^2] + (s^2 - 2rs)J''(J')^2 + (r^2 - 2rs)j''(j')^2\big\}/32 \\
&\quad + 0.25\beta a_0^{-2}(\Psi_2'j - \psi_2'J + \psi_2J' - \Psi_2j' + r\psi_2'j' - s\Psi_2'J').
\end{aligned}
\tag{71}
$$

The secular terms are eliminated in eq. (71) if

$$J_3(r) = \left(\frac{1}{32}\beta^2 a_0^{-4} - \frac{1}{12}\beta_1 a_0^{-2}\right) r(J')^3 + \frac{1}{32}\beta^2 a_0^{-4} r^2 J''(J')^2 + \frac{1}{4}\beta a_0^{-2} r\Psi_2' J' + \Psi_3. \tag{72}$$

$$j_3(s) = \left(\frac{1}{32}\beta^2 a_0^{-4} - \frac{1}{12}\beta_1 a_0^{-2}\right) s(j')^3 + \frac{1}{32}\beta^2 a_0^{-4} s^2 j''(j')^2 - \frac{1}{4}\beta a_0^{-2} s\psi_2' j' + \psi_3. \tag{73}$$

Here $\Psi_3 = \Psi_3(r)$ and $\psi_3 = \psi_3(s)$. Then in eqs (64) and (65) we assume that

$$J_4(r) = \beta_2 a_0^{-2} r(J')^4/16, \quad j_4(s) = -\beta_2 a_0^{-2} s(j')^4/16, \tag{74}$$

$$j_5(r) = -0.05\beta_3 a_0^{-2} s(j')^4 - 0.25\mu a_0^{-1} rJ'' - 0.25k a_0^{-2} rJ''', \tag{75}$$

$$j_5(s) = -0.05\beta_3 a_0^{-2} s(j')^4 - 0.25\mu a_0^{-1} sj'' - 0.25k a_0^{-2} sj'''. \tag{76}$$

Using eq. (51), and expressions (57), (68), (71)–(73), (64), (74) and (65), (75), (76), we can write the approximate general bounded solution of eq. (45):

$$\begin{aligned} u_1 = {} & J + j + \Psi_2 + \psi_2 + \Psi_3 + \psi_3 + x_1 d + d_1 - 0.5a_0^{-2}x_1[R_e(J' - j') + a_{tt}(J - j)] \\ & - \beta a_0^{-2}[x_1(J')^2 + x_1(j')^2 - jJ' + j'J]/4 + \frac{1}{32}\beta^2 a_0^{-4}(J''j^2 + j''J^2 - 2j'J'J - 2j'J'j) \\ & - \frac{1}{4}(\beta_1 a_0^{-2} - 5\beta^2 a_0^{-4}/8)[j(J')^2 + J(j')^2] + \frac{1}{4}(\beta_1 a_0^{-2} - 0.5\beta^2 a_0^{-4})\left[j'\int (J')^2\,dr + J'\int (j')^2 ds\right] \\ & + (\beta_1 a_0^{-2}/6 - \beta^2 a_0^{-4}/16)x_1[(J')^3 - (j')^3] + \frac{1}{8}\beta^2 a_0^{-4} x_1[Jj'j'' - jJ'J'' - 0.5J'(j')^2 + 0.5j'(J')^2 \\ & + x_1 J''(J')^2 + x_1 j''(j')^2] - \beta_2 a_0^{-2} x_1[(j')^4 + (J')^4]/8 - 0.1\beta_3 a_0^{-2} x_1[(j')^5 + (J')^5] \\ & - 0.5\mu a_0^{-1} x_1(j'' - J'') - 0.5k a_0^{-2} x_1(j''' - J''') + \frac{1}{4}\iint a_0^{-2}[X + \rho_0^{-1}h^{-1}\tau_{31} + \rho_0^{-1}X_N^p + g(h_r - h_s) \\ & + g(0.5\eta_1^+ - \eta_1^-)]\,dr ds + \frac{1}{4}\beta a_0^{-2}(\Psi_2' j - \psi_2' J + \psi_2 J' - \Psi_2 j' - 2x_1\psi_2' j' - 2x_1\Psi_2' J'). \end{aligned} \tag{77}$$

It is assumed that the integrals in eq. (77) do not generate secular terms. One can consider expression (77) as the approximate bounded solution of 2-D equations of deformable media under conditions (1)–(3) on the surfaces of the layers. The solution is valid for finite layers. If the effect of the interaction of the waves J' and j' is negligible and $X_N^p = X = \eta_1^+ = \eta_1^- = 0$, then eq. (77) reduces to the following expression:

$$\begin{aligned} u_1 = {} & J + j + \Psi_2 + \psi_2 + \Psi_3 + \psi_3 + x_1 d + d_1 - 0.5a_0^{-2}x_1[R_e(J' - j') + a_{tt}(J - j)] \\ & - \frac{1}{4}\beta a_0^{-2} x_1[(J')^2 + (j')^2] + (\beta_1 a_0^{-2}/6 - \beta^2 a_0^{-4}/16)x_1[(J')^3 - (j')^3] + \frac{1}{8}x_1\{\beta^2 a_0^{-4} x_1[J''(J')^2 + j''(j')^2] \\ & - \beta_2 a_0^{-2}[(j')^4 + (J')^4]\} - 0.1\beta_3 a_0^{-2} x_1[(j')^5 + (J')^5] - 0.5\mu a_0^{-1} x_1(j'' - J'') \\ & - 0.5k a_0^{-2} x_1(j''' - J''') + 0.25\iint a_0^{-2}\left[\rho_0^{-1}h^{-1}\tau_{31} + g(h_r - h_s)\right] dr ds - 0.5\beta a_0^{-2} x_1(\psi_2' j' + \Psi_2' J'). \end{aligned} \tag{78}$$

Let us consider a one-sided travelling wave of displacement u_1^-. In this case, $j = 0$ and from eq. (78) we have

$$\begin{aligned} u_1^- = {} & J + d_1 - 0.5a_0^{-2}x_1(R_e J' + a_{tt}J) - \frac{1}{4}x_1\beta a_0^{-2}(J')^2 + \left(\beta_1 a_0^{-2}/6 - \beta^2 a_0^{-4}/16\right)x_1(J')^3 \\ & + \frac{1}{8}x_1^2\beta^2 a_0^{-4} J''(J')^2 - \beta_2 a_0^{-2} x_1(J')^4 - 0.1\beta_3 a_0^{-2} x_1(J')^5. \end{aligned} \tag{79}$$

For simplicity it was assumed that $\Psi_2 = \Psi_3 = 0$ and $\psi_2 = \psi_3 = 0$. We also eliminated some terms in eq. (79). Expression (79) explicitly demonstrates the non-linear effect. Indeed, according to the linear theory $u_1^- = J$ and a seismic wave propagates with an unvarying shape. Because of the non-linear terms in eq. (79), the shape deforms as the coordinate x_1 varies. Harmonics are generated within the wave. For example, if we have at a given point, say $x_1 = 0$, a sinusoidal wave with frequency ω, then, according to eq. (79), harmonics with frequencies 2ω, 3ω, 4ω and 5ω appear in $x_1 > 0$.

The above effect depends strictly on frequency and the mechanical properties of the material. In particular, for earthquake-induced waves in hard rocks the non-linear effects are very small. However, for porous, soft sediments, liquified, gassy and weakly cohesive soils, non-linear terms in eqs (66) and (77)–(79) may be important. The solutions eqs (77) and (78) explicitly include the dependence of wavefields on the dissipative, dispersive and topographic effects. We shall use these solutions to consider different boundary problems in Sections 5 and 6.

3.4 Strongly non-linear waves and transresonant evolution of eq. (45)

We have derived the perturbed wave equation (45) assuming that the non-linear terms are smaller than the linear terms. For example, if a linear term is of order 0.3 then a non-linear term can be of the order of 0.1. Therefore, one might expect that any attempt to study strongly non-linear waves with the help of these equations would fail. However, this is not the case if the same linear terms annihilate each other. As a result, the influence of non-linearity becomes more important than the influence of the linear terms, although every linear term may to be larger than the non-linear terms. In eq. (45) the annihilation takes place if $u_{1,tt} \approx a_0^2 u_{1,11}$.

The perturbation method was also based on the assumption that the non-linear terms are smaller than the linear ones. In particular, the series (79) diverges if the function J is sufficiently large. However, sometimes, we may wish to simulate the generation of strongly non-linear seismic waves.

While the general solution for strongly non-linear seismic waves is unknown, we consider a special solution that can be readily obtained (Galiev 1988; Galiev & Galiev 2001). Let the solution of eq. (45) be the sum or the difference of oppositely travelling localized waves:

$$u_1 = J(r) \pm j(s). \tag{80}$$

In this case, if $\tau_{31} = 0$ and $X_N^p = \eta_1^- = 0$, we have directly from eq. (49) that

$$a_t^{-1} a_{tt}^2 u_{1,t} - \left(a_0^2 - a_t^2\right) u_{1,11} = X - gh_1 + \left(\beta u_{1,1} + \beta_1 u_{1,1}^2 + \beta_2 u_{1,1}^3 + \beta_3 u_{1,1}^4\right) u_{1,11} + \mu u_{1,11t} + k u_{1,1111} + 0.5 g \eta_1^+ . \tag{81}$$

Here $u_1 = u_1(r, s)$. If $a_t^2 = a_0^2$, [see conditions (50)] and $a_{tt} \approx 0$ occur, eq. (81) yields

$$\mu \xi_t + k \xi_{11} = gh - 0.5\beta\xi^2 - \beta_1 \xi^3/3 - \beta_2 \xi^4/4 - \beta_3 \xi^5/5 - \int \left(X + 0.5 g \eta_1^+\right) dx_1 + C(t), \tag{82}$$

where $\xi = u_{1,1}(r, s)$ and $C(t)$ is an arbitrary function. The perturbed wave equation (45) is transformed into non-linear diffusion eqs (81) or (82) (see also Section 8.2). In particular, eq. (82) yields $\mu \xi_t + k \xi_{11} = -0.5\beta\xi^2$. Near resonance the evolution and the interaction of non-linear, dissipative, diffusive and dispersive effects may be very complex (Prigogine 1997). Eq. (82) may be reduced to an algebraic equation with respect to $u_{1,1}$, if $\mu = 0$, $k = 0$, $X = 0$. In this case, if $C(t) = gh_0$ and $\eta_1^+ = 0$, we have

$$g(h - h_0) = 0.5\beta\xi^2 + \beta_1 \xi^3/3 + \beta_2 \xi^4/4 + \beta_3 \xi^5/5. \tag{83}$$

For a flat layer $g(h - h_0) = 0$, then the equation of free non-linear oscillations follows from eq. (83):

$$\beta + 2\beta_1 \xi/3 + \beta_2 \xi^2/2 + 2\beta_3 \xi^3/5 = 0. \tag{84}$$

We have obtained eqs (82)–(84) using eq. (50). However, there is a special case, when $a_t^2 \neq a_0^2$, but $\mu = 0$, $k = 0$, $X = 0$ and $gh_1 \approx 0$. Then we have from eq. (81) the following algebraic equation:

$$a_t^2 - a_0^2 = \beta\xi + \beta_1 \xi^2 + \beta_2 \xi^3 + \beta_3 \xi^4. \tag{85}$$

The results presented in this section may be useful for studying wave evolution in elongated topographies. First the sign in eq. (80) should be chosen so that boundary conditions are satisfied at the ends of the topography. Then the form and the amplitude of the waves are determined from eqs (82), (83), (84) or (85)(82), (83), (84) or (85) (Galiev 1999, 2000; Galiev & Galiev 2001).

3.5 Non-linear, non-linear-topographic and dispersive effects. Solitary and shock waves

Let us assume $j(s) = j = 0$ in eq. (80) and consider non-linear, non-linear-topographic and dispersive effects on the one-sided travelling wave.

(1) Non-linear effect. Let $\beta = \beta_2 = \beta_3 = 0$, then eq. (85) yields $\xi = u_{1,1} = \pm(a_t^2 - a_0^2)^{1/2} \beta_1^{-0.5}$. Using these solutions and eq. (80), we can construct the following discontinuous solution:

$$u_{1,1} = (a_t^2 - a_0^2)^{1/2} \beta_1^{-0.5} \{H[a(t) - x_1] - H[-a(t) + x_1]\}, \tag{86}$$

where H is the Heaviside function, which defines here the travelling shock wave. Solution (86) takes into account the cubic non-linear effect. This solution describes a surface shock wave, since $u_{1,1}$ is proportional to the vertical displacement η.

(2) Non-linear-topographic resonant effect. Let $\beta_1 = \beta_2 = \beta_3 = 0$ in eq. (83). In this case eq. (83) yields $u_{1,1} = \pm[2g(h - h_0)\beta^{-1}]^{1/2}$. Using these solutions and eq. (80) we can construct the following discontinuous resonant solution $u_{1,1} = [2g(h - h_0)\beta^{-1}]^{1/2}\{H[a(t) - x_1] - H[-a(t) + x_1]\}$. For a flat layer we have $u_{1,1} = 0$.

(3) Dispersive non-linear-topographic effect. It is assumed that the non-linear, dissipative and dispersive terms are of the same order and a_0, a_t, β, β_1, β_2, β_3, μ and k are approximately constant. In this case, from eq. (81) we have

$$kJ'''' + \mu a_t J''' - \left[a_t^2 - a_0^2 + \beta J' - \beta_1 (J')^2 + \beta_2 (J')^3 - \beta_3 (J')^4\right] J'' = gh_1 - 0.5 g \eta_1^+ - X. \tag{87}$$

This is the ordinary differential equation for a travelling wave J'. Eq. (87) describes the interaction of non-linear, dissipative, dispersive and topographic effects. We shall consider a variety of particular cases of eq. (87) in Sections 5–7.

Eq. (87) is integrated if $\mu = 0$. Let $X = 0$, $h = h_0$ and $\eta^+ = 0$. In this case eq. (87) yields

$$k^{1/2} \int \left[\left(a_t^2 - a_0^2\right)(J')^2 + \frac{1}{3}\beta (J')^3 - \frac{1}{6}\beta_1 (J')^4 + \frac{1}{10}\beta_2 (J')^5 - \frac{1}{15}\beta_3 (J')^6 + C_1 J' + C_2\right]^{-0.5} dJ' = r + C_3. \tag{88}$$

Here C_1, C_2 and C_3 are arbitrary constants. It is possible to derive different expressions for J' from eq. (88). Let us consider the much studied solitary wave using eq. (88) and assuming that $\beta_1 = \beta_2 = \beta_3 = C_1 = C_2 = C_3 = 0$. Following Remoissenet (1996) and Akhmediev & Ankiewicz (1997), we can write the solitary wave solution

$$u_{1,1} = -J' = 3\beta^{-1}\left(a_t^2 - a_0^2\right)\operatorname{sech}^2\left\{0.5\sqrt{k^{-1}\left(a_t^2 - a_0^2\right)}[a(t) - x_1]\right\}. \tag{89}$$

This solution describes a localized surface wave. Thus, dispersion can transform the shock wave (86) into the solitary wave (89). The shape and size of this wave depend on the difference $a_t^2 - a_0^2$. Solitary waves were first observed in a canal by J. Scott Russell in 1834. The waves travel in a canal for miles without changing form (Lamb 1932). We suggest that an earthquake can generate a similar wave on the surface of liquified layers. The localized waves are known in structural geology (Hunt *et al.* 1997).

Integrating eq. (89) we find that $u_1 = -6\beta^{-1}\sqrt{k(a_t^2 - a_0^2)}\tanh\{0.5\sqrt{k^{-1}(a_t^2 - a_0^2)}[a(t) - x_1]\}$. It is the shock-like solution for the horizontal displacement. The width of the shock (jump) becomes infinitely small if the dispersive coefficient $k \to 0$. The amplitude of u_1 is a function of non-linearity and dispersion.

4 2-D NONLINEAR THEORY FOR COMPRESSIBLE MATERIAL

We have constructed a set of solutions of 1-D equations of the general theory. Below, a 2-D theory of non-linear surface seismic waves is developed and a set of 2-D analytical solutions is presented.

Let us introduce the displacement potential φ and assume that

$$u_1 = \partial\varphi/\partial x_1 = \varphi_1, \quad u_2 = \partial\varphi/\partial x_2 = \varphi_2. \tag{90}$$

For this case, eq. (32) yields

$$\rho^{-1} = \rho_0^{-1}(1 + \eta/h)\left(1 + \nabla^2\varphi + \varphi_{11}\varphi_{22} - \varphi_{12}^2\right). \tag{91}$$

Now using eqs (90) and (91) we transform eqs (29) and (30) into the following form:

$$\varphi_{1tt}(1 + \varphi_{11}) + (\varphi_{2tt} - Y)\varphi_{12} - X_* = -\rho_0^{-1}(1 + \eta/h)\left(1 + \nabla^2\varphi + \varphi_{11}\varphi_{22} - \varphi_{12}^2\right)P_1^*, \tag{92}$$

$$\varphi_{2tt}(1 + \varphi_{22}) + (\varphi_{1tt} - X)\varphi_{21} - Y_* = -\rho_0^{-1}(1 + \eta/h)\left(1 + \nabla^2\varphi + \varphi_{11}\varphi_{22} - \varphi_{12}^2\right)P_1^*, \tag{93}$$

where $X_* = X + \rho_0^{-1}(h^{-1}\tau_{31} + X_N^p) + g(0.5\eta_1^+ - \eta_1^-)$, $Y_* = Y + \rho_0^{-1}(h^{-1}\tau_{32} + Y_N^p) + g(0.5\eta_2^+ - \eta_2^-)$ and

$$P_i^* = \partial\left(P + \frac{2}{3}h^{-1}G\eta - \frac{4}{3}G\nabla^2\varphi\right)\Big/\partial x_i. \tag{94}$$

Let us consider two limiting cases of plane waves when

$$\varphi_1 \approx \varphi_2, \quad \varphi_{11} \approx \varphi_{22}, \quad X_* - \rho_0^{-1}P_1^* \approx Y_* - \rho_0^{-1}P_2^* \quad \text{or} \tag{95}$$

$$\varphi_1 \gg \varphi_2, \quad \varphi_{11} \gg \varphi_{22}, \quad \rho_0 Y_* - P_2^* \approx 0. \tag{96}$$

Thus, it is assumed that $\varphi = \varphi\,[a(t) \pm f(k_1x_1 \pm k_2x_2)]$, where f is an arbitrary function, k_1 and k_2 are arbitrary constants, and $k_1 \approx k_2$ (case 95) or $k_2 \approx 0$ (case 96).

In the case of eq. (95), expressions (92) and (93) yield the same equation:

$$\varphi_{1tt} - X_* = -\rho_0^{-1}(1 + \eta/h)P_1^*. \tag{97}$$

If conditions (96) occur, then the influence of the coordinate x_2 is small and $\varphi_2 = \partial\,\varphi/\partial x_2 \approx 0$. In this case, eq. (92) reduces to eq. (97). Let us rewrite eq. (97) using eq. (94) so that

$$\varphi_{1tt}(1 - \eta h^{-1} + \eta^2h^{-2} + \cdots) - X_* = -\rho_0^{-1}\partial\left(P + \frac{2}{3}h^{-1}G\eta - \frac{4}{3}G\nabla^2\varphi\right)\Big/\partial x_1. \tag{98}$$

Thus, we have an equation of state (23), equation of continuity (91) and eqs (28) and (98) for four unknown functions: ρ, φ, P and η.

4.1 Pressure and vertical displacement

Now, using the iterative method, we find $P - P_0$ and η as functions of φ. It is assumed that X_*, topographic and dispersive effects are of third order with respect to φ. This allows us to take into account the influence of X_*, topographic and dispersive effects in the final expression for $P - P_0$ and η.

As a first approximation, from eq. (98) we find

$$P - P_0 \approx -\rho_0\varphi_{tt} - \frac{2}{3}h^{-1}G\eta + \frac{4}{3}G\nabla^2\varphi. \tag{99}$$

Now taking into account eqs (33) and (99), one can write

$$\eta \approx A^*\left(2GB_*^{-2} - \rho_0\right)\varphi_{tt}. \tag{100}$$

We assume that

$$A^* = (g\rho_0 + 2h^{-1}G)^{-1}. \tag{101}$$

In eq. (100) we have used the linear relation

$$\nabla^2\varphi \approx B_*^{-2}\varphi_{tt}, \tag{102}$$

where B_* will be defined in Section 4.2. Now we can take into account the quadratic terms. In this case, eqs (98) and (100) yield

$$\varphi_{1tt}(1 + 2a_1\varphi_{tt}) = -\rho_0^{-1}\partial\left(P + \frac{2}{3}h^{-1}G\eta - \frac{4}{3}G\nabla^2\varphi\right)\Big/\partial x_1, \tag{103}$$

where $a_1 = 0.5A^*\,h^{-1}(\rho_0 - 2B_*^{-2}G)$. Integrating eq. (103), we obtain

$$P - P_0 \approx -\rho_0\varphi_{tt}(1 + a_1\varphi_{tt}) - \frac{2}{3}h^{-1}G\eta + \frac{4}{3}G\nabla^2\varphi. \tag{104}$$

Then using eqs (33) and (104) we find that

$$\eta \approx A^*[2G\nabla^2\varphi - \rho_0\varphi_{tt}(1 + a_1\varphi_{tt})]. \tag{105}$$

Now the pressure $P - P_0$ and η may be calculated by taking into account the third-order terms. First we rewrite eq. (98) using eqs (100) and (105):

$$\varphi_{1tt}[1 - 2h^{-1}A^*G\nabla^2\varphi + h^{-1}\rho_0A^*(1 + a_1\varphi_{tt})\varphi_{tt} + h^{-2}(A^*)^2(2GB_*^{-2} - \rho_0)\varphi_{tt}^2] - X_* = -\rho_0^{-1}\partial\left(P + \frac{2}{3}h^{-1}G\eta - \frac{4}{3}G\nabla^2\varphi\right)\Big/\partial x_1. \tag{106}$$

Integrating this equation we use the following relation:

$$\nabla^2\varphi \approx B_*^{-2}(\varphi_{tt} - \beta^*B_*^{-4}\varphi_{tt}^2), \tag{107}$$

where β^* will be determined in Section 4.2. As a result, one can find that

$$\varphi_{1tt}(1 + 2a_1\varphi_{tt} + 3a_2\varphi_{tt}^2) - X_* = -\rho_0^{-1}\partial\left(P + \frac{2}{3}h^{-1}G\eta - \frac{4}{3}G\nabla^2\varphi\right)\Big/\partial x_1. \tag{108}$$

Integration of eq. (108) yields

$$P - P_0 = -\rho_0\varphi_{tt}(1 + a_1\varphi_{tt} + a_2\varphi_{tt}^2) - \frac{2}{3}h^{-1}G\eta + \frac{4}{3}G\nabla^2\varphi + \rho_0\int X_*\,dx_1, \tag{109}$$

where $a_2 = A^*[2h^{-1}\beta^*B_*^{-6}G - A^*h^{-2}(1.5\rho_0 - 2B_*^{-2}G)(2B_*^{-2}G - \rho_0)]/3$. The final expression for η is determined from eqs (33) and (109),

$$\eta = A^*\left[2G\nabla^2\varphi - \rho_0\varphi_{tt}(1 + a_1\varphi_{tt} + a_2\varphi_{tt}^2) + \rho_0\int X_*\,dx_1 - \frac{1}{3}hA^*(B_*^2\rho_0 - G)(2G - \rho_0B_*^2)\nabla^4\varphi - \rho_0g(h - h_0)\right]. \tag{110}$$

Now one can find $P - P_0$ from eqs (109) and (100) as a function of φ:

$$P - P_0 = \rho_0\left(\frac{2}{3}h^{-1}GA^* - 1\right)\left(\varphi_{tt} + a_1\varphi_{tt}^2 + a_2\varphi_{tt}^3 - \int X_*\,dx_1\right) + \frac{4}{3}(1 - h^{-1}GA^*)G\nabla^2\varphi$$
$$+ \frac{2}{9}G(A^*)^2(B_*^2\rho_0 - G)(2G - \rho_0B_*^2)\nabla^4\varphi + \frac{2}{3}g\rho_0h^{-1}GA^*(h - h_0). \tag{111}$$

4.2 Governing equation

The equation of state (23) and continuity eq. (91) may be reduced to the following form:

$$\eta + (\eta + h)\nabla^2\varphi \approx -hb(P - P_0) + h\phi_0P_0^{-2}(P - P_0)^2 - h\phi_0P_0^{-3}(P - P_0)^3. \tag{112}$$

Let us substitute in the last equation expressions (110) and (111). Then, after some algebra, one can find the following perturbed wave equation:

$$\varphi_{tt} - a_*^2\nabla^2\varphi = \mu^*\nabla^2\varphi_t + k^*\nabla^4\varphi + I_* - g_*(h - h_0) + \beta^*(\nabla^2\varphi)^2 + \beta_1^*(\nabla^2\varphi)^3, \tag{113}$$

where

$$a_*^2 = Z^{-1}[h + 2E_1G_* + 4bh(1 - h^{-1}E_1G_*)G_*/3], \tag{114}$$

$$\beta^* = -Z^{-1}\left[bCh\rho_0a_1B_*^4 + hC_1\phi_0P_0^{-2}B_*^2\left(\rho_0CB_*^2 - \frac{8}{3}G_*C^*\right) + \rho_0a_1E_1B_*^4 - 2E_1G_* + \rho_0E_1B_*^2\right], \tag{115}$$

$$\beta_1^* = -Z^{-1}\left\{h\phi_0P_0^{-3}\left(C\rho_0B_*^2 - \frac{4}{3}C^*G_*\right)^3 + h\phi_0\rho_0CP_0^{-2}\left[2\rho_0\beta^*CB_*^2 - \frac{8}{3}\beta^*C^*G_* + 2a_1a_*^4\left(\rho_0CB_*^2 - \frac{4}{3}C^*G_*\right)\right]\right.$$
$$\left. + Cbh\rho_0(2\beta^*a_1B_*^2 + a_2B_*^6) + \rho_0E_1B_*^2(2\beta^*a_1 + a_2B_*^4) + \rho_0E_1(\beta^* + a_1B_*^4)\right\}, \tag{116}$$

$$\mu^* = Z^{-1}\eta^*(1-\alpha_\nu\phi_0)E_1\left\{2+\rho_0 B_*^2\left[\frac{2}{3}b\left(1-2h^{-1}E_1G_*\right)+2h^{-1}E_1\right]-4h^{-1}E_1G_*+4bh(E_1^{-1}-h^{-1}G_*)-\frac{4}{3}bG_*\left(1-2h^{-1}E_1G_*\right)\right\}, \tag{117}$$

$$k^* = \frac{1}{3}h\rho_0 B_*^2 Z^{-1}E_1^2\left(\frac{2}{3}bG_*-1\right)(2G_*B_*^{-2}-\rho_0)(B_*^2-\rho_0^{-1}G_*), \tag{118}$$

$$I_* = \rho_0 Z^{-1}(1+bhC)\int X_*\,dx_1, \tag{119}$$

$$g_* = g\rho_0 E_1 Z^{-1}\left(1-\frac{2}{3}bG_*\right). \tag{120}$$

Here we used the following notation:

$$Z = hb\rho_0+\rho_0E_1-\frac{2}{3}b\rho_0E_1G_*, \tag{121}$$

$$E_1 = (g\rho_0+2h^{-1}G_*)^{-1}, \quad C^* = 1-h^{-1}E_1G_*, \tag{122}$$

$$C = 1-2h^{-1}E_1G_*/3, \quad a_1 = 0.5h^{-1}E_1(\rho_0-2G_*B_*^{-2}), \tag{123}$$

$$a_2 = 2\beta^*h^{-1}E_1G_*B_*^{-6}-h^{-2}E_1^2(2G_*B_*^{-2}-\rho_0)(1.5\rho_0-2G_*B_*^{-2})/3. \tag{124}$$

It is assumed that $B_* = a_*(h_0, t)$.

Eq. (113) may be approximately rewritten for η. Considering eqs (100) and (102)

$$\nabla^2\varphi \approx b_0\eta, \tag{125}$$

where $b_0 = E_1^{-1}(2G^*-\rho_0B_*^2)^{-1}$, we find from eq. (113) that

$$\eta_{tt}-a_*^2\nabla^2\eta = \mu^*\nabla^2\eta_t+k^*\nabla^4\eta+b_0^{-1}\nabla^2I_*-g_*b_0^{-1}\nabla^2h+b_0\beta^*\nabla^2\eta^2+b_0^2\beta_1^*\nabla^2\eta^3. \tag{126}$$

Eqs (113) and (126) generalize the 1-D model suggested in Section 3. These equations describe approximately the propagation of the waves. In particular, we used approximate conditions (95) or (96). At the same time, the equations describe a wide spectrum of plane waves in different media and elongated bodies. Indeed, we took into account the strength, compressibility and viscous properties of media. In particular, in eqs (113) and (126) the dispersive terms depend on the effective shear modulus G_*. In addition, these equations take into account both underlying and overlying topographies as well as the porosity of the surface material. The variation of porosity is determined by the expression (22): $\phi = P_0\phi_0P^{-1}$.

4.2.1 Limiting expressions for a_* and the thickness effect on a_*

The expression for the local wave speed a_*, eq. (114), is complicated. However, there are cases when it can be simplified.

(1) Let $h\to\infty$ (see also Section 3.1), then we have the speed of elastic waves in the infinite space:

$$a_*^2 = [\rho_0\lambda(1-\phi_0)+\rho_0\phi_0P_0^{-1}]^{-1}+\frac{4}{3}\nu\rho_0^{-1}(1-\alpha_s\phi_0). \tag{127}$$

(2) Let $g=0$, then

$$a_*^2 = 4\nu\rho_0^{-1}\left\{3+\nu\left[\lambda(1-\phi_0)+\phi_0P_0^{-1}\right]\right\}\left\{3+4\nu\left[\lambda(1-\phi_0)+\phi_0P_0^{-1}\right]\right\}^{-1}. \tag{128}$$

If $\phi_0=0$, expression (128) determines the velocity of longitudinal waves in plates (Kolsky 1953). For compressible liquified materials $\nu\approx 0$ and $a_*^2 = 4\nu\rho_0^{-1}$.

(3) Let us consider an incompressible material ($\lambda=0$). In this case, if $\phi_0P_0^{-1}\to 0$,

$$a_*^2 = gh+4\nu\rho_0^{-1}(1-\alpha_s\phi_0). \tag{129}$$

If $\phi_0\to 0$, then from eq. (129) we have $a_*^2 = gh+4\nu\rho_0^{-1}$.

(4) If $\alpha_s\phi_0\to 1$ in eq. (129), then we have liquified media and $a_*^2 = gh$.

From eqs (114) and (127)–(129) it follows that the velocity a_* depends on the thickness of the layer. This dependence is interesting for rock-like geomaterials. However, it is more important for weakly cohesive soils, liquefiable soils and soft materials. For example, for very soft muddy sediments and gassy and liquified soils, the shear velocity is of the order of 10 m s^{-1}. In these cases we can have in eq. (129) that $gh > 4\nu\rho_0^{-1}(1-\alpha_s\phi_0)$. Mexico City clay has a shear velocity close to 80 m s^{-1} (Singh *et al.* 1988). During the 1985 September 19 Michoacan earthquake, the greatest damage occurred there where a layer thickness changes from 38 to 50 m and $(gh)^{1/2}\approx 20$ m s^{-1}. Thus the effect of thickness may be important for surface seismic waves. On the other hand, from eqs (114) and (127)–(129) it follows that the effect of porosity and the vertical acceleration ($g = g_0+g_d(t)$) may be also important.

4.2.2 Limiting cases of eqs (113) and (126)

It is assumed for liquified layers that $\alpha_s\phi_0 \approx 1$, $\lambda = 0$ and $\eta^* = 0$. The coefficients containing ϕ_0 are often very small. In this case, eq. (113) yields

$$\varphi_{tt} - gh\nabla^2\varphi = \frac{1}{3}gh^3\nabla^4\varphi - g(h-h_0) - 1.5gh(\nabla^2\varphi)^2 + 2gh(\nabla^2\varphi)^3. \tag{130}$$

For simplicity we eliminated I_* from eq. (130). We can expect that eq. (130) describes shallow waves in water. Indeed, since eq. (125) holds, from eq. (130) we have

$$\eta_{tt} - gh_0\nabla^2\eta = \frac{1}{3}h_0^2\nabla^2\eta_{tt} + 1.5g\nabla^2\eta^2 + 2gh_0^{-1}\nabla^2\eta^3. \tag{131}$$

If the cubic term is negligible, eq. (131) coincides with eq. (4.3) from Beji & Nadaoka (1997) for 2-D water waves.

For the 1-D case, eq. (130) yields

$$u_{1,tt} - gh_0u_{1,11} = \frac{1}{3}gh_0^3u_{1,1111} - 3gh_0u_{1,1}u_{1,11} + 6gh_0u_{1,11}u_{1,1}^2, \tag{132}$$

since $u_1 = \partial\varphi/\partial x_1$ (90). Eq. (132) may be considered as a modified form of the Airy equation (see also eq. 46). From another perspective, this equation may be regarded as the Boussinesq-type equation written using the Lagrangian coordinate system (Galiev 2000a).

4.3 General wave solution for plane waves

Eq. (113) is the 2-D analogue of the 1-D equation (45) that was studied using the perturbation method. Therefore, the solution of eq. (113) will be constructed by the method developed in Section 3.3. Let us introduce new variables:

$$r = k_{12}a(t) - k_1x_1 - k_2x_2,\ s = k_{12}a(t) + k_1x_1 + k_2x_2. \tag{133}$$

Here k_1, k_2 and k_{12} are arbitrary constants. It follows that

$$\partial^2\varphi/\partial x_i^2 = k_i^2(\varphi_{rr} - 2\varphi_{rs} + \varphi_{ss}), \qquad \varphi_{tt} = k_{12}^2a_t^2(\varphi_{rr} + 2\varphi_{rs} + \varphi_{ss}) + k_{12}a_{tt}(\varphi_r + \varphi_s), \tag{134}$$

$$\nabla^2\varphi_t = k_{12}a_t\left(k_1^2 + k_2^2\right)(\varphi_{rrr} - \varphi_{rrs} - \varphi_{rss} + \varphi_{sss}), \tag{135}$$

$$\nabla^4\varphi = \left(k_1^2 + k_2^2\right)^2(\varphi_{rrrr} - 4\varphi_{rrrs} + 6\varphi_{rrss} - 4\varphi_{rsss} + \varphi_{ssss}). \tag{136}$$

We consider plane waves for which $k_1 \approx k_2$ or $k_1 \gg k_2$ (see conditions 95 and 96).

Eq. (113) may be rewritten as

$$\begin{aligned}[k_{12}^2a_t^2 - a_*^2\left(k_1^2 + k_2^2\right)](\varphi_{rr} + \varphi_{ss}) + k_{12}a_{tt}(\varphi_r + \varphi_s) + 2[k_{12}^2a_t^2 + a_*^2\left(k_1^2 + k_2^2\right)]\varphi_{rs}\\ = -g_*(h-h_0) + I_* + \beta^*\left(k_1^2 + k_2^2\right)^2(\varphi_{rr} - 2\varphi_{rs} + \varphi_{ss})^2 + \beta_1^*\left(k_1^2 + k_2^2\right)^3(\varphi_{rr} - 2\varphi_{rs} + \varphi_{ss})^3\\ + \mu^*k_{12}a_t\left(k_1^2 + k_2^2\right)(\varphi_{rrr} - \varphi_{rrs} - \varphi_{rss} + \varphi_{sss}) + k^*\left(k_1^2 + k_2^2\right)^2(\varphi_{rrrr} - 4\varphi_{rrrs} + 6\varphi_{rsrs} - 4\varphi_{rsss} + \varphi_{ssss}).\end{aligned} \tag{137}$$

Let $\varphi_{rs} = 0$ and $a_*^2 > k_{12}^2a_t^2(k_1^2 + k_2^2)^{-1}$. Then eq. (137) yields the following non-linear diffusion-type equation:

$$a_{tt}a_t^{-1}\varphi_t - [a_*^2 - k_{12}^2a_t^2\left(k_1^2 + k_2^2\right)^{-1}]\nabla^2\varphi = \mu^*\nabla^2\varphi_t + k^*\nabla^4\varphi + I_* - g_*(h-h_0) + \beta^*(\nabla^2\varphi)^2 + \beta_1^*(\nabla^2\varphi)^3. \tag{138}$$

We assume site resonant conditions

$$|R_e| \ll 1, \quad |a_{tt}| \ll 1, \quad \varphi_{rs} \approx 0, \tag{139}$$

where a transresonant parameter $R_e = k_{12}^2a_t^2 - a_*^2(k_1^2 + k_2^2)$ depends weakly on x_1, x_2 and t: $(R_e)_1 \approx 0$, $(R_e)_2 \approx 0$ and $(R_e)_t \approx 0$. We have the exact resonance if $R_e = 0$. Conditions (139) and the left-hand side of eq. (137) yield

$$\varphi_{tt} - a_*^2\nabla^2\varphi = R_e(\varphi_{rr} + \varphi_{ss}) + k_{12}a_{tt}(\varphi_r + \varphi_s) + 2(2a_t^2k_t^2 - R_e)\varphi_{rs} \approx 0. \tag{140}$$

In Section 3.3 relations similar to eq. (137) and conditions (139) were used. We take this circumstance into account here. The solution of eq. (137) is sought with the aid of the perturbation method:

$$\varphi = \varphi^{(1)} + \varphi^{(2)} + \varphi^{(3)} + \cdots, \tag{141}$$

where $\varphi^{(1)} \gg \varphi^{(2)} \gg \varphi^{(3)}$. We assume that at the resonance the amplitude of the waves becomes significantly larger than the amplitude of the forcing oscillations. Substituting the sum (141) into eqs (137), (140) and equating terms of the same order, we obtain the following linear differential equations:

$$\varphi_{rs}^{(1)} = 0, \tag{142}$$

$$4a_*^2\left(k_1^2 + k_2^2\right)\varphi_{rs}^{(2)} = -R_e[\varphi_{rr}^{(1)} + 2\varphi_{rs}^{(1)} + \varphi_{ss}^{(1)}] - k_{12}a_{tt}[\varphi_r^{(1)} + \varphi_s^{(1)}] + \beta^*\left(k_1^2 + k_2^2\right)^2\left[\varphi_{rr}^{(1)} - 2\varphi_{rs}^{(1)} + \varphi_{ss}^{(1)}\right]^2, \tag{143}$$

$$4a_*^2\left(k_1^2+k_2^2\right)\varphi_{rs}^{(3)} = -R_{\rm e}\left[\varphi_{rr}^{(2)}+2\varphi_{rs}^{(2)}+\varphi_{ss}^{(2)}\right]-k_{12}a_{tt}\left[\varphi_r^{(2)}+\varphi_s^{(2)}\right]$$
$$-g_*(h-h_0)+I_*+2\beta^*\left(k_1^2+k_2^2\right)^2\left[\varphi_{rr}^{(1)}-2\varphi_{rs}^{(1)}+\varphi_{ss}^{(1)}\right]\left[\varphi_{rr}^{(2)}-2\varphi_{rs}^{(2)}+\varphi_{ss}^{(2)}\right]^2$$
$$+\beta_1^*\left(k_1^2+k_2^2\right)^3\left[\varphi_{rr}^{(1)}+\varphi_{ss}^{(1)}\right]^3+\mu^*k_{12}a_t\left(k_1^2+k_2^2\right)\left[\varphi_{rrr}^{(1)}-\varphi_{rrs}^{(1)}-\varphi_{rss}^{(1)}+\varphi_{sss}^{(1)}\right]$$
$$+k^*\left(k_1^2+k_2^2\right)^2\left[\varphi_{rrrr}^{(1)}-4\varphi_{rrrs}^{(1)}+6\varphi_{rrss}^{(1)}-4\varphi_{rsss}^{(1)}+\varphi_{ssss}^{(1)}\right]. \tag{144}$$

Let the approximate solution of eq. (142) be

$$\varphi^{(1)} = J(r)+j(s). \tag{145}$$

Solution (145) resembles the d'Alembert-type solution, but here the velocity of waves $J(k_{12}a-k_1x_1-k_2x_2)$ and $j(k_{12}a+k_1x_1+k_2x_2)$ can be variable. Then, following Section 3.3, we assume that $a_{tt}[\varphi_r^{(1)}+\varphi_s^{(1)}]\approx 0$, and $R_{\rm e}$, $\beta^*a_*^{-2}\left(k_1^2+k_2^2\right)$, $\beta_1^*a_*^{-2}\left(k_1^2+k_2^2\right)^2$, $\mu^*k_{12}a_ta_*^{-2}$, $k^*a_*^{-2}\left(k_1^2+k_2^2\right)$ are approximately constant.

Now we correct solution (145) taking into account $\varphi^{(2)}$ and $\varphi^{(3)}$. Substituting eq. (145) into eq. (143), after integrating, we find

$$\varphi^{(2)} = J_2(r)+j_2(s)-0.25a_*^{-2}\left(k_1^2+k_2^2\right)^{-1}[R_{\rm e}(sJ'+rj')+k_{12}a_{tt}(sJ+rj)]$$
$$+0.25\beta^*a_*^{-2}\left(k_1^2+k_2^2\right)\left[s\int (J'')^2\,dr+2J'j'+r\int (j'')^2\,ds\right]+d(k_1x_1+k_2x_2)+d_1. \tag{146}$$

Expressions (145) and (146) are substituted in eq. (144). For simplicity it is assumed that $R_{\rm e}\approx 0$. Then, following Section 3.3, we find $\varphi^{(3)}$. Solution (141) is written using the expressions for $\varphi^{(i)}(i=1,2,3)$:

$$\varphi = J+j+J_2(r)+j_2(s)+d(k_1x_1+k_2x_2)+d_1+J_3(r)+j_3(s)-0.25a_*^{-2}\left(k_1^2+k_2^2\right)^{-1}[s(R_{\rm e}J'+k_{12}a_{tt}J)+r(R_{\rm e}j'+k_{12}a_{tt}j)]$$
$$+\frac{1}{4}\beta^*a_*^{-2}\left(k_1^2+k_2^2\right)\left[s\int (J'')^2\,dr+2J'j'+r\int (j'')^2ds\right]+\frac{1}{24}(\beta^*)^2a_*^{-4}\left(k_1^2+k_2^2\right)^2[s^2(J'')^3-r^2(j'')^3]$$
$$+\frac{1}{4}a_*^{-2}\left(k_1^2+k_2^2\right)^2\left[\beta_1^*-(\beta^*)^2a_*^{-2}\right]\left[s\int (J'')^3\,dr+r\int (j'')^3ds\right]$$
$$+\frac{1}{4}\mu^*a_*^{-1}\left(k_1^2+k_2^2\right)^{1/2}(sJ''+rj'')+\frac{1}{4}k^*a_*^{-2}\left(k_1^2+k_2^2\right)(sJ'''+rj''')-I^*, \tag{147}$$

where $I^*=0.25k_{12}^{-2}\iint a_*^{-2}[g_*(h-h_0)-I_*]\,drds$, and neglecting the third-order terms in eq. (147), which took into account interaction of the waves J, $J_2(r)$ and j, $j_2(s)$. The solution (147) is the approximate general solution of the equations of deformable media for certain plane waves (see conditions 95 and 96).

4.3.1 Bounded solution

Expression (147) contains the secular terms if $a=a_0t$. Following Section 3.3.1 we can eliminate these terms (Galiev 1999a). In particular, the expression (146) is rewritten so that

$$\varphi^{(2)} = \Psi_2(r)+\psi_2(j)-0.25a_*^{-2}\left(k_1^2+k_2^2\right)^{-1}(s-r)[R_{\rm e}(J'-j')+k_{12}a_{tt}(J-j)]$$
$$+0.25\beta^*a_*^{-2}\left(k_1^2+k_2^2\right)\left[(s-r)\int (J'')^2\,dr+2J'j'+(r-s)\int (j'')^2ds\right]+d(k_1x_1+k_2x_2)+d_1. \tag{148}$$

Expressions (145) and (148) are substituted in eq. (144). Then, after integrating eq. (144), we obtain

$$\varphi^{(3)} = J_3(r)+j_3(j)+\frac{1}{12}(\beta^*)^2a_*^{-4}\left(k_1^2+k_2^2\right)^2\iint (s-r)\left\{[(J'')^3]'-[(j'')^3]'\right\}drds$$
$$+0.25a_*^{-2}\left(k_1^2+k_2^2\right)^2\left[\beta_1^*-(\beta^*)^2a_*^{-2}\right]\left[s\int (J'')^3\,dr+r\int (j'')^3\,dr\right]$$
$$+0.25\mu^*a_*^{-1}\left(k_1^2+k_2^2\right)^{1/2}(sJ''+rj'')+0.25k^*a_*^{-2}\left(k_1^2+k_2^2\right)(sJ'''+rj''')-I^*, \tag{149}$$

neglecting the third-order terms in eq. (149), which took into account interaction of the waves J, $\Psi_2(r)$ and j, $\psi_2(s)$. The double integral in eq. (149) is calculated according to eq. (70). Then, using $J_3(r)$ and $j_3(j)$, we eliminate the singular terms. In particular, it was assumed that

$$J_3(r) = \frac{1}{24}(\beta^*)^2a_*^{-4}\left(k_1^2+k_2^2\right)^2r^2(J'')^3-0.25a_*^{-2}\left(k_1^2+k_2^2\right)^2r\left[\beta_1^*-\frac{2}{3}(\beta^*)^2a_*^{-2}\right]\int (J'')^3\,dr$$
$$-0.25\mu^*a_*^{-1}\left(k_1^2+k_2^2\right)^{1/2}rJ''-0.25ka_*^{-2}\left(k_1^2+k_2^2\right)rJ'''+\Psi_3(r). \tag{150}$$

The expression for $j_3(s)$ is similar to eq. (150). We assume in eq. (149) that the integral I^* does not generate the singular terms. As a result, the secular terms in eq. (149) are eliminated. The final bounded solution is

$$\varphi = J + j + \Psi_2(r) + \psi_2(s) + \Psi_3(r) + \psi_3(s) + d(k_1x_1 + k_2x_2) + d_1 + I^* + 0.5\beta^* a_*^{-2}\left(k_1^2 + k_2^2\right)J'j'$$
$$-0.5a_*^{-2}\left(k_1^2 + k_2^2\right)^{-1}(k_1x_1 + k_2x_2)[R_e(J' - j') + k_{12}a_{tt}(J - j)]$$
$$+ \frac{1}{6}(\beta^*)^2 a_*^{-4}\left(k_1^2 + k_2^2\right)^2(k_1x_1 + k_2x_2)^2[(J'')^3 + (j'')^3] + 0.5a_*^{-2}\left(k_1^2 + k_2^2\right)(k_1x_1 + k_2x_2)\left\{\beta^*\left[\int (J'')^2\,dr - \int (j'')^2 ds\right]\right.$$
$$\left. + \mu a_*\left(k_1^2 + k_2^2\right)^{-0.5}(J'' - j'') + k(J'''' - j'''') + \left(k_1^2 + k_2^2\right)\left[\beta_1^* - \frac{2}{3}(\beta^*)^2 a_*^{-2}\right]\left[\int (J'')^3\,dr - \int (j'')^3\,ds\right]\right\}. \quad (151)$$

The expression (151) may be considered as a particular case of eq. (147).

4.4 2-D strongly non-linear waves and the transresonant evolution of eq. (113)

Approximate solutions of eq. (113) were constructed. This equation also has other solutions. Some new resonant solutions may be found following Sections 3.4 and 3.5 without using the perturbation method.

There are solutions of the equation that can be obtained by requiring that

$$I_* = f_*(r), \quad \varphi = F(r), \quad (152)$$

where

$$r = a_0k_{12}t - k_1x_1 - k_2x_2 \quad (153)$$

and $f_* = f_*(r)$ is a travelling seismic wave. In this case, eq. (113) reduces to an ordinary differential equation in r, so

$$\left[k_{12}^2a_0^2 - a_*^2\left(k_1^2 + k_2^2\right)\right]F'' = f_* - g_*(h - h_0) + \mu^* a_t\left(k_1^2 + k_2^2\right)F'''' + k^*\left(k_1^2 + k_2^2\right)^2F'''''' + \beta^*\left[\left(k_1^2 + k_2^2\right)F''\right]^2 + \beta_1^*\left[\left(k_1^2 + k_2^2\right)F''\right]^3. \quad (154)$$

The solution of this equation for a linear, inviscid and non-dispersive medium is

$$F'' = [f_* - g_*(h - h_0)]\left[k_{12}^2a_0^2 - a_*^2\left(k_1^2 + k_2^2\right)\right]^{-1}. \quad (155)$$

Taking into account eqs (125) and (152) we find the vertical displacement

$$\eta = b_0^{-1}[f_* - g_*(h - h_0)]\left[k_{12}^2a_0^2\left(k_1^2 + k_2^2\right)^{-1} - a_*^2\right]^{-1}. \quad (156)$$

The 1-D case of solution (156) was considered by Lamb (1932, p. 264). Solution (156) has a singularity when

$$k_{12}^2a_0^2 = a_*^2\left(k_1^2 + k_2^2\right). \quad (157)$$

Thus, solution (156) is not valid and we must take into account non-linear effects when the resonant condition (157) occurs. Let us take into account the quadratic term in eq. (154). In this case, eq. (154) has two resonant solutions:

$$F'' = \pm(\beta^*)^{-0.5}\left(k_1^2 + k_2^2\right)^{-1}[g_*(h - h_0) - f_*]^{1/2}. \quad (158)$$

Using these solutions, we can construct the following discontinuous solution:

$$\eta = b_0^{-1}(\beta^*)^{-0.5}[g_*(h - h_0) - f_*]^{1/2}[H(a_0k_{12}t - k_1x_1 - k_2x_2) - H(-a_0k_{12}t + k_1x_1 + k_2x_2)]. \quad (159)$$

Thus, the effects of non-linearity and topography may be very strong. Indeed, solutions (156) and (159) are quite different. The full equation (154) may be considered in the transresonant band following Galiev (1999a). He found that shock-, soliton- and oscillon-like resonant waves may be excited in non-linear, dissipative–dispersive systems (see also Section 3.5).

Galiev (1999a) also modelled transresonant oscillations of Tarzana Hill. The results are presented in Fig. 1. There is a large difference between the linear and non-linear models. According to the linear model there is very localized amplification of seismic waves near resonance. At the same time, the non-linear theory predicts strong amplification in the wide transresonant band. Fig. 1 qualitatively explains the observed amplification of seismic waves by non-linear and resonant effects. It would seem that, since peaks of the linear resonances are very narrow, the complex 2-D and 3-D numerical methods (Rial *et al.* 1992; Bouchon & Barker 1996; Rial 1996; Yeh *et al.* 1998) lose these resonances and predict a much lower degree of amplification than was observed. Of course, our analysis is purely qualitative. There are other explanations for the discrepancy between the numerical results and the field observations (Reiter 1990, p. 162).

Topographic and resonant effects can be very complex and highly variable. In particular, the resonant condition (157) may be a function of the relief, since $a_* = a_*(x_1, x_2, t)$. Therefore, the non-linear effect may be very localized and the linear model may be valid everywhere except for specific valleys and mountains.

4.4.1 Condition of common resonance

Thus, the seismic waves depend on the surface relief. Therefore, the condition of resonance should depend on the relief. Eq. (113), which was written for $\varphi = \varphi\,[a(t) \pm f(k_1x_1 \pm k_2x_2)]$, takes into account this dependence, since the coefficients are functions of coordinates (relief). Let

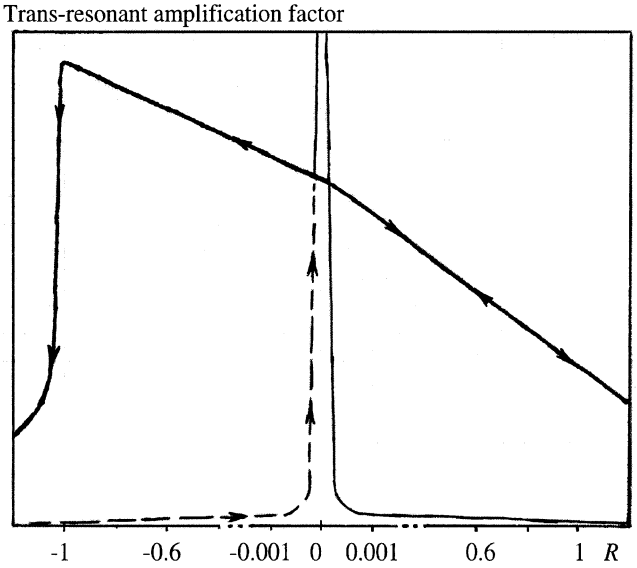

Figure 1. Influence of frequency on linear and non-linear hysteretic responses of an undamped model of Tarzana Hill (- → — → — the frequency increases, → the frequency increases further and ← the frequency decreases).

us rewrite eq. (113) using the following variables, which can explicitly take into account the relief effect

$$r = a(t)k_{12} - k_1(x_1) - k_2(x_2) - K_{12}(x_1, x_2), \quad s = a(t)k_{12} + k_1(x_1) + k_2(x_2) + K_{12}(x_1, x_2), \tag{160}$$

where $k_1(x_1)$, $k_2(x_2)$ and $K_{12}(x_1, x_2)$ are functions, which are determined by the geometry of the relief. As a result, we have that

$$k_{12}a_{tt}(\varphi_r + \varphi_s) + a_*^2(k_{1,11} + K_{12,11} + k_{2,22} + K_{12,22})(\varphi_r - \varphi_s) + \{k_{12}^2 a_t^2 - a_*^2[(k_{1,1} + K_{12,1})^2 + (k_{2,2} + K_{12,2})^2]\}(\varphi_{rr} + \varphi_{ss})$$
$$+ 2\{k_{12}^2 a_t^2 + a_*^2[(k_{1,1} + K_{12,1})^2 + (k_{2,2} + K_{12,2})^2]\}\varphi_{rs} = -g_*(h - h_0) + \beta^*(\nabla^2\varphi)^2 + \beta_1^*(\nabla^2\varphi)^3 + \mu^*\nabla^2\varphi_t + k^*\nabla^4\varphi + I_*. \tag{161}$$

If the earthquake-induced waves are not large ($-g_*(h - h_0) + I_* \approx 0$) and the topographic-resonant effect is weak, then the linearized equation (161) may be used. However, in the remaining cases, we should use the full equation (161). Let us consider critical (resonant) points for which $\varphi_{tt} \approx a_*^2\nabla^2\varphi$ and eq. (161) yields

$$k_{12}a_{tt}(\varphi_r + \varphi_s) + a_*^2(k_{1,11} + K_{12,11} + k_{2,22} + K_{12,22})(\varphi_r - \varphi_s) + \{k_{12}^2 a_t^2 - a_*^2[(k_{1,1} + K_{12,1})^2 + (k_{2,2} + K_{12,2})^2]\}(\varphi_{rr} + \varphi_{ss}) = 0\,, \tag{162}$$

$$\mu^*\Phi_t + k^*\nabla^2\Phi = g_*(h - h_0) - \beta^*\Phi^2 - \beta_1^*\Phi^3 - I_*. \tag{163}$$

We assumed that $\varphi_{rs} \approx 0$ and $\Phi = \nabla^2\varphi\,(r, s)$, where $\nabla^2\varphi\,(r, s) = \partial^2\varphi\,(r, s)/\partial x_1^2 + \partial^2\varphi\,(r, s)/\partial x_2^2$. Thus, the perturbed wave equation (161) is transformed into the non-linear diffusion eq. (163) if the condition of common resonance (162) occurs (Galiev & Galiev 2001). If near the critical points $\varphi_r \approx \varphi_s$, then eq. (162) yields the diffusion equation

$$k_{12}a_{tt}a_t^{-1}\varphi_t - \{a_*^2 - k_{12}^2 a_t^2[(k_{1,1} + K_{12,1})^2 + (k_{2,2} + K_{12,2})^2]^{-1}\}\nabla^2\varphi = 0. \tag{164}$$

If the effects of dissipation and dispersion are small, and $I_* = 0$ in eq. (163), then we have the algebraic equation for $\nabla^2\varphi$: $g_*(h - h_0) = \beta^*(\nabla^2\varphi)^2 + \beta_1^*(\nabla^2\varphi)^3$.

We treat three cases of a simplification of the resonant condition (162).

(1) Let

$$\varphi_r \approx \varphi_s \approx 0, \tag{165}$$

then we have resonance if

$$a_t^2 = k_{12}^{-2}a_*^2[(k_{1,1} + K_{12,1})^2 + (k_{2,2} + K_{12,2})^2]. \tag{166}$$

(2) Let

$$a_{tt} \approx 0, \qquad k_{1,11} \approx 0, \qquad k_{2,22} \approx 0, \qquad K_{12,11} \approx 0, \qquad K_{12,22} \approx 0, \tag{167}$$

then we again have the resonant condition (166).

(3) In the third case, if eq. (165) holds, we have a set of resonant conditions as follows:

$$a_t \approx k_{1,1} \approx k_{2,2} \approx K_{12,1} \approx K_{12,2} \approx 0. \tag{168}$$

Thus, at the resonance the governing equation and motion of seismic waves can change (see also Sections 3.4 and 8.2). Near resonance the complex interaction of non-linear, dissipative, and dispersive effects may be (Prigogine 1997).

5 TOPOGRAPHIC-RESONANT AMPLIFICATION OF WEAKLY NONLINEAR SEISMIC WAVES

The theory has been developed for weakly cohesive materials overlying a rigid bedrock. This theory allows us to estimate the effects of site conditions. As examples of the application of the theory, we consider transresonant non-linear waves in a sediment-filled shallow valley and a small elongated island. The perturbation method developed in Section 3 is used.

5.1 The 1-D resonance of the sediment-filled valley

We can assume approximately that the horizontal displacement of the valley having steep edge slopes is fixed by the rock at the edges. In this case

$$u_1 = 0 \quad (x_1 = 0 \quad \text{and} \quad L), \tag{169}$$

where L is the length of the valley. This boundary problem is similar to those considered by Galiev (1997b, 1998, 1999, 2000a) and Galiev & Galiev (1998). It was found that *unfamiliar* surface waves may be generated in elongated resonators. Therefore, we can expect that anomalous waves may be excited on the surface of the shallow valley.

We assumed that $g = g_0 + g_d$. Let $g_d = \delta\cos\,\omega t$. Here g_d is the earthquake-induced vertical component of the bedrock acceleration. This acceleration, the slope of the valley bottom and the surface relief excite horizontal waves. For these waves, we assume in eq. (47) that $a(t) = a_0 t$.

Perturbations of the sediment thickness (surface relief) may be described by the standard Fourier expansion. Let us assume for the gradient of the thickness that

$$h_1 = \partial h/\partial x_1 = \sum_i H_i \cos i\pi x_1/L \qquad (i = 0, 1, 2, 3, \ldots, I). \tag{170}$$

Following Galiev (1999, 2000a) and Galiev & Galiev (1998) we study first linear and then non-linear oscillations. We do not take into account the influence of relief on the velocity a_0.

5.1.1 Linear oscillations

Considering the linear waves we shall use the inviscid model of the material. Using eq. (78), $g_d = \delta\cos\,\omega t$ and $a(t) = a_0 t$,

$$u_1 = J + j + \delta\cos\omega t \sum_i H_i\left(\omega^2 - i^2\pi^2 a_0^2 L^{-2}\right)^{-1}\cos i\pi x_1/L - g_0\sum_i H_i L^2 i^{-2}\pi^{-2}a_0^{-2}\cos i\pi x_1/L + 0.5x_1 k(J''' - j'''). \tag{171}$$

The boundary condition (169) at $x_1 = 0$ is satisfied if

$$J = F(r) - \varphi_*\cos\omega r + d_*, \quad j = -F(s) - \varphi_*\cos\omega s + d_*, \tag{172}$$

where

$$\varphi_* = 0.5\delta\sum_i H_i[\omega^2 - (\pi i a_0/L)^2]^{-1}, \quad d_* = 0.5g_0 L^2\pi^{-2}a_0^{-2}\sum_i H_i i^{-2}. \tag{173}$$

Now, using the boundary condition at $x_1 = L$

$$F(r) = \frac{\delta\sin\omega a_0^{-1}r}{2\sin\omega L a_0^{-1} + kL\omega^3 a_0^{-3}\cos\omega L a_0^{-1}}\sum_i \frac{H_i[(-1)^i - \cos\omega L a_0^{-1}]}{[\omega^2 - (\pi i a_0/L)^2]^{-1}} - 0.5d_2 L^{-1}r. \tag{174}$$

Here $d_2 = g_0 L^2\pi^{-2}a_0^{-2}\sum_i[(-1)^i - 1]H_i i^{-2}$. Thus, travelling horizontal waves are excited by the vertical excitation and the gradient (170). The resonant frequencies of the layer are approximately $\Omega_{lN} = \Omega_{Nl} + \omega^*$, where $\Omega_{Nl} = N\pi a_0/L$ and $\omega^* = ka_0 L^{-3}\pi^3 N^3(-1)^{N+1}/2$ ($N = 1, 2, 3, \ldots$). If the dispersive coefficient k is very small, we obtain $\Omega_{lN} = \Omega_{Nl}$. Thus, the dispersion shifts the resonant frequencies.

According to eqs (171) and (173) at resonance, if $i = N$, the topographic term can increase considerably. Therefore, we should take into account that the double integral in eq. (78) must be recalculated if $\omega^2 = (\pi\ ia_0/L)^2$ and $i = N$. As a result, instead of eq. (171), we have

$$\begin{aligned} u_1 = {} & J + j + \delta\cos\omega t \sum_{i(i\neq N)} H_i(\omega^2 - i^2\pi^2 a_0^2 L^{-2})^{-1}\cos i\pi x_1/L - \frac{1}{8}\delta\omega^{-1}a_0^{-1}(s\sin\omega a_0^{-1}r + r\sin\omega a_0^{-1}s) \\ & - g_0\sum_i H_i L^2 i^{-2}\pi^{-2}a_0^{-2}\cos i\pi x_1/L + 0.5x_1 k(J''' - j'''). \end{aligned} \tag{175}$$

The topographic term may be limited at the resonance and the boundary condition (169) at $x_1 = 0$ is satisfied if $J = F(r) + \frac{1}{8}\delta\omega^{-1}a_0^{-1}r\sin\omega a_0^{-1}r - \varphi_*\cos\omega r + d_*$, $j = -F(s) + \frac{1}{8}\delta\omega^{-1}a_0^{-1}s\sin\omega a_0^{-1}s - \varphi_*\cos\omega s + d_*$. These expressions are similar to eq. (172). However, here the symbol $\sum_i$, in the expression for φ, eq. (175), must be replaced by $\sum_{i(i\neq N)}$.

5.1.2 Non-linear analysis

Near the resonant frequencies, linear analysis is not valid. Let us consider resonant oscillations neglecting cubic terms and arbitrary functions Ψ_2, ψ_2, Ψ_3 and ψ_3 in eq. (78). In this case, we assume $d_1 = 0$, $a_{tt} \approx 0$ and

$$|F(r)| \gg \varphi_*\cos\omega r - d_*, \quad |F(s)| \gg \varphi_*\cos\omega s - d_*. \tag{176}$$

Then, using eqs (78), (172) and (176), we consider boundary condition (169) at $x_1 = L$. The function $F(s)$ is expanded in a Taylor's series at $x_1 = L$:

$$F(s) = F[r + 2N\pi a_0/\omega + 2\omega^{-1}L(\omega_1 + \omega^*)]$$
$$= F(r) + 2\omega^{-1}L(\omega_1 + \omega^*)F'(r) + 2\omega^{-2}L^2(\omega_1 + \omega^*)^2F''(r) + 4\omega^{-3}L^3(\omega_1 + \omega^*)^3F'''(r)/3 + \cdots,$$

where $\omega = \Omega_{lN} + \omega_1$ and ω_1 is a perturbation of a resonant frequency. It was assumed that $F(r + 2N\pi a_0/\omega) = F(r)$. Then following Galiev (1999) and Galiev & Galiev (1998), the boundary problem is reduced to the perturbed Burgers–Korteweg–de Vries equation written for the travelling wave. This equation is

$$-L[2(\omega_1 + \omega^*)\omega^{-1} + a_0^{-2}R_e]F' + L[a_0^{-1}\mu + h^{-1}\rho_0^{-1}a_0^{-1}\mu_f - 2(\omega_1 + \omega^*)^2L\omega^{-2}]F''$$
$$+ L\left[ka_0^{-2} - \tfrac{4}{3}(\omega_1 + \omega^*)^3L^2\omega^{-3}\right]F''' - 0.5\beta La_0^{-2}(F')^2 = l\cos\omega t - dL, \tag{177}$$

where $l = \delta\sum_i H_i[\omega^2 - (\pi i a_0/L)^2]^{-1}[\cos\omega La_0^{-1} - (-1)^i]$. According to Section 3 (see eq. 45) we approximated the boundary friction as a function $\tau_{31} = \mu_f u_{1,11t}$. At the exact resonance, $\sum_i$ must be replaced by $\sum_{i(i\neq N)}$ in the last expression. Far from the resonance, the acoustic solution follows from eq. (177) (Galiev & Galiev 1998). Let $\mu_* = \mu + h^{-1}\rho_0^{-1}\mu_f - 2a_0\omega^{-2}L(\omega_1 + \omega^*)^2$, $k_* = ka_0^{-2} - 4\omega^{-3}L^2(\omega_1 + \omega^*)^3/3$. Eq. (177) yields

$$(f - 2R_*\pi^{-1}\sqrt{\varepsilon})^2 - \mu_*\omega a_0\beta^{-1}f' - 0.5k_*a_0\omega^2\beta^{-1}f'' = \varepsilon\cos^2\tau + 4\varepsilon\pi^{-2}R_*^2. \tag{178}$$

Here $f = a_0F'(\tau)$, $\varepsilon = -4la_0^4(\beta L)^{-1}$, $R_* = -\pi a_0[0.5R_e + a_0^2(\omega_1 + \omega^*)\omega^{-1}]/\beta\varepsilon^{1/2}$ and $d = l/L$.

We introduced a modified time variable $\tau = \omega t/2$ and $f' = \partial F'/\partial\tau$, where $F' = \partial F/\partial r$. R_* is a transresonant parameter. The resonant band is between $R_* = 1$ and -1 (Chester 1964; Galiev *et al.* 1970; Galiev 1972a, 1988). Linear terms in eq. (178) depend on the frequency of excitation. For example, if $\mu = 2a_0\omega^{-2}L(\omega^* + \omega_1)^2 - h^{-1}\rho_0^{-1}\mu_f$, the viscous term disappears. Then eq. (178) transforms into the perturbed Korteweg–de Vries-type equation written for the travelling wave, and cnoidal waves and solitary waves may be excited. If

$$ka_0^{-2} = 4\omega^{-3}L^2(\omega^* + \omega_1)^3/3,$$

then eq. (178) transforms into the perturbed Burgers-type equation written for the travelling wave and describes continuous shock-like waves. On the other hand, the dissipative effect increases, respectively, the dispersive effect if $h \to 0$. Therefore, the evolution of the wave structure and the amplitude may be very complex within the resonant band. Let us write that

$$f = a_0F'(\tau) = \sqrt{\varepsilon}[2R_*\pi^{-1} + \Phi(\tau)]\cos\tau. \tag{179}$$

The equation for $\Phi(\tau)$ follows from eq. (178):

$$\mu_*\omega a_0\beta^{-1}\Phi' + 0.5k_*a_0\omega^2\beta^{-1}(\Phi'' - \Phi) = -\sqrt{\varepsilon}(1 - \Phi^2)\cos\tau. \tag{180}$$

We assumed that $\sin\tau \approx 0$ (Chester 1964) near the wave front.

5.2 Transresonant evolution of waves. Non-linear, dissipative and dispersive effects

According to eqs (37) and (77) the wave of the vertical displacement $\eta \approx -h(1 - u_{1,1})u_{1,1}$, where $u_{1,1} = -F'(r) - F'(s) + \frac{3}{4}\{[F'(r)]^2 + [F'(s)]^2\} + \frac{3}{2}x_1[F'(r)F''(r) - F'(s)F''(s)]$.

5.2.1 Non-linear effects on the transresonant evolution

For a non-dispersive and inviscid medium, and at the exact resonance ($R_* = 0$) eq. (178) becomes $(a_0F')^2 = \varepsilon\cos^2\omega t/2$. The last equation has two solutions. Using these solutions, the expression for periodic discontinuous resonant waves may be constructed. In the case where $R_* \neq 0$, we have that

$$\eta \approx -ha_0^{-1}\varepsilon^{1/2}\left\{2R_*\pi^{-1} + H[\sin(\xi_- - \Delta_*)]\cos\xi_- + H[\sin(\xi_+ - \Delta_*)]\cos\xi_+\right\}, \tag{181}$$

where H is the Heaviside function, which here determines the pair of waves travelling in opposing directions, since $\xi_\pm = \frac{1}{2}\omega t \pm \frac{1}{2}(\omega a_0^{-1}x_1 - \pi N)$ and $\Delta_* = \arcsin R_*$. N shock-like surface waves are excited according to eq. (181) if $\omega \approx N\pi a_0/L$. These waves travel back and forth in the valley being repeatedly reflected from the edges. The patterns that these shock-like waves yield in the x_1–t-plane are presented in Figs 2 and 3. At the same time, eq. (181) describes cnoidal-like waves if $R_* = \pm 1$. These waves transform into shock-like waves when $|R_*| < 1$ (Chester 1964; Galiev *et al.* 1970). A finite-amplitude wave excited in a medium becomes stronger when the excitation frequency approaches the resonance frequency ($R_* \to 0$).

5.2.2 The effect of frequency on wave structure

We seek a solution of eq. (180) as an asymptotic expansion:

$$\Phi = \Phi_0 + \Phi_1 + \cdots, \tag{182}$$

where $\Phi_0 \gg \Phi_1$. Here Φ_0 takes into account the non-linear and dispersive (or dissipative) effects, Φ_1 takes into account dissipative (or dispersive) effects.

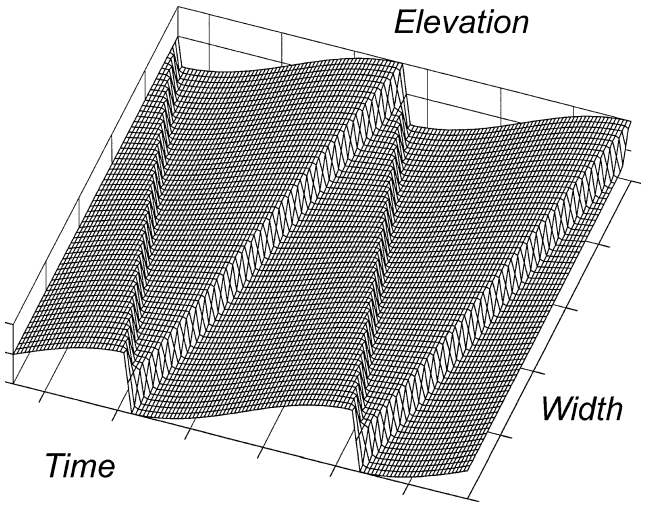

Figure 2. Shock-like resonant seismic wave $\varepsilon^{-0.5}\eta$ travelling to and fro in a valley being repeatedly reflected from the sides ($N = 1$, the fundamental resonance).

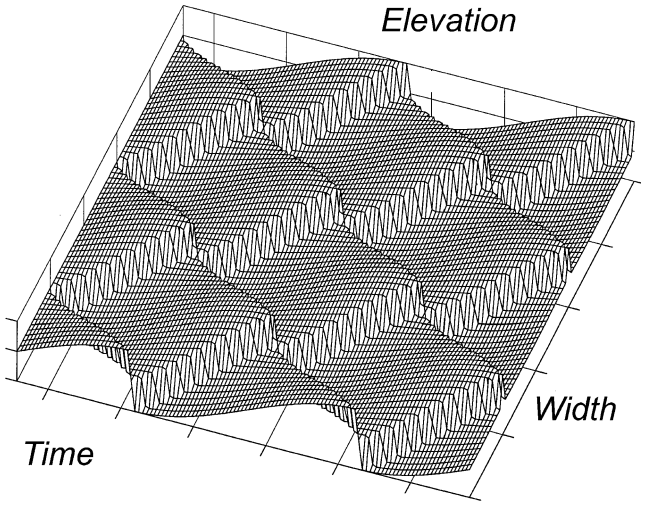

Figure 3. Interaction of the five shock-like resonant seismic waves $\varepsilon^{-0.5}\eta$ travelling to and fro in the valley. At the fifth resonance ($N = 5$) the five shock-like waves are excited.

First, we consider the thin layer ($k \approx 0$) and the frequencies when the dissipative (viscous) effect exceeds the dispersive effect [$(\omega_1 + \omega^*)^3 \approx \frac{3}{4}ka_0^{-2}\omega^3 L^{-2}$ and $k_* \approx 0$]. In this case (Chester 1964), $\Phi_0 = \tanh[2\sqrt{q}(\sin\tau - R_*)]$ and

$$a_0F'(a_0t \pm x_1) \approx 2\varepsilon^{1/2}R_*\pi^{-1} + \varepsilon^{1/2}\tanh[2\sqrt{q}(\sin\xi_\pm - R_*)]\cos\xi_\pm.$$

The period of $F'(a_0t \pm x_1)$ is 4π if $R_* \neq 0$. However, the solution is most conveniently defined as a periodic function with the same period as the earthquake-induced oscillations, namely $2\pi/\omega$ in t. Therefore, we assume that

$$F'(a_0t \pm x_1) \approx \varepsilon^{1/2}a_0^{-1}\{2R_*\pi^{-1} + \tanh[2\sqrt{q}\sin(\xi_\pm - \Delta_*)]\cos\xi_\pm\}, \tag{183}$$

where $\sqrt{q} = -\beta\sqrt{\varepsilon}/2\omega a_0\mu_*$. According to eq. (183) the transresonant surface waves always have a shock structure in weakly viscous systems. The discontinuous solutions are the limit of eq. (183) if $\mu_* \to 0$. On the other hand, a finite-amplitude wave excited in a medium becomes steeper when the excitation frequency approaches the exact resonance (Chester 1964). Using eqs (179)–(183) we find that near the wave front

$$\begin{aligned} a_0F'(a_0t \pm x_1) = {} & 2\varepsilon^{1/2}R_*\pi^{-1} + \varepsilon^{1/2}\tanh[2\sqrt{q}\sin(\xi_\pm - \Delta_*)]\cos\xi_\pm \\ & + \varepsilon^{1/2}q_1\{1 - \tanh^2[2\sqrt{q}\sin(\xi_\pm - \Delta_*)]\}\{\cos\xi_\pm - 2\ln\cosh[2\sqrt{q}\sin(\xi_\pm - \Delta_*)]\}\cos\xi_\pm, \end{aligned} \tag{184}$$

where $q_1 = k_*\beta\varepsilon^{1/2}/2a_0\mu_*^2$ (Galiev & Galiev 1998). According to eq. (184) a soliton-like wave is generated in the shock structure due to weak dispersion. The amplitude of the soliton depends on the competition of the dispersive and dissipative effects. If $(\omega_1 + \omega^*)^2 \approx \frac{1}{2}(\mu + h^{-1}\rho_0^{-1}\mu_f)a_0^{-1}\omega^2 L^{-1}$ then this amplitude increases.

Let us consider the thick layer and frequencies when $\mu_*\omega a_0\beta^{-1}f' \ll 0.5k_*a_0\omega^2\beta^{-1}f''$ in eq. (178).

In this case we have from eqs (182), (180) and (179) the following approximate expression:

$$a_0F'(a_0t \pm x_1) = \varepsilon^{1/2}\{6q_0\gamma^2 \operatorname{sech}^2[\gamma \sin(\xi_\pm - \Delta_*)] + C_{1,2}\}\cos^2\xi_\pm$$
$$- 2\varepsilon^{1/2}\mu_*(k_*\omega)^{-1}\{6q_0\gamma \tanh[\gamma \sin(\xi_\pm - \Delta_*)] + C_{1,2}\sin\xi_\pm\}\cos\xi_\pm, \quad (185)$$

where $q_0 = -k_*a_0\omega^2/2\beta\varepsilon^{1/2}$, $\gamma^2 = 0.5(1 - C_{1,2}/q_0)$ and $C_{1,2} = \frac{4}{3}(q_0 \pm \sqrt{q_0^2 + \frac{3}{4}})$ (Galiev & Galiev 1998). This solution is valid if the dispersive effect exceeds the dissipative (viscous) effect. The soliton-like waves can be generated within the transresonant band. According to eq. (185) within the soliton structure the shock wave may be generated if $\mu_* \neq 0$. Our calculations show that solutions (184) and (186) qualitatively describe experimental (Chester & Bones 1968; Verhagen & Van Wijngaarden 1995) and numerical (Cox & Mortell 1986; Smith 1998) data.

5.2.3 Competition of viscous and dispersive effects. The transresonant evolution of surface waves

Let us consider the case when dissipative and dispersive effects are approximately equal ($\mu_*\omega a_0\beta^{-1}f' \approx 0.5k_*a_0\omega^2\beta^{-1}f''$ in eq. 178). For this case solutions of eq. (178) were constructed by Galiev (1999a). A few scenarios for the competition of the non-linear, dissipative and dispersive effects were considered. Here we write solution (53) from Galiev (1999a):

$$a_0F'(a_0t \pm x_1) = 2\varepsilon^{1/2}R_*\pi^{-1} + A\tanh(e\sin M^{-1}\xi_\pm - eR_*)\cos\xi_\pm - B\tanh^2(e\sin M^{-1}\xi_\pm - eR_*)\cos^2\xi_\pm$$
$$+ B_1\sin^2\omega_k(\xi_\pm - \Delta_*)\cos\xi_\pm H(\cos\xi_\pm - R_*), \quad (186)$$

where A and B are determined by non-linear algebraic equations (Galiev 1999a) and $B_1 = [1 - (A - B)^2 + q_0(A - B)](A - B - 0.5q_0)^{-1}$, $\omega_k^2 = 0.5[(A - B)q_0^{-1} - 0.5]$. Let us rewrite the solution using eq. (184) so as to determine constants A, B and e. As a result, we have near the wave front

$$a_0F'(a_0t \pm x_1) = 2\varepsilon^{1/2}R_*\pi^{-1} + \varepsilon^{1/2}\tanh[2\sqrt{q}\sin(\xi_\pm - \Delta_*)]\cos\xi_\pm - 0.5\varepsilon^{1/2}\{\tanh[2\sqrt{q}\sin(\xi_\pm - \Delta_*)] + 1\}$$
$$\times\{q_1\tanh^2[2\sqrt{q}\sin(\xi_\pm - \Delta_*)] - B_1\sin^2\omega_k(\xi_\pm - \Delta_*)\}\cos\xi_\pm. \quad (187)$$

We used the property that $\cos\xi_\pm \approx 1$ (Chester 1964) near the wave front. The period of function (187) is 4π. I emphasize that solutions (184)–(187) are valid for vertically or horizontally vibrated valleys (Galiev & Galiev 1998).

Let us compare the results of the theory with data from experiments with horizontally excited resonant water waves (Verhagen & Van Wijngaarden 1965; Chester & Bones 1968) using solution (187). One period of the exciting oscillations will be considered. First we examine the amplification of the vertical displacement during the reflection of the wave from the boundary (the wall of the resonator). In Fig. 4, results of calculations according to solution (187) (continuous and dashed curves) are presented. We use the expression (37) for η. The dotted-dashed curve is calculated according to eq. (183).

The dashed and dotted-dashed curves correspond to the experimental curve (measured at the wall) in Fig. 4 from Verhagen & Van Wijngaarden (1965). Following their experiments, we assumed $\omega^* = 0$, $L = 60$ cm, $l = 0.314$ cm, $h = 9$ cm, $N = 1$ and $R_* = 0$. Boundary friction is simulated by taking $h^{-1}\rho_0^{-1}\mu_f = 82$ cm^2 s^{-1}. It is seen that the dispersion (dashed curve) can strongly modify the effects of non-linearity and viscosity (dotted-dashed curve). The continuous curve corresponds to the third experimental curve in Fig. 10 from Chester & Bones (1968) ($\omega^* = 0$, $h^{-1}\rho_0^{-1}\mu_f = 30$ cm^2 s^{-1}, $L = 60$ cm, $l = 0.31$ cm, $h = 5$ cm, $N = 1$ and $R_* = 0$). Fig. 4 shows that solution (187) describes the experimental data.

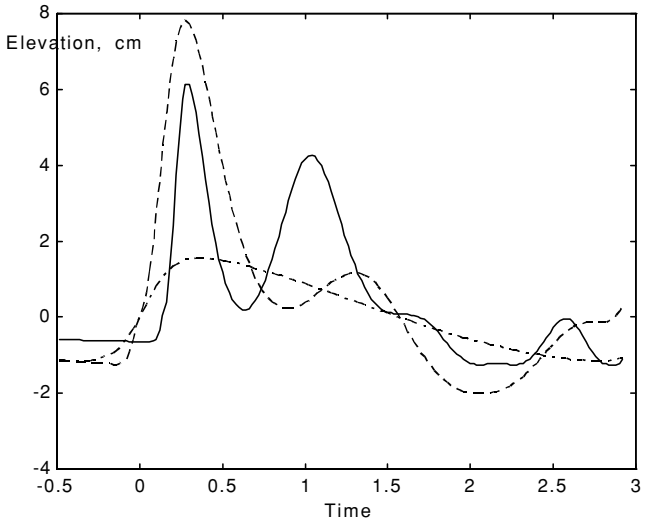

Figure 4. Non-linear amplification of non-linear waves at the side and the shock-structure: dashed and solid lines illustrate the dispersion effect (formation of the soliton-like wave), dot–dash wave illustrates the dissipative effect (formation of the shock-like wave).

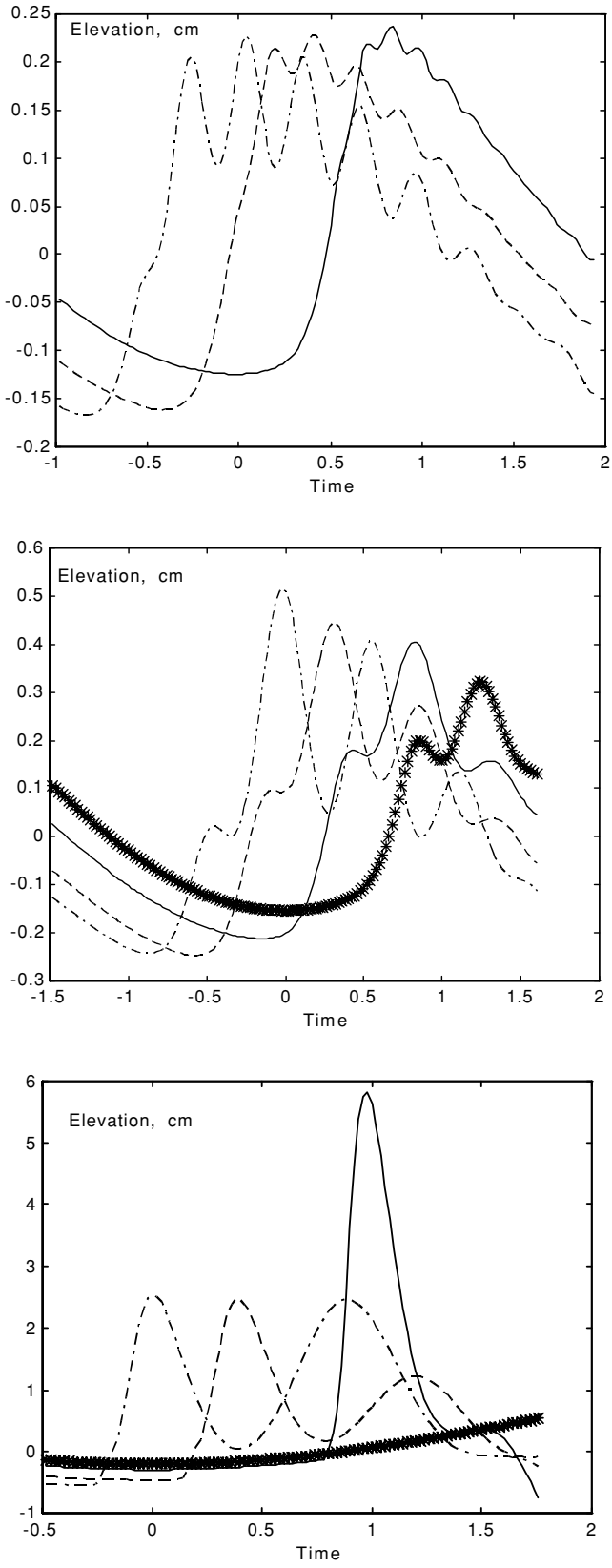

Figure 5 Transresonant transformation of profiles of surface waves and the effect of dispersion (layer thickness) on this transformation calculated for: (a) $h = 1.25$ cm and $R_* = -0.56$ (dot–dash), -0.07 (dashed) and 0.5 (solid); (b) $h = 2.5$ cm and $R_* = -0.62$ (dot–dash), -0.3 (dashed), 0.23 (solid) and 0.64 (asterisks); (c) $h = 5$ cm and $R_* = -0.39$ (dot–dash), 0 (dashed), 0.53 (solid) and 0.6 (asterisks).

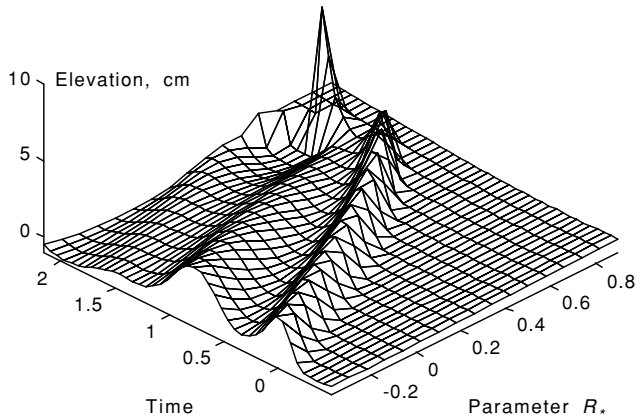

Figure 6. The transresonant evolution of profiles of surface waves from the dark soliton ($R_* = 0.3$) to the bright soliton ($R_* = 0.8$) calculated according to eq. (187) for $N = 1$, $h = 5$ cm, $L = 60$ cm, $\mu_f/h\rho_0 = 35$ cm^2 s^{-1}, $l = 0.155$ cm.

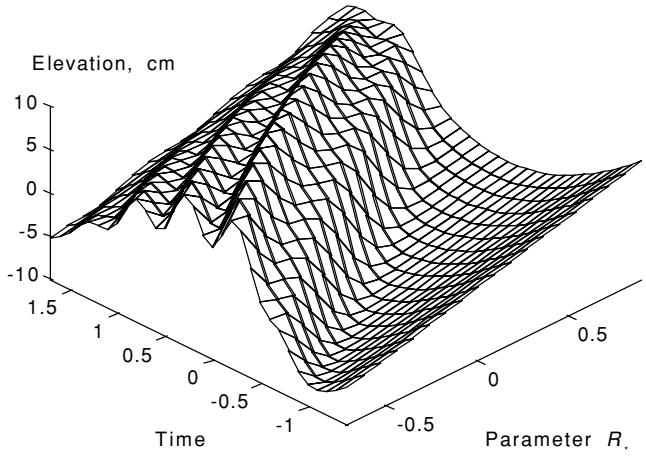

Figure 7. The transresonant evolution of profiles of surface waves from an oscillating shock-like wave ($R_* = -0.7$) to a harmonic wave ($R_* = 0.7$). The evolution was calculated according to eq. (187) for $N = 1$, $h = 20$ m, $L = 250$ m, $\mu_f/h\rho_0 = 10^5$ cm^2 s^{-1}, $l = 0.1$ cm.

Let us study the transresonant wave evolution using the experimental data of Chester & Bones (1968) and solution (187). The results of these calculations are presented in Figs 5 and 6. Fig. 5(a) corresponds to Fig. 5 ($h = 1.25$ cm, $l = 0.31$ cm), Fig. 5(b) corresponds to Fig. 7 ($h = 2.5$ cm, $l = 0.165$ cm), Figs 5(c) and 6 correspond to Fig. 9 ($h = 5$ cm, $l = 0.165$ cm) of Chester & Bones (1968), respectively. Figs 5(a) and (b) demonstrates a variety of oscillating profiles of the shock-like waves. The unloading wave occurs at (Fig. 5a) or in front of (Fig. 5b) the jump. Figs 5(c) and 6 show the transformation of a two-wave configuration ($R_* = -0.39$) into a bright soliton ($R_* = 0.53$) which instantly annihilates if $R_* \approx 0.77$.

It follows from Figs 5 and 6 that increasing the layer thickness amplifies the surface waves. The oscillating shock wave (Figs 5a and b) is transformed into a two-wave configuration (dark soliton) and then into soliton-like excitation (Figs 5c and 6). There is a strong amplification of the waves at the wall because of dispersion. This result is quite different from the result predicted by linear acoustics. The analogous amplification is well known for bubbly liquids (Nigmatulin 1991).

Consideration of Figs 5 and 6 suggests that increasing the thickness also intensifies the transresonant effect. It is important that maximal oscillations can be generated when $R_* \to 1$ (see Figs 5c and 6). The dispersion forms oscillating shock-like waves. We also note that soliton-like unloading waves and oscillating shock waves reminiscent of the waves presented in Figs 5 and 6 have been observed in bubbly liquids and granular materials (Van der Grinten *et al.* 1987; Nakoryakov *et al.* 1989, 1996; Nigmatulin 1991; Britan *et al.* 1997).

Thus, there is agreement between the theory and the experiments. The agreement is better than might be expected. In fact, eq. (45) and the solution (77) were obtained only for weakly non-linear waves, and small dispersive and dissipative effects. In particular, the boundary friction was approximated as $\tau_{31} = \mu_f u_{1,11t}$ instead of the integral form considered by Chester & Bones (1968) and Cox & Mortell (1986). We used the approximate solution (187), which was derived for very small dispersion. However, in experiments, strongly non-linear waves were excited (their amplitude was sometimes close to h), and the influence of dispersion was not small.

Resonant water waves called seiches have been observed in lakes in various parts of the world. The amplitude of these waves can be up to 2 m (the lake at Geneva in Switzerland) and more (up to 3 m, Lake Michigan) (Stoker 1957, p. 423). These waves can be excited by earthquakes. Tides are amplified (up to 15 m) at the top of the Bay of Fundy (Nova Scotia, Canada) due to the resonance.

Many cities are built on sedimentary basins. When there are sharp changes of mechanical properties between sedimentary material and the bedrock, seismic waves transmitted into the resonator may be trapped. The frequency of the reverberations of the trapped waves may vary, for example, because of a slope of the boundaries. As a result, the transresonant process can occur.

Consider a sedimentary basin with $L = 250$ m, $h = 20$ m and shear wave speed 250 m s^{-1}. Assume that the frequency of excitation of the bedrock equals the natural horizontal resonance of the basin, and $l = 0.1$ cm. The non-linear parameter β corresponds to the fluidized state of the sediments. Solution (187) was used.

In Fig. 7 the transresonant waves are presented calculated for the viscous parameter $h^{-1}\rho_0^{-1}\mu_f = 10^5$ cm^2 s^{-1} and various R_*. The amplitude of the surface waves may be as much as 100 times greater than the amplitude of the bedrock oscillations. We found that the waveform is varied from an oscillating shock-like wave to a smooth wave within the transresonant band. Dissipation can strongly modify the amplitude of the excited waves. The amplitude is reduced by about three times when $h^{-1}\rho_0^{-1}\mu_f = 5 \times 10^5$ cm^2 s^{-1}.

5.3 Charles Darwin's seismic evidence and the 1-D resonance of the island

On 1835 February 20 a violent earthquake affected the coastal area (about 1000 km) of Chile parallel to the Andes. This earthquake was one of the largest for several centuries and was observed by Charles Darwin, who gave an interesting description of the earthquake (Darwin 1839). The coincidence of the earthquake with the eruption of volcanoes in the Andes led Darwin to conclude that the volcanic activity and earthquakes were related. This description has been quoted in the literature (Yeats *et al.* 1997). However, we know of no attempt at mathematical simulation of the reported events except Galiev (1999a, 2000b). Charles Darwin described catastrophic waves and very complex, anomalous seismic phenomena. In this section we consider earthquake-induced oscillations of the small island of Quiriquina.

Quiriquina is considered as an elongated natural resonator located on the continental shelf. Darwin (1839, p. 370) noted the following results of the earthquake on this small island '*...The ground was fissured in many parts, in north and south lines; which direction perhaps was caused by the yielding of the parallel and steep sides of the narrow island. Some of the fissures near the cliffs were a yard wide...*'. The fissures were a result of earthquake-induced vibrations. Very long seismic waves shook the shelf and vibrated the base of the island. It is known that earthquakes can generate large vertical displacements of the coast [the 1835 Chilian earthquake lifted the island of Santa Maria by up to 3 m (Darwin 1839, p. 375); the Alaska 1899 earthquake lifted the coast of Haenke Island from 5.1 to 5.7 m and the west coast of Disenchantment Bay up to 14.5 m (Davison 1936, p. 167)]. Because of the slope of the shelf a horizontal component of the disturbing acceleration is generated in the topography (Galiev & Galiev 1998; Galiev 1999a). As a result, surface waves are excited in the island. We suggest that the frequency of excitation was close to some natural frequency of the horizontal oscillations of the island and resonant ground waves were induced. These waves may be reminiscent of vertically excited resonant surface waves in water or granular layers (Galiev 1999a). Since the shelf slope is perpendicular to the long axis of the island, a strong directional resonance, and surface waves and fissures, oriented approximately parallel to the long axis of the island, might be excited.

As a result of the shape of the island (width approximately 500 m, length 4000 m; the island has 'the parallel and steep sides' Darwin 1839), we can use the 1-D theory of Section 3.

Let us consider boundary conditions for the island. Quiriquina is located near the coast of Chile, where the water depth is less than 50 m. The velocity of water waves for this depth is approximately 20 m s^{-1} (see the Airy-type equation 46). As a result of the sharp impedance contrast between the island material and the water, an earthquake-induced wave loses only a small part of its energy because of reflections from the cliffs. Thus, the reflection from the cliffs is reminiscent of the reflection of waves from free boundaries. In the last case the cliffs are free from stress (18) and $u_{1,1} = 0$ if $x_1 = 0$ or L, where L is the width of the island. Therefore, we assume that the coefficient of the energy loss b^* is very small and write the following boundary conditions at the cliffs

$$u_{1,1} = b^* u_{1,t} \quad (x_1 = 0 \quad \text{and} \quad L). \tag{188}$$

Here b^* is the second-order value ($b^* \ll 1$).

First, the linear oscillations will be considered. Assume that $d = 0$ and the relief yields that $h_1 = \sum_i H_i \sin i\pi x_1/L$ in eq. (78). The linearized boundary conditions (188) (see also eq. 191) are used. According to Section 5.1 the linearized boundary condition (191) at $x_1 = 0$ implies that

$$J' = F'(r) + \varphi^* \cos \omega a^{-1} r - d^*, \quad j' = F'(s) - \varphi^* \cos \omega a^{-1} s + d^*, \tag{189}$$

where $\varphi^* = 0.5\delta\pi L^{-1} \sum_i i H_i [\omega^2 - (\pi i a_0/L)^2]^{-1}$, $d^* = 0.5 g_0 L \pi^{-1} a_0^{-2} \sum_i i^{-1} H_i$ (see also eq. 175). Function $F'(a_0 t \pm x_1)$ in eq. (189) is determined from the boundary condition (188) at $x_1 = L$:

$$F'(a_0 t \pm x_1) = 0.5\delta\pi L^{-1} \frac{\sin \omega a_0^{-1}(a_0 t \pm x_1)}{\sin \omega L a_0^{-1}} \sum_i \frac{i H_i [\cos \omega L a_0^{-1} - (-1)^i]}{[\omega^2 - (\pi i a_0/L)^2]} - 0.5 g_0 \pi^{-1} a_0^{-2} (a_0 t \pm x_1) \sum_i H_i i^{-1} [1 - (-1)^i], \tag{190}$$

neglecting dissipative and dispersive effects. From eq. (190) the resonant horizontal natural frequencies of the island are given by $\Omega_N = N\pi a_0/L (N = 1, 2, 3, \ldots)$. At the exact resonance the expression for φ^* in eq. (189) is not valid and the double integral in eq. (178) must be recalculated. It has been found (see eq. 194) that the topographic effect is limited at the exact resonance.

It follows from consideration of the linear problem that the topographic effect on the island oscillations is complex. This effect is determined by the shelf slope, the relief of the island and the frequency of excitation.

5.3.1 Resonant cubic basic equation

Here, we assume that the effects of dissipation and dispersion are negligible. From eqs (78) and (188) neglecting terms of fourth and fifth order, we have if $R_e = d = d_1 = 0$,

$$\begin{aligned}
&j' - J' - \Psi_2' + \psi_2' - \Psi_3' + \psi_3' - \frac{1}{4}\beta a_0^{-2}[(J')^2 + (j')^2 - 2x_1(J'J'' - j'j'') - 2J'j' + J''j + Jj''] \\
&\quad - \frac{1}{4}a_0^{-2}\left[\iint g(h_s - h_r)\,dr\,ds\right]_1 + \frac{1}{32}\beta^2 a_0^{-4}(J''j^2 + j''J^2 - 2JJ'j' - 2jj'J')_1 \\
&\quad - \frac{1}{4}(\beta_1 a_0^{-2} - 5\beta^2 a_0^{-4}/8)[j(J')^2 + J(j')^2]_1 + \frac{1}{4}(\beta_1 a_0^{-2} - 0.5\beta^2 a_0^{-4})\left[j'\int (J')^2\,dr + J'\int (j')^2 ds\right]_1 \\
&\quad + (\beta_1 a_0^{-2}/6 - \beta^2 a_0^{-4}/16)[(J')^3 - (j')^3] - (\beta_1 a_0^{-2}/2 - 7\beta^2 a_0^{-4}/16)x_1[(J')^2 J'' + (j')^2 j''] \\
&\quad + \frac{1}{8}\beta^2 a_0^{-4}[Jj'j'' - jJ'J'' - 0.5J'(j')^2 + 0.5j'(J')^2] \\
&\quad + \frac{1}{8}\beta^2 a_0^{-4}x_1[J(j'')^2 - 2J'j'j'' + Jj'j''' - 2j'J'J'' + j(J'')^2 + jJ'J''' + 0.5J''(j')^2 + 0.5j''(J')^2] \\
&\quad - \frac{1}{8}\beta^2 a_0^{-4}x_1^2[J'''(J')^2 - j'''(j')^2 + 2J'(J'')^2 - 2j'(j'')^2] - \frac{1}{2}\beta a_0^{-2}[\psi_2'j' + \Psi_2'J' + x_1(\psi_2'j' + \Psi_2'J')_1] \\
&= b^* a_0[j' + J' + \Psi_2' + \psi_2' - \frac{1}{4}\beta a_0^{-2}(2x_1 J'J'' + 2x_1 j'j'' - 2J'j' + jJ'' + Jj'')].
\end{aligned} \tag{191}$$

The boundary condition (191) is satisfied at $x_1 = 0$ if

$$J' = F'(r),$$

$$\Psi_2' = -\frac{1}{4}\beta a_0^{-2}JJ'' - b^* a_0 J' + \varphi^* \cos\omega a^{-1} r - d^* + d_2 r, \tag{192}$$

$$\Psi_3' = -b^*\beta a_0^{-1}[(J')^2 - JJ''] - 0.5\beta a_0^{-2}J'\Psi_2';$$

$$j' = F'(s), \qquad \psi_2' = \frac{1}{4}\beta a_0^{-2} jj'' + b^* a_0 j' - \varphi^* \cos\omega a^{-1} s + d^* + d_2 s, \tag{193}$$

$$\psi_3' = b^*\beta a_0^{-1}[(j')^2 - jj''] + 0.5\beta a_0^{-2} j'\psi_2',$$

where d_2 is an arbitrary constant. The expression for the topographic terms in eqs (191)–(193) depends on the frequency of excitation ω. At the exact resonance, if $i = N$, we have from eq. (191) that

$$\Psi_2' = -\frac{1}{4}\beta a_0^{-2}JJ'' - b^* a_0 J' + \frac{1}{8}\delta\pi^{-1}a_0^{-2}LN^{-1}H_N(\cos\omega a_0^{-1}r + rN\pi L^{-1}\sin\omega a_0^{-1}r) + \varphi^*\cos\omega a_0^{-1}r - d^* + d_2 r, \tag{194}$$

where $\varphi^* = 0.5\delta\pi L^{-1}\sum_{i(i\neq N)} i H_i[\omega^2 - (\pi i a_0/L)^2]^{-1}$. The expression for $\psi_2{}'$ is similar to the above expression for $\Psi_2{}'$.

Now, assume that $F(a_0 t - L + 2N\pi a_0\omega^{-1}) = F(a_0 t - L)$ and consider the boundary condition at $x_1 = L$. First, function $F(s)$ is expanded in a Taylor's series at $x_1 = L$:

$$F(a_0 t + L) = F(a_0 t - L) + \Delta F'(a_0 t - L) + 0.5\Delta^2 F''(a_0 t - L) + \cdots, \tag{195}$$

where $\Delta = 2\omega^{-1}L\omega_1$ and ω_1 is a perturbation of the resonant frequency. The boundary condition (188) at $x_1 = L$ may be reduced, using eqs (191) and (195), to the following equation:

$$\begin{aligned}
&\Delta F'' - (\beta_1 a_0^{-2} - 7\beta^2 a_0^{-4}/8)L(F')^2 F'' + 4b^*\beta L a_0^{-1}F'F'' - b^* a_0\Delta F' + \frac{1}{8}\beta^2 L a_0^{-4}F(F'F'')' - \beta L a_0^{-2}(\Psi_2'F')' \\
&\quad = \delta\pi L^{-1}\sum_i i H_i\frac{\cos\omega L a_0^{-1} - (-1)^i}{\omega^2 - i^2\pi^2 a_0^2 L^{-2}}\cos\omega t + g_0\pi^{-1}L a_0^{-2}\sum_i i^{-1}H_i[(-1)^i - 1] - 2L\,d_2.
\end{aligned} \tag{196}$$

Let $b^* a_0\Delta F' \approx 0$, $\frac{1}{8}\beta^2 L a_0^{-4}F(F'F'') \approx 0$, $\beta L a_0^{-2}(\Psi_2'F')' \approx 0$ and $d_2 = \frac{1}{2}g_0\pi^{-1}a_0^{-2}\sum_i i^{-1}H_i[(-1)^i - 1]$. Then, after some algebra, eq. (196) yields

$$(l_* F')^3 + r_*(l_* F')^2 + 3Rl_* F'/2^{2/3} + \sin\omega t + C = 0. \tag{197}$$

Here $l_* = [-\frac{1}{3}Ll_1^{-1}(\beta_1 a_0^{-2} - 7\beta^2 a_0^{-4}/8)]^{1/3}$, $r_* = 2b^*\beta l_1^{-1}a_0^{-1}l_*^{-2}L$, $R = 2^{2/3}\Delta l_1^{-1}l_*^{-1}/3$ [R is a transresonant parameter (Galiev 1999)], $l_1 = \delta\pi a_0\omega^{-1}L^{-1}\sum_i i H_i\frac{(-1)^i - \cos\omega L a_0^{-1}}{\omega^2 - i^2\pi^2 a_0^2 L^{-2}}$ and C is a constant of integration. If $i = N$, then $\sum_i$ must be replaced by $\sum_{i(i\neq N)}$. Eq. (197) may be transformed to the cubic eq. (199). Let us introduce a new function F_*':

$$l_* F_*' = l_* F' + r_*/3. \tag{198}$$

As a result, eq. (197) yields

$$(l_* F_*')^3 + (3R/2^{2/3} - r_*^2/3)l_* F_*' + 2r_*^3/27 - r_* R/2^{2/3} + \sin\omega t + C = 0. \tag{199}$$

In Sections 5.3.2 and 5.3.3 special cases of eq. (199) will be considered.

5.3.2 Resonant solutions and waves

Let us consider the cliffs as free surfaces. In this case $b^* = 0$ ($r_* = 0$) in eq. (198) and we have $F'_* = F'$. Let $C = 0$. Then eq. (199) yields

$$(l_* F')^3 + (3R/2^{2/3}) l_* F' + \sin \omega t = 0. \tag{200}$$

It is necessary to distinguish four cases.

(1) Let $R = 0$, then eq. (200) is satisfied if

$$l_* F' = (-\sin \xi^{\pm})^{1/3}. \tag{201}$$

Here and below $\xi^{\pm} = \omega a_0^{-1}(a_0 t \pm x_1)$.

(2) Let $R > 0$, then the function F' is unique, single-valued and continuous

$$l_* F' = -2D \sinh\left[\frac{1}{3} \operatorname{arcsin} h(|R|^{-1.5} \sin \xi^{\pm})\right], \tag{202}$$

where $D = (\operatorname{sign} \sin \omega t)(|R|2^{-2/3})^{1/2}$.

(3) Let $R < 0$ and $0.25[R^3 + \sin^2 \omega a_0^{-1}(a_0 t \pm x_1)] \le 0$. In this case there is no continuous single-valued solution and a solution with discontinuities was constructed (Sibgatullin 1972; Galiev 1999a). However, Nature often manifests multi-valued solutions (for example, breaking waves and turbulence). Indeed, non-linear systems often exhibit two or more dynamic equilibrium states for the same values of parameters. Some states may be chaotic, while others are periodic. Here we will construct regular multi-valued solutions with the help of the following smooth single-valued solutions:

$$l_* F'_i = -2D \cos\left[\frac{1}{3} \arccos(|R|^{-1.5} \sin \xi^{\pm}) + 2i\pi/3\right], \tag{203}$$

where $i = 0, 1, 2$.

(4) If $R < 0$ and $0.25[R^3 + \sin^2 \omega a_0^{-1}(a_0 t \pm x_1)] > 0$, we have one real and two complex solutions:

$$l_* F' = -2D \cosh\left[\frac{1}{3} \arccos h(|R|^{-1.5} \sin \xi^{\pm})\right], \tag{204}$$

$$l_* F'_{\pm} = D \cosh\left[\frac{1}{3} \arccos h(|R|^{-1.5} \sin \xi^{\pm})\right] \pm \sqrt{-3} D \sinh\left[\frac{1}{3} \operatorname{arcsin} h(|R|^{-1.5} \sin \xi^{\pm})\right]. \tag{205}$$

Thus, we have obtained a set of solutions (201)–(205), which describe waves on the island surface generated within and near the transresonant band.

Some results of calculations of dimensionless vertical displacement $\eta/h = -u_{1,1}$ and wave patterns in the x_1–t plane are given in Fig. 8. The dimensionless coordinate (x_1/L) is used. We assumed that $N = 3$ (Figs 8a–c), $a_0 = 249$ m s^{-1} and used solution (203) for $i = 2$, $R = -0.001$ (Fig. 8a) and $R = -0.999\,999\,91$ (Fig. 8c). Fig. 8(b) was calculated for $i = 2$ or 0 in eq. (203) and $R = -0.999\,9999$. One can see the transformation of the step-like waves (Fig. 8a) into pyramid-like waves (Fig. 8c). Fig. 8(d) is calculated for $N = 1$ ($i = 2$ or 0) and $R = -0.999\,9999$. It is interesting that strictly localized jet-like waves can be excited on the island surface in the case $R = -0.999\,9999$ (Figs 8b and d). These waves are reminiscent of the jet-like waves that were observed in water and granular layers (Longuet-Higgins 1983; Goodridge *et al.* 1996; Umbanhowar *et al.* 1996; Jiang *et al.* 1998; Zeff *et al.* 2000; Lohse 2003; James *et al.* 2003). Indeed, eq. (45) and the solutions (201)–(205) are valid for these layers. The step-like surface waves (Fig. 8a) were observed by Lioubashevski *et al.* (1999). The vertically excited pyramid-like waves
(Fig. 8c) on a liquid surface were observed by Longuet-Higgins (1983). Let $C = 1$ in eq. (199). Then we have

$$(l_* F')^3 + (3R/2^{2/3}) l_* F' + 2\cos^2 \frac{1}{2}(\omega t - \pi/2) = 0. \tag{206}$$

Solutions for this case may be written according to eqs (201)–(205), where $\sin \omega t$ must be replaced by $2\cos^2 \frac{1}{2}(\omega t - \pi/2)$. Taking this into account we considered the transresonant evolution of solutions of eq. (206) (Fig. 9). Patterns corresponding to $R = -0.9$ (Fig. 9a) and $R = -1.587$ (Fig. 9b) are calculated according to eq. (203), where $i = 1$. Patterns corresponding to $R = -1.5875$ (Fig. 9c) are calculated according to eq. (204). One can see the transformation of the shock-like waves into cnoidal-like waves. The latter were observed recently on the surface of deep and thin granular layers (Wassgren *et al.* 1996; Cerda *et al.* 1997).

5.3.3 Free oscillations

A sole seismic shock can be trapped by the island and free oscillations may be generated (Galiev 1999a). In this case, if $C = 0$ in eq. (199), we have $(l_* F')^2 = -3R/2^{2/3}$. At resonance, $R = 0$ and $F' = 0$. If $R < 0$, then we have $l_* F'_{\pm} = \pm(-3R/2^{2/3})^{1/2}$. Using this solution we can construct a step-like periodic function. This function determines the free resonant shock waves reverberating in the island. The stress near the island surface is proportional to

$$(-3R/2^{2/3})^{1/2}\{H[\sin(\omega t - \omega a_0^{-1} x_1)] - H[\sin(\omega t + \omega a_0^{-1} x_1)]\}. \tag{207}$$

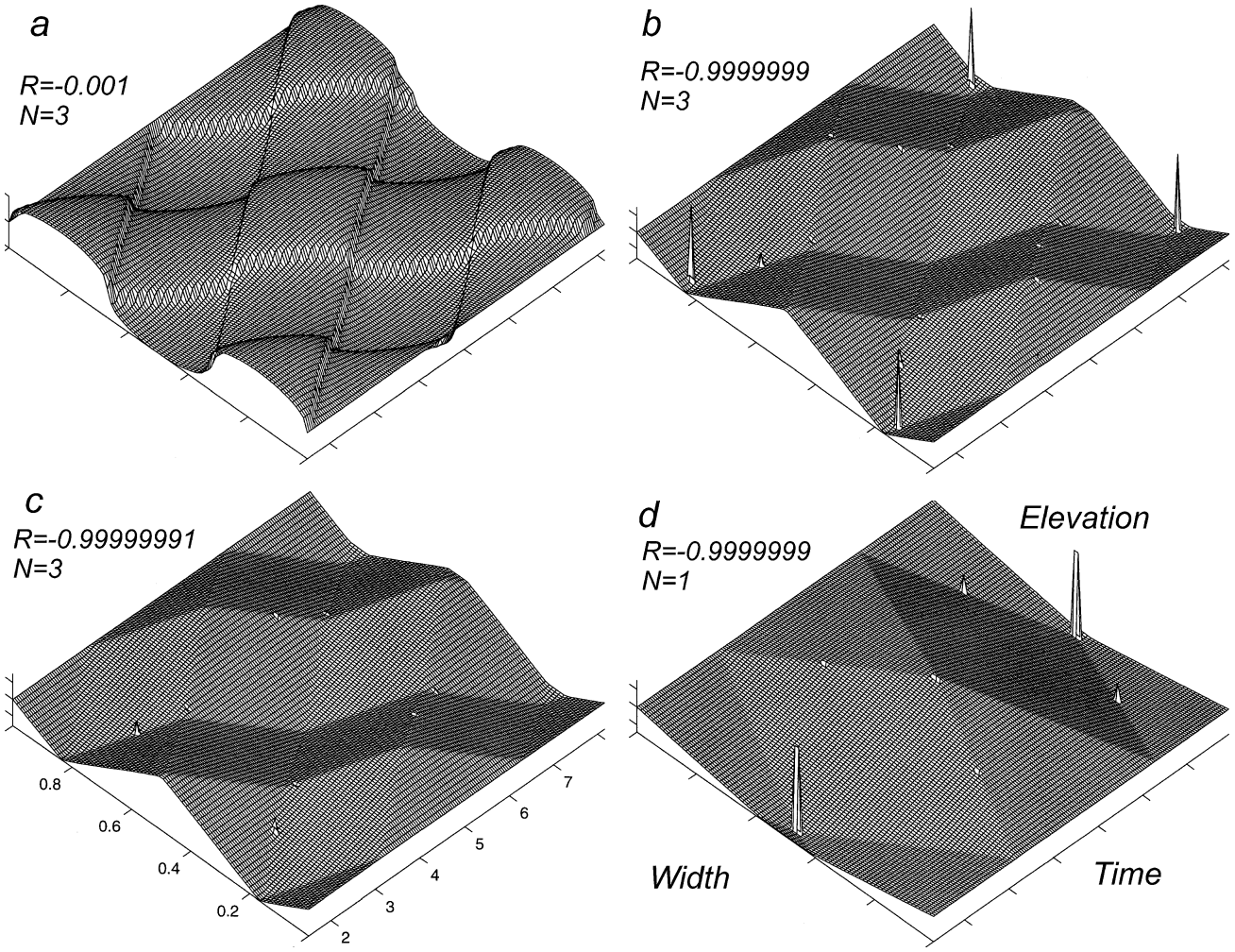

Figure 8. Resonant wave patterns generated in the x_1-t plane by the equation $(l_*F')^3 + (3R/2^{2/3})l_*F' + \sin\omega t = 0$, eq. (200) and calculated for $N = 3$ (a)–(c) and $N = 1$ (d). The evolution of shock-like waves ($R = -0.001$, case a) into jet- and pyramid–like waves ($\approx -0.999\,9999$, cases b–d).

Thus, $2N$ shock waves appear travelling back and forth along the width of the island within the resonant band with number $N(N = 1, 2, 3, \ldots)$. Expression (207) qualitatively describes the waves presented in Figs 8(a) and 9(a).

The amplitude of the free waves (207) is determined only by the properties of the material and by the frequency of reverberation of the waves from the cliffs. These shock-like waves are reinforced along lines parallel to the long sides. As a result, on these lines the stress changes instantly from maximal compression to maximal tension. We suggest that the ground fissures were generated along these lines.

5.4 Scenarios of transresonant evolution and comparisons with experiments

Figs 8 and 9 show anomalous surface wave phenomena that occur near certain critical values of R ($R \approx 0$ and -1 (Fig. 8) or $R \approx -0.9$ and -0.5π (Fig. 9)). These phenomena are associated with single-valued solutions. However, multi-valued waves may be excited within the transresonant band.

Figs 10 and 11 show discontinuous curves calculated according to solutions (203) (Figs 10a and 11a) and (204) (Figs 10b and 11b). These solutions form continuous multi-valued periodic figures in Figs 10(c) and 11(c). According to these figures mushroom-like waves can form on the surface under intense vertical excitation (Wright *et al.* 2000; Galiev & Galiev 2001). Thus, near $R \approx -1$ there is a tendency for drops (jets) to form on the surface. It is known that similar mushroom-like waves may be formed in the Earth's mantle (Davies 1999) and magma chambers (Couch *et al.* 2001). On the other hand, the closed loops in Figs 10(c) and 11(c) may be treated as vortices (Galiev & Galiev 2001, see also Sections 5.4.1, 7.1.1 and 7.2). It is possible to construct a few scenarios for the transresonant evolution of the waves with the help of the figures.

Here we consider some scenarios for the transresonant evolution of waves F', which are qualitatively supported by experiments. Four scenarios, calculated according to solutions (203)–(205), are presented in Fig. 12. Scenarios B, D, E correspond to $C = 0$ in eq. (199). Scenario F corresponds to $C = 1$ in eq. (199). It is seen from Fig. 12(B) that periodic shock- and saw-like waves may be generated on the surface (see

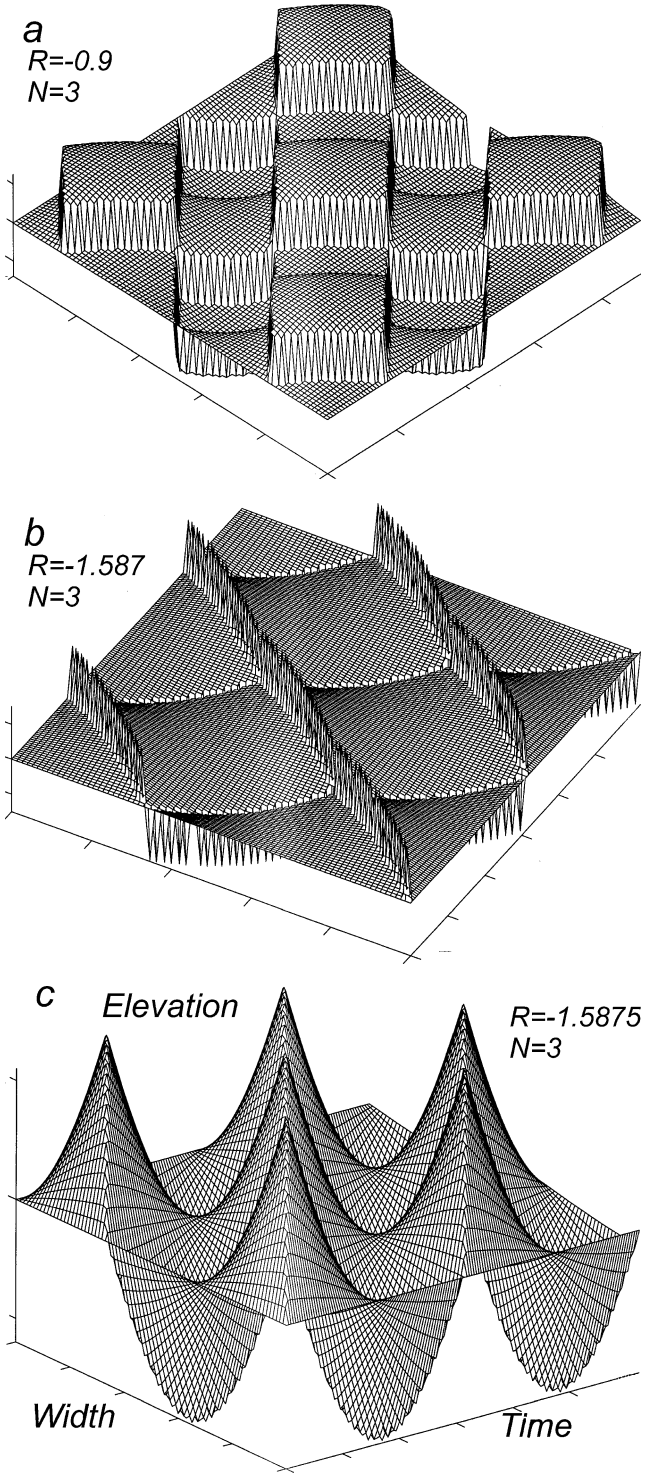

Figure 9 Resonant wave patterns generated in the x_1–t plane by the equation $(l_* F')^3 + (3R/2^{2/3}) l_* F' + 2\cos^2 \frac{1}{2}(\omega t - \pi/2) = 0$, eq. (200) and calculated for $N = 3$. The evolution of shock-like waves ($R = -0.9$, case a) into jet-like ($R = -1.587$, case b) and cnoidal-like ($R = -1.5875$, case c) waves.

also Figs 8a, c, 10c and 11c). Near the critical value of the resonant excitation, when $R \approx -1$, jets are ejected from the surface (see also Figs 8b, d and 11c). This result is quite different from the predictions of the linear theory (harmonic curves in Figs 10 and 11). According to scenarios *D* and *E*, stripe-like, stable breaking-like and mushroom-like travelling waves may be excited. Indeed, stable breaking stripe-like waves were observed recently on liquid (Kataoka & Troian 1999). The steepening of the breaking waves, when R reduces, is displayed in Fig. 12(D). These anomalous travelling waves were observed (Fineberg 1996; Lioubashevski *et al.* 1996; Lioubashevski *et al.* 1999). The mushroom-like waves are often formed due to the instability of rods (see Figs 48–51 from Love 1944), shells (Karagiozova & Jones 2001), thin jets of viscous

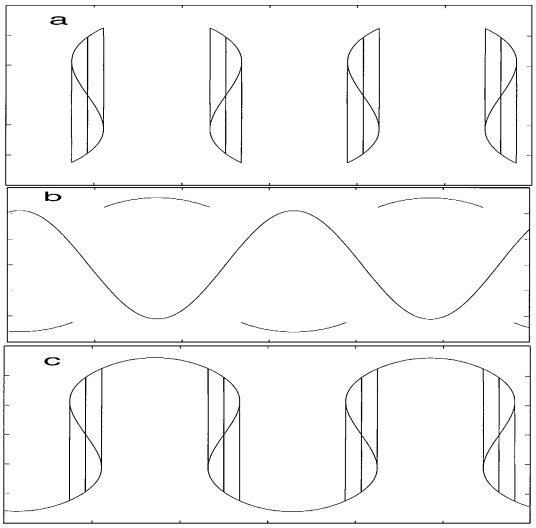

Figure 10. Multi-valued continuous mushroom-like waves (d) determined by solutions of the equation $(l_* F')^3 + (3R/2^{2/3}) l_* F' + \sin \omega t = 0$ (200), calculated for $R = -0.5$. The waves are constructed from the multi-valued solution (203) (a) and the discontinuous solution (204) (b). The harmonic wave (b) is determined by the linearized eq. (200) calculated for $R = -0.5$.

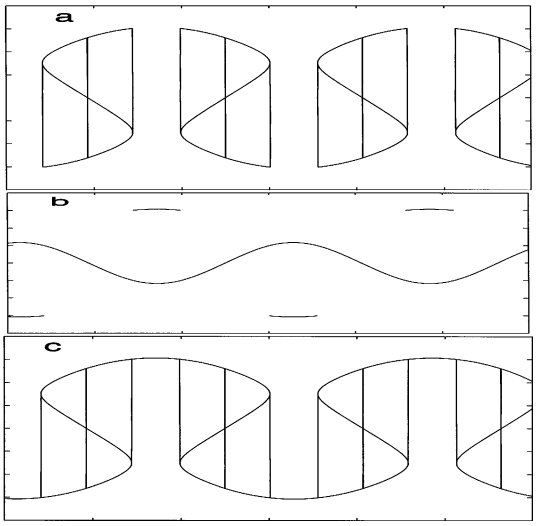

Figure 11. Waves and curves similar to those presented in Fig. 10 calculated for $R = -0.9$.

fluid (Taylor 1969) and gas (Suplee 1999). If $R \approx -1$, then the solutions separate and surfaces 1, 2 and 3 form (see Fig. 12E). It is possible to give different interpretations of the last result. Here we note only that these surfaces may qualitatively describe the generation of fissures parallel to the surface or the generation of foam and surface cavitation (Goodridge *et al.* 1996). Fountain- and step-like waves are presented in Fig. 12(F). These waves can have a crater on the top. This crater was recently observed on step-like waves in a vertically vibrated colloidal suspension (Lioubashevski *et al.* 1999). On the other hand, Fig. 12(F) can be interpreted as a picture of the generation and transresonant evolution of particles (drops) on the crest of the waves. Vertically excited waves with a drop on the crest are also known (Longuet-Higgins 1983; Goodridge *et al.* 1997, see also Fig. 20).

Because of the vertical excitation the wave velocity a_0 and R can vary according to a periodic law. We consider the case when in (200) $R = 2^{2/3} \Delta l_1^{-1} \gamma_*^{-1}/3 + \delta_* \cos {}^k\omega t/K$, where k and K are integers, and δ_* is constant. Here the term $\delta_* \cos {}^k\omega t/K$ may be very small. At the same time, this term is important near the critical value R: $R \approx -1$. Results of calculations for varying R are shown in Fig. 13. Fig. 13(D) is calculated for $2^{2/3} \Delta\, l_1^{-1} \gamma_*^{-1}/3 = -0.978$, Figs 13(B) and (E) are calculated for $2^{2/3} \Delta\, l_1^{-1} \gamma_*^{-1}/3 = -1$. We also assumed that $k = 5$, $K = 5$ and $\delta_* = -0.05$. These figures show the process of formation of stable breakers (Fig. 13D), jet-like (Fig. 13B) and mushroom-like (Fig. 13E) waves, when $R \approx -1$. In Fig. 13(D) the harmonic curve corresponds to the acoustic solution. According to these calculations, sawtooth waves are generated, if $R < -1$. These waves transform into harmonic waves if $R < -1.1$.

It follows from the theory that non-linear resonant effects are important for earthquake hazard analysis. Natural resonators can trap seismic waves. The frequency of the reverberations of the trapped waves can slowly reduce or increase. According to the theory, the amplitude

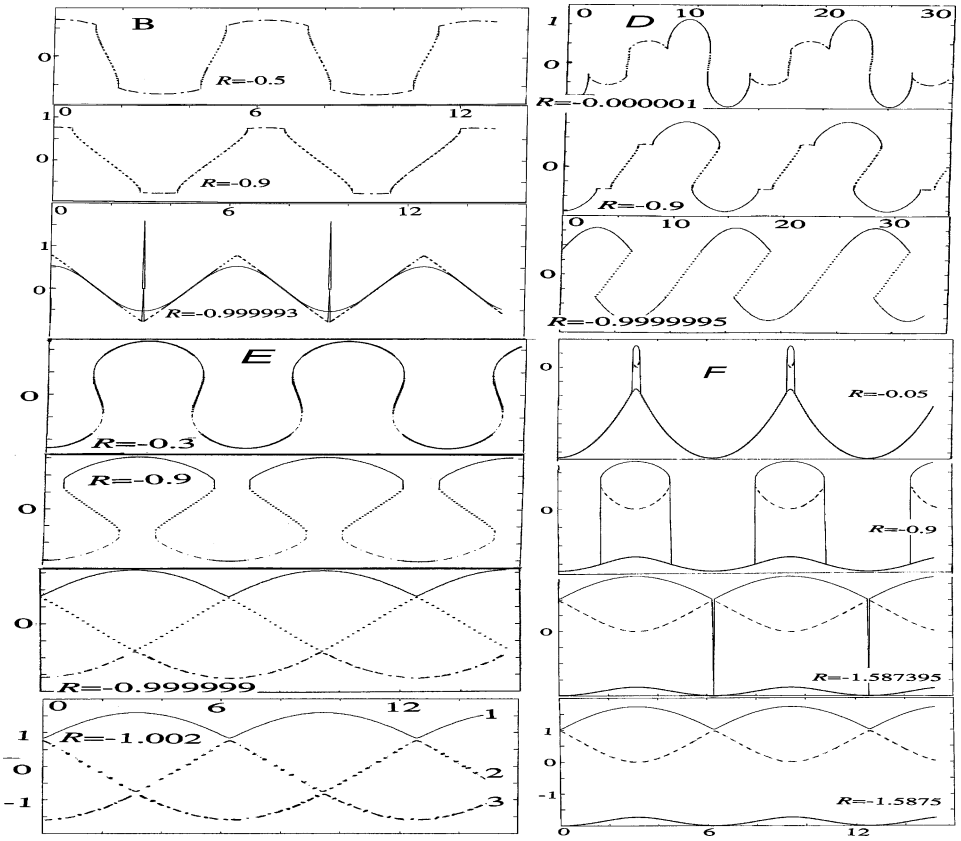

Figure 12. Different scenarios for the transresonant evolution of seismic waves calculated according to the equations $(l_* F')^3 + (3R/2^{2/3}) l_* F' + \sin \omega t = 0$ (200) (cases *B*, *E*, *D*) and $(l_* F')^3 + (3R/2^{2/3}) l_* F' + 2\cos^2 \frac{1}{2}(\omega t - \pi/2) = 0$, eq. (206) (case *F*): generation of jets (*B*), generation of breaker (*D*), generation of mushroom-, saw- and cnoidal-like waves (*E*), generation and evolution of particles (drops) on the crest of the waves (*F*).

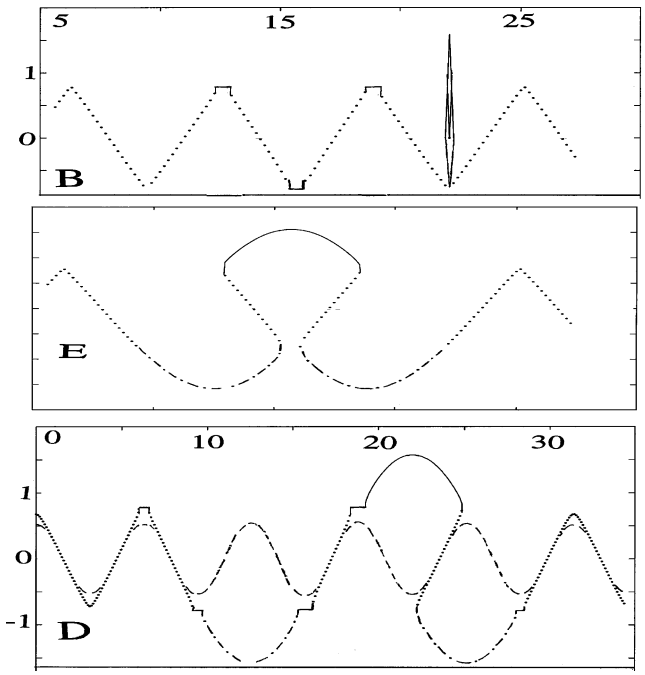

Figure 13. Transresonant effects calculated according to solutions (203)–(205) for *R* disturbed near the critical value of −1. Transition of sawtooth waves into breaker (*D*), jet- and mushroom-like waves (*B*, *E*).

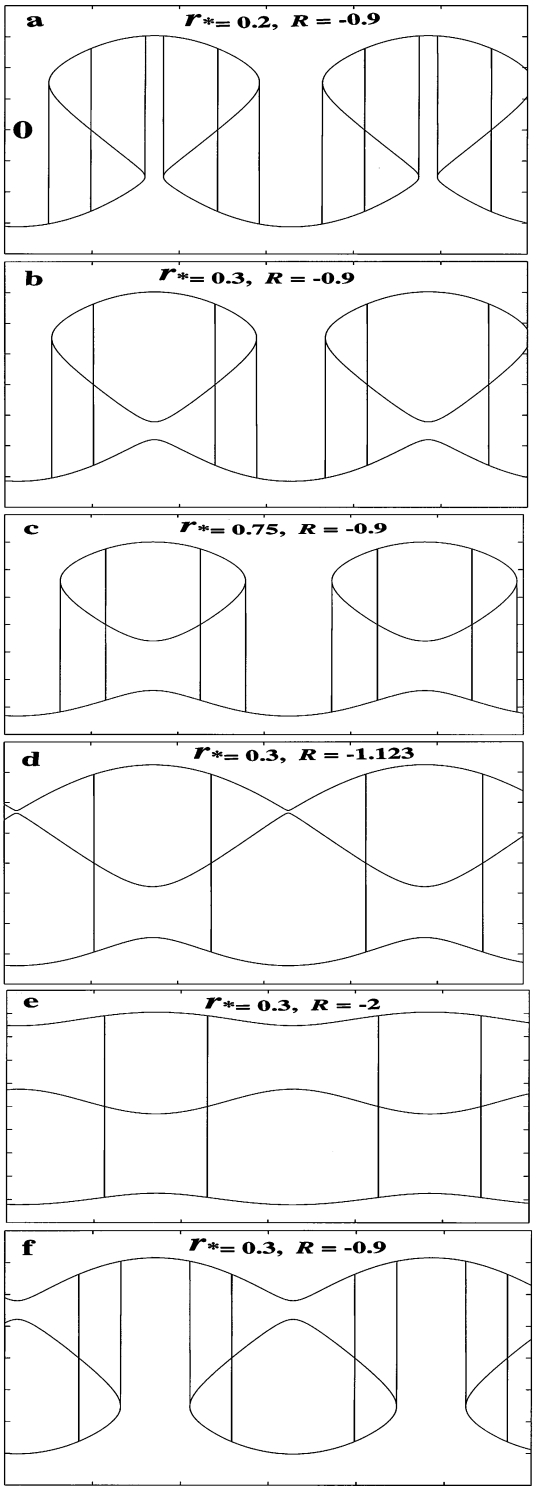

Figure 14. Quadratic non-linearity effect studied using equation $(l_*F')^3 + r_*(l_*F')^2 + 3Rl_*F'/2^{2/3} + \sin\omega t = 0$, eq. (197). Evolution of mushroom-like waves (a) into particles (drops) above the wave crests (b, c) or bubbles below the wave troughs (f).

of the trapped waves is greatly increased if this frequency passes through a resonance. In particular, collapse of buildings on the resonator surface may occur after the initial seismic waves have passed.

5.4.1 The effect of ocean water and quadratic non-linearity

We have considered the cliffs as the free surface. Let us take into account the influence of ocean water. In this case $b^* \neq 0$ in eq. (188) and a quadratic term is kept in eq. (197). Using eq. (198) and solutions (201)–(205) we studied the influence of b^* on the transresonant evolution of surface waves. Some results of the calculations are presented in Figs 14 and 15. These figures show a dependence of the wave shape on

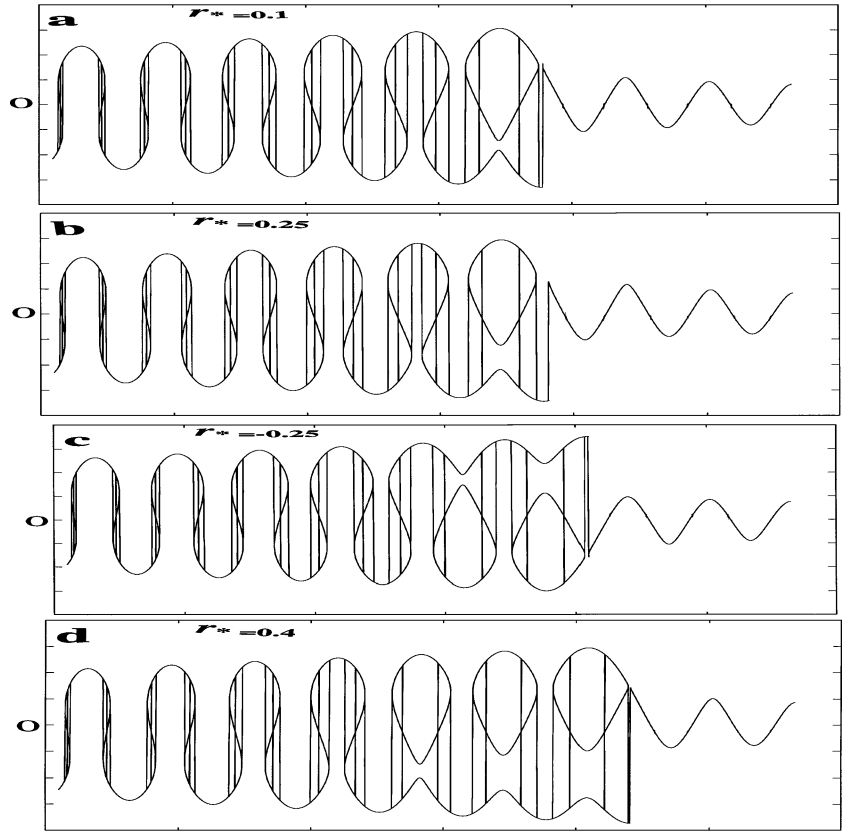

Figure 15. Quadratic non-linearity effect: the transresonant evolution of mushroom-like waves into particles (drops) (a, b, d) or bubble-like structures (c) if $R > -1$, and harmonic waves if $R < -1$.

r_* (or b^*) and R. The value of r_* is varied from –0.3 (Fig. 14f) and 0 (Fig. 11c) to $r_* = 0.75$ (Fig. 14c) (the dimension of r_* is time/length). This variation transforms mushroom-like waves (Fig. 11c) into drop- and bubble-like structures (Figs 14b, c and f), cnoidal-like waves (Fig. 14d) and harmonic waves (Fig. 14e). The shape of the drop-like structures depends on R. These structures transform into pairs of cnoidal-like waves if R reduces from -0.9 to -1.123. The linear solution (harmonic wave) follows when $R = -2$ (Fig. 14e).

The evolution of the shock-like waves into mushroom-like waves, and the drop-, bubble- and vortex-like structures in the transresonant band is shown in Fig. 15. The parameter R is varied from -0.3 to -1.4. If $R < -1$ then harmonic waves can be generated on the surface. It is seen that the transresonant evolution of the waves depends upon the quadratic non-linearity. In particular, for $r_* = 0.1$ we have one drop-like structure, but for $r_* = 0.4$ four drop-like structures are generated during the transresonant evolution of the ripples. We emphasize that the results were obtained with the aid of the analytic solutions (201)–(204) of the cubic equation (199).

It is possible to give different interpretations of the results presented in Figs 14 and 15. They qualitatively simulate generation of drops (Longuet-Higgins 1983; Goodridge *et al.* 1996; Goodridge *et al.* 1997; Jiang *et al.* 1998; Zeff *et al.* 2000; Lohse 2003; James *et al.* 2003) and bubbles (Taylor 1953) at water wave crests, or the ejection of particles above a granular layer (Umbanhowar *et al.* 1996) under resonant excitation. In particular, according to Fig. 15 the analytic solutions can describe the drop formation process which has previously been studied using numerical methods (Wright *et al.* 2000). The solutions also describe bubbles that can be formed in liquid (Zeff *et al.* 2000) and granular (Pak & Behringer 1994) vertically vibrated layers. Some structures (closed loops) may also be considered as vortices. Therefore, Figs 14 and 15 simulate qualitatively the generation of vortices by non-linear waves. This ill-understand phenomenon has only lately begun to be studied (Bühler & Jacobson 2001; Dunn *et al.* 2001; Galiev & Galiev 2001; Galiev 2002).

The drop-like structures generated above the free surface were studied by Galiev & Galiev (2001) using fourth- or fifth-order non-linear algebraic equations. Here they were studied using the cubic equation (197). Thus, under the simple vertical harmonic excitation, surface waves can manifest complex development of harmonic waves into shock-like waves, jets, cnoidal- and mushroom-like waves, drops, bubbles and vortices (see also Sections 7.1.1 and 7.2).

6 EXAMINATION OF EARTHQUAKE–VOLCANO INTERACTIONS NOTED BY CHARLES DARWIN AND STRONGLY NONLINEAR WAVE PHENOMENA

In this section we study strongly non-linear earthquake-induced phenomena. In particular, the dynamics of volcano craters, ridges and volcano eruptions will be considered.

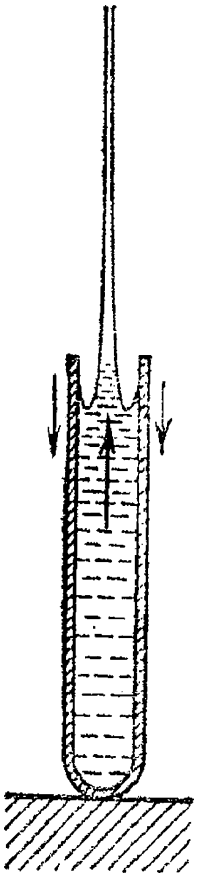

Figure 16. Jet generated by the interaction of a converged water surface (the rim at the tube wall and the trough at the centre) with an underwater shock wave.

6.1 Earthquake-induced resonant surface waves and column in a volcano crater

Charles Darwin (1839, p. 380) reported that, after the 1835 Chilean earthquake *'. . . a train of volcanoes situated in the Andes. . .instantaneously spouted out a dark column. . .*' and '*. . . in the immediate neighbourhood, these eruptions entirely relieve the trembling ground. . .*'. These notes suggest that there was a common mechanism creating the eruptions of the volcanoes separated by the long distances. Here I propose that the mechanism is the interaction of the volcano craters with an upward shock wave generated by the rapid vertical displacement (up to a few feet Darwin 1839) of the volcano bases.

The volcano shape is a cone truncated by a crater (funnel). The crater surface is formed of weakly cohesive media (snow, ice, granular materials, sediments, water and magma). The crater is connected to the base of the volcano by a conduit containing bubbly liquid-like magma (see Fig. 19 in Section 6.2). For example, the Soufriere Hills volcano in Montserrat, West Indies, has a 30 m diameter conduit, a 300 m diameter and a 100 m deep crater, and a vent fill (estimated as 20 m thick). Axisymmetric topography surrounds the vent ($\sim 22^{\circ}$ slope) (Clarke *et al.* 2002). Thus, the volcano can be visualized as a conduit truncated by a funnel.

The generation of a vertical column of matter in such a system may be demonstrated with the help of a tube filled by water. When the tube falls from a height of 10–20 cm and the bottom receives shock loading, the centre of the water surface ejects a thin vertical column (see Fig. 16, taken from Lavrentev & Shabat 1977). This is a result of the interaction of the concave surface of the water with the upward wave of the acceleration. The height of the ejected column can be more than 1 m. The deformation of the concave surface and the formation of the column during the experiment are shown for six points in time (from 0 to 0.009 s and for 0.16 s) in Fig. 108 which may be found in Lavrentev & Shabat (1977). The form of the funnel (crater) can be important. Under a high-pressure shock wave the walls of the funnel are caused to collapse so that the surface material is forced to concentrate on the axis giving rise to the jet (see Plate 48 from Johnson 1972). The experiments are described qualitatively by calculations (fig. 107 of Lavrentev & Shabat 1977 and fig. 5.47 of Frohn & Roth 2000). These calculations also simulate the dynamics of the water surface cavity and the generation of the central jet from the cavity (Worthington 1908; Kientzler *et al.* 1954).

Two distinct phenomena can take place during the interaction of the upward seismic wave with the crater surface. First, interaction of the wave with the free surface generates the vertical velocity (Cole 1948; Johnson 1972; Lavrentev & Shabat 1977; Galiev 1988; Bourne & Field 1992). Material near the centre of the crater rises perpendicular to the shock front, and moves more rapidly, and for a longer time than material near the rim. As a result, because of surface tension, the material collapses and transforms into a liquified state. The plume is then

generated. The motion of this plume is described by hydrodynamic laws. Experiments with water surface cavities have shown (Bourne & Field 1992) that the plume velocity increases with the surface curvature and/or the intensity of the shock.

Secondly, due to the topographic effect, the radial force directed from the crater rim to the centre is generated and a radial surface wave is formed. This wave focuses and forms a vertical jet of fragmented material in the centre of the crater at the same time or a little later than the vertical plume formed. Surface waves in cavities were studied by Bourne & Field (1992). The waves originate at the edges of the cavity and move to the centre.

To study this phenomenon we use eq. (126). This equation contains a topographic term which can describe the rim effect. Let us consider a circular crater of radius R_{12} and use the polar radial coordinate r_1. In this case, we have

$$\eta_{tt} - a_*^2\nabla^2\eta = -g_* b_0^{-1}\nabla^2 h + b_0\beta^*\nabla^2\eta^2. \tag{208}$$

Here $\nabla^2\eta = \partial^2\eta/\partial r_1^2 + r_1^{-1}\partial\eta/\partial r_1$. We employed the quadratic non-linear theory and neglected some small terms in eq. (126). It is assumed that the approximate solution of eq. (208) is a sum of oppositely travelling localized waves:

$$\eta = A_1(r_1)[J(r) + j(s)], \tag{209}$$

where $r = a_*\, t - r_1 + R_{12}$ and $s = a_*\, t + r_1 - R_{12}$. As a result, the left-hand side of eq. (208) yields

$$(\partial^2 A_1/\partial r_1^2 + r_1^{-1}\partial A_1/\partial r_1)(J + j) = (2\partial A_1/\partial r_1 + r_1^{-1}A_1)(J' - j'). \tag{210}$$

This equation has two approximate solutions: $A_1(r_1) = (Cr_1)^{-0.5}$ and $A_1(r_1) = \ln(Cr_1)$ (Landau & Lifshitz 1987), where C is an arbitrary constant. The first expression is valid far from the crater centre. For a large enough crater, near the rim $C^{-0.5}r_1^{-2.5}a_*^2(J + j) \approx 0$. Then from eqs (208) and (209) the resonant algebraic equation follows:

$$\eta^2 = g_* b_0^{-2}(h - h_0)/\beta^*. \tag{211}$$

Here g_* includes both the static and dynamic parts of the vertical acceleration. We shall consider only the dynamic part. Let us assume that

$$g_* = g_{12}\,\mathrm{sech}^4\alpha_{12}t \quad \text{and} \quad h - h_0 = h_{12}(Cr_1)^{-1}\,\mathrm{sech}^4\gamma_{12}(r_1 - R_{12}). \tag{212}$$

Here g_{12}, α_{12} and h_{12} and γ_{12} are constants related to the earthquake-induced impulse and the shape of the rim. Using eq. (212) we have from eqs (209) and (211)

$$J(r) + j(s) = \frac{1}{2}[(\beta^*)^{-1}b_0^{-2}g_{12}h_{12}]^{1/2}[\cosh(\alpha_{12}t + \gamma_{12}r_1 - \gamma_{12}R_{12}) + \cosh(\alpha_{12}t - \gamma_{12}r_1 + \gamma_{12}R_{12})]^{-2}. \tag{213}$$

We consider the localized waves interacting only if $r_1 \approx R_{12}$. Therefore, eq. (213) yields

$$J(r) \approx \frac{1}{2}[(\beta^*)^{-1}b_0^{-2}g_{12}h_{12}]^{1/2}\,\mathrm{sech}^2\gamma_{12}(a_*t - r_1 + R_{12}), \tag{214}$$

where we assume that $a_* = \alpha_{12}/\gamma_{12}$. The expression for $j(s)$ is similar to eq. (214). Now we can write the following formula for the earthquake-induced vertical displacement of the crater surface:

$$\eta = \frac{1}{2}[(\beta^*)^{-1}b_0^{-2}g_{12}h_{12}]^{1/2}r_1^{-0.5}[\mathrm{sech}^2\gamma_{12}(a_*t - r_1 + R_{12}) + \mathrm{sech}^2\gamma_{12}(a_*t + r_1 - R_{12})] + F(r_1). \tag{215}$$

The first term in eq. (215) describes localized converging and diverging radial waves propagating from the crater rim and the jet. The second term describes the volcano top. Calculations of η eq. (215) are presented in Fig. 17. Wave patterns for three points in time are shown.

It is important for the theory presented that Fig. 17 qualitatively describes the experimental observations of the water rim collapse, the generation and evolution of the water plume and the water column from the centre of the surface crater (Worthington 1908; Kientzler *et al.* 1954, see also the discussion in Section 6.3). The realization presented in Fig. 17 is also reminiscent of oscillon oscillations excited on the surface of a layer of vertically vibrated brass balls (Umbanhowar *et al.* 1996). The oscillon may be started by touching the surface of brass balls with a pencil (Mukerjee 1996). After formation of the surface crater, the oscillon begins to bounce up and down while the material around stays in place. During one cycle of the excitation, it is a peak; on the next cycle it is a crater (Umbanhowar *et al.* 1996). Oscillons do not occur only in granular media. They have also been observed in water and suspension layers (Lioubashevski *et al.* 1999). Galiev (1999a) has shown that localized, oscillon-like waves may be excited during earthquakes on the top of some hills.

A rough approximation of the height of the earthquake-induced column can be deduced using Longuet-Higgins' experiments (1983). In these experiments, a small vertical harmonic excitation (amplitude 0.5 mm) of a beaker ultimately produced a surface water jet rising to a height of over 1.7 m. For volcanoes this effect may be amplified by the crater form. Thus, if we assume that the shock vertical displacement of the volcano base was of the order of 1 m, then the jet (column) height could reach the order of 1–2 km (see also Section 6.3).

The mathematical model and the experiments discussed have demonstrated that the reported phenomena can occur if there is a strong enough vertical excitation. As a result of the earthquake-induced vertical shock, the surface material of the craters is transformed into a liquified state. Then, according to the hydrodynamic theories and the experiments, the liquified matter can be ejected from the volcano craters. Thus, the earthquake-induced volcanoes separated by very long distances could eject instantaneously the 'dark columns of matter'. The surface non-linear wave processes in the craters generate this ejection. The fluidization of the crater surface and the fountain-like eruption absorb considerable seismic energy. Therefore, immediately after the eruption, surface oscillations near the volcano are reduced.

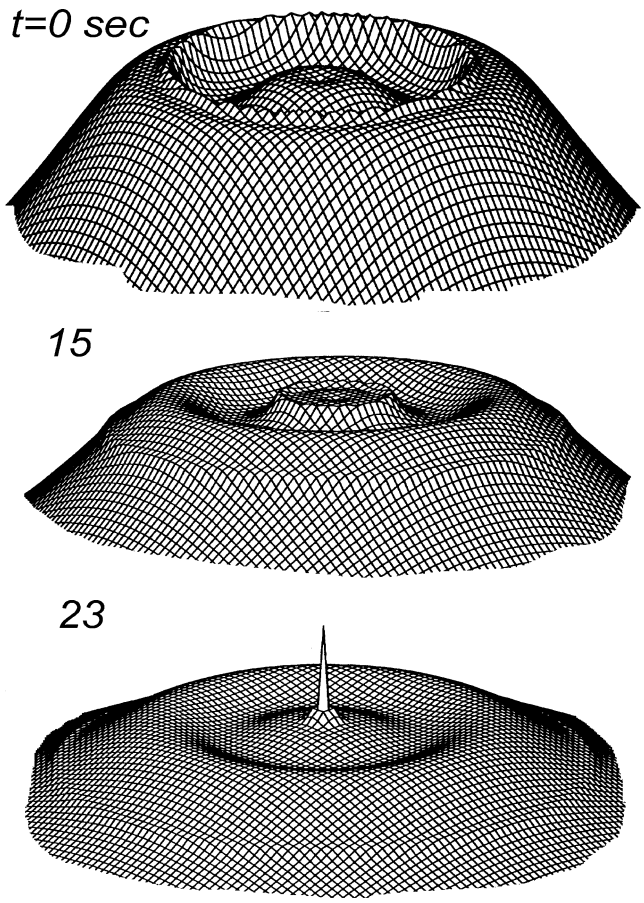

Figure 17. 2-D simulation of results of the interaction of an upward seismic shock wave and a volcano crater. Evolution of the plume, generation of the converging and diverging radial waves (a, b), and the eruption (c) from the centre.

6.2 Earthquake-induced non-linear wave phenomena in cone volcanoes

Large earthquakes can stimulate large-scale volcano eruptions. The cause of a naturally triggered earthquake is not clear, although a few interesting mechanisms are proposed (see short reviews by Sturtevant *et al.* 1996; Linde & Sacks 1998; Hill *et al.* 2002). In particular, it has been proposed that seismic waves may have caused the triggering (Nakamura 1975). Apparently, it is impossible to explain all documented events through a single mechanism. In the section below, attention is focused on the documented simultaneous eruptions from four volcanoes during the 1835 Chilean earthquake (Brodsky *et al.* 1998; Linde & Sacks 1998). Darwin (1839, p. 380) reports that '*. . . several of the great chimneys in the Cordillera of central Chile commenced a fresh period of activity'*. Let us consider these eruptions using the results of Section 6.1 and taking into account the volcano shape and the conduit. Three of the volcanoes (Minchinmavida 2404 m, Cerro Yanteles 2050 m and Peteroa 3603 m) are stratovolcanos and are formed of symmetrical cones with steep sides. Robinson Crusoe (922 m) is a shield volcano and is formed of a cone with gently sloping sides. The above volcanoes are not very active. The last large eruption of Minchinmavida, Cerro Yanteles and Robinson Crusoe was in 1835. Peteroa also erupted in 1837 and 1937. Now it has a small crater lake. Thus, all of these volcanoes are conical. We may surmise that their vents had a large sealing plug (vent fill) in 1835. These common features are important for our triggering model which will be discussed below. Darwin (1839, p. 276) reports that the craters of Minchinmavida and Yanteles were covered by snow.

It is known (Kolsky 1953) that when a compression wave is propagated along a cone from the bottom, the wave amplitude and the form change. In particular, the amplitude increases strongly. At the same time, a tension tail develops along the axis behind the compression region and the length of the compression becomes shorter and shorter as the tip is approached. At the same time, the tensional stress increases. As a result, the tip may break and fly off at high velocity (see Plate III from Kolsky 1953). Experiments with wedge-shaped plates explosively loaded along and at the centre of the base agree with Kolsky's experimental data. For different triangular plates the fractures were localized near the angles and along the height (see Plates 8 and 9 from Johnson 1972).

Thus, the experiments showed that the fractures group near the tip and the axis of the cone. In particular, the axis fractures recall cavitation bubbles in a liquid.

Fractures can also occur in earthquake-induced conic volcanoes having large vents. The vent fill material usually has a very low tensional strength and can easily be fragmented by tension waves. When a compressional vertical wave is reflected from the vent surface then a large number of fractures ('bubbles') occur. As a result, the material is transformed into a gas-fluidized state. This process recalls the generation of transient cavitation during the reflection of an underwater shock wave from a water surface (see Fig. 18, taken from Galiev 1988). A similar

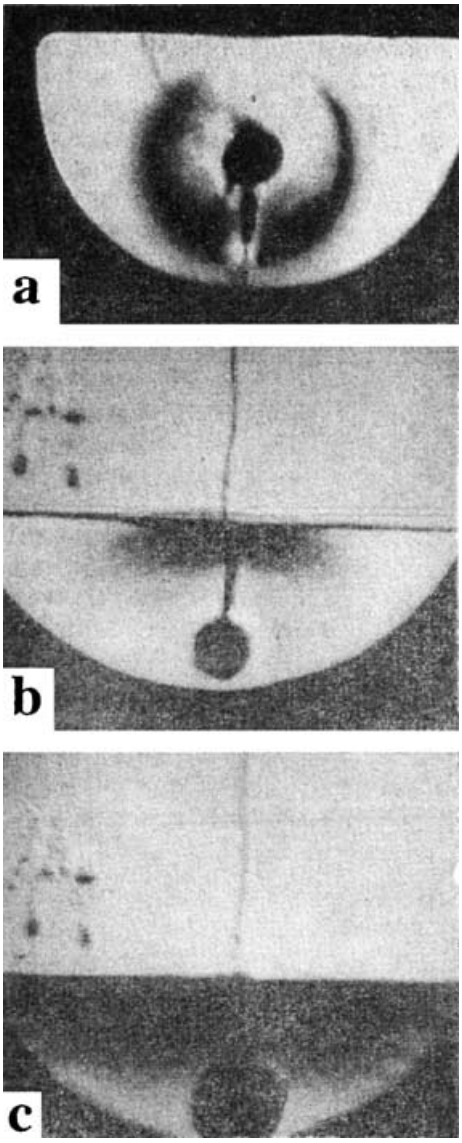

Figure 18. Interaction of an underwater explosion with a free water surface: the spherical wave generated by the explosion (a), and the propagation of the reflected tension wave and the transient cavitation from the free surface (b, c).

phenomenon can be also generated on the surface of metal, glass, polymethymethacrylate, concrete and rock-like materials (Kolsky 1953; Rinehart 1960; Johnson 1972). Johnson (1972, Plate 3) shows a section of a mild steel plate after surface detonation. A large surface bubble is formed by a thin layer of the metal which separated from the mass of the plate. Once the shallow surface cavity has formed, the remainder of the incident compressive impulse is reflected from a fresh free surface. As a results, new fractures and bubble-like voids localized near the axis are generated.

We emphasize that the vertical motion and the surface fractures just discussed are not limited to small phenomena. Localization of fractures in a cone-type mountain was observed following a 1.7 kiloton underground nuclear blast (Rinehart 1960). Near the top the stress wave produced three slabs of equal thicknesses (≈35 m). The slabs moved upward with initial velocities, approximately, 2.4, 1.5 and 0.7 m s^{-1}, respectively. The surface slab of consolidated tuff, situated about 230 m above the blast, rose to a height of 22.5 cm. The converging seismic waves can explain the violent crest amplification, which was observed in Quiriquina. Charles Darwin (1839, p. 370) reports about this amplification *'. . . The effect of the vibration on the hard primary slate, which composes the foundation of the island, was still more curious: the superficial parts of some narrow ridges were as completely shivered, as if they had been blasted by gunpowder. This effect . . . , be confined to near the surface . .'*.

The reflection of the upward wave from the volcano slope may produce tensional stresses which are sufficiently large to cause fractures and bubbles within the volcano (Fig. 19a). The conduit magma is held at high pressure by the weight and the strength of the vent fill. This fill may collapse (Fig. 19b) and fly off (Fig. 19c) when the upward wave is reflected from the volcano crater. After this the pressure on the magma surface drops to atmospheric P_a and a decompression front begins to move downward (Fig. 19c). In particular, large gas bubbles can begin to form in the magma within the conduit. The resulting bubble growth provides the driving force at the beginning of the eruption (Anilkumar

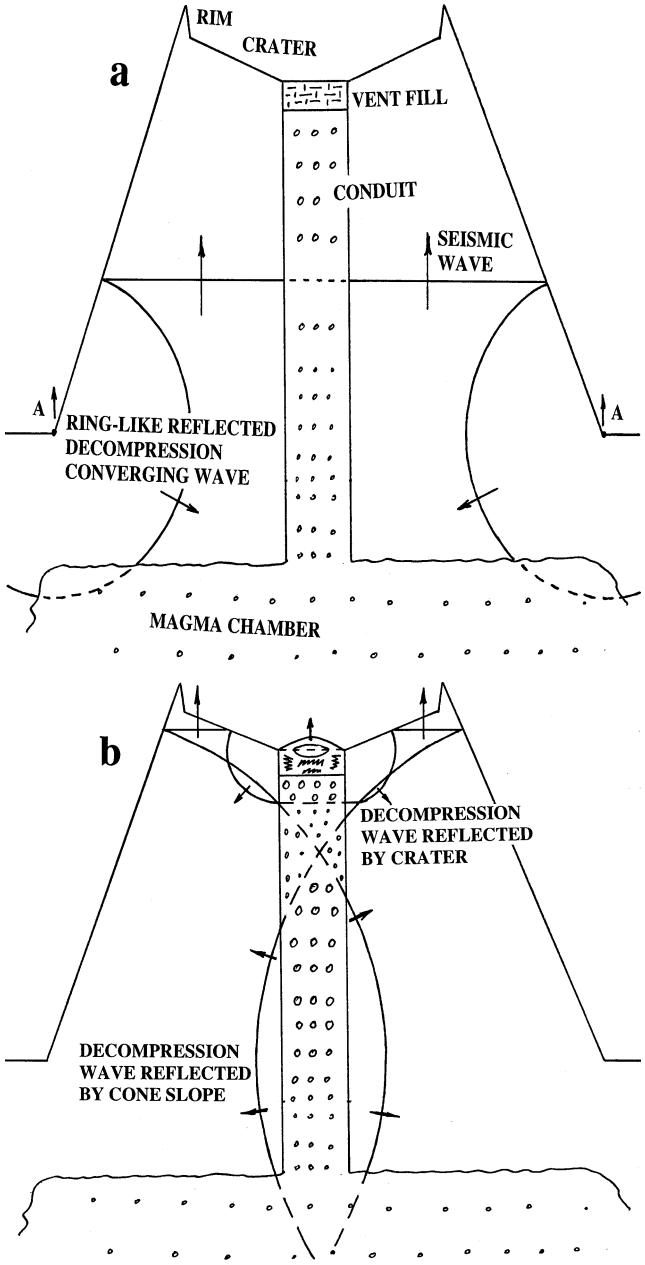

Figure 19 Dynamics of the interaction of a conical volcano truncated by a crater with an upward seismic shock wave. The volcano scheme (mountain, crater, vent fill, conduit and magma chamber) and the tension waves reflected from the lateral surface (a). The tension waves reflected from the crater surface, the beginning of vent fill collapse and the growth of bubbles in magma due to the tension (b). The failure of the vent fill, the growth of the magma bubbles and the beginning of the larger-scale eruption (c).

et al. 1993; Alidibirov & Dingwell 1996; Mader 1998; Morrissey & Mastin 2000). Thus, the earthquake-induced non-linear wave phenomena can qualitatively explain the spectacular simultaneity of large eruptions after large earthquakes. The model will be discussed further in Section 6.3.

The amplitude of the decompression wave is of the order of P_a. This wave is reflected by the high-pressure magma chamber as a compression wave with amplitude close to P_0 (Fig. 19c). As a result, the pressure difference between a region of low pressure (atmosphere) and the magma chamber can cause a large-scale eruption (Fig. 19c). The beginning and the process of the eruption depend on many circumstances. In particular, due to reverberations and transformations of the wave in the conduit the eruption can become pulsatory (Dobran *et al.* 1993). For example, if the chamber is located at depth and P_0 is large then explosion-like phenomena can occur during the reflection of the compression wave from the vent. According to Clarke *et al.* (2002) the initial conduit gas pressure can be of the order of 10 MPa. Let us estimate the period of the pulsations. The conduit magma contains a lot of gas, therefore the wave speed C_m can vary from a few m s^{-1} (Kieffer 1977) to several tens of m s^{-1} (Puzyrev & Kulikov 1980; Galiev & Galiev 1994; Galiev & Panova 1995; Morrissey & Mastin 2000). Indeed, according to eqs (21) and (22) we have

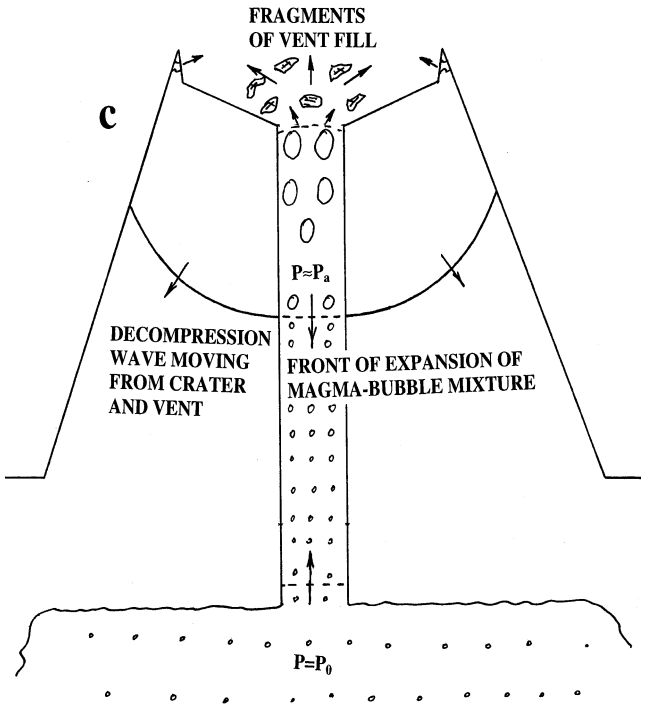

Figure 19. (*Continued.*)

$$C_m^2 = \frac{dp}{d\rho} = \frac{\{(1-\phi_0)[1-\lambda(p-p_0)]+\phi_0 p_0/p\}^2}{\rho_0[(1-\phi_0)\lambda+\phi_0 p_0 p^{-2}]}. \tag{216}$$

Thus, the sound velocity C_m is a complex function of ϕ_0, p_0 and p. It follows from Galiev & Galiev (1994) that C_m can depend strongly on the gas content. In particular, if ϕ_0 increases from 0 then C_m can drop from 2000 to 10 m s^{-1}. If ϕ_0 decreases from 1 then C_m drops from the velocity of sound (300 m s^{-1}) to 10 m s^{-1}. When the conduit length is of the order of 10 km, then the period of the pulsatory explosions can lie in the range from minutes to hours. Resonant shock waves similar to shock waves in tubes containing bubbly liquid or gas (Chester 1964; Galiev *et al.* 1970; Galiev 1988; Galiev & Galiev 1994; Ilgamov *et al.* 1996) may be generated in a conduit.

Remark. We have illustrated the model using the experimental data for short waves (Figs 18 and 19). These figures illustrate wave reflection and generation of the tension waves in thick vent fills and in the conduit magma. However, for thin vent fills it is better to describe them as a thin plate closing the conduit (Galiev 1981; Galiev 1988).

6.3 Discussion of the models of Sections 6.1 and 6.2

The theory of Section 6.1 describes the dynamics of a crater on the surface of liquified material. There is an analogy between these dynamics and the evolution of a crater generated by a bubble bursting at a free water surface (Kientzler *et al.* 1954) or the collision of a liquid drop with the surface of a deep liquid (Worthington 1908). The experimental data were obtained by high-speed photography. The photographs and calculations (Hobbs & Kezweeny 1967) show the behaviour of the free surface through the following sequence of events: (1) the crater and a rim (crown) are formed; (2) the height of the rim reduces and liquid rushes to the crater centre; (3) the rush forms a jet in the crater centre. It can be seen from Fig. 20 (Fig. 20a taken from Worthington 1908, 20(b, f) taken from Hobbs & Kezweeny 1967) that the height of the jet (column) can reach 2.5 R_{12}. The radial rush of liquid is reminiscent of the plume and converging wave in the volcano crater. Indeed, the photographed liquid column (Fig. 20a) is similar to the column of matter calculated for the volcano crater (Fig. 17). Using this analogy we can estimate the height of the ejected column. Let $R_{12} = 200$ m. Then according to Fig. 20(a), this height can reach 500 m. If $R_{12} = 500$ m, then the height is 1250 m. On the whole, these values agree with the result of Section 6.1 (height 1–2 km).

Linde & Sacks (1998) indicated clearly that a great earthquake can be a trigger mechanism for large eruptions. In particular, it was shown that there is a sharp peak in the number of eruptions on the same day as an earthquake. We have constructed a model that explains this peak. The model takes into account the amplification of the upward seismic wave near the top of a conical volcano and the interaction of this wave with the crater surface. The elements of the model are fragmentation of the vent fill, connection of the atmosphere and the high-pressure conduit, growth of bubbles (cavitation) and the beginning of the eruption (generation of the column of ejected matter).

The results presented in Sections 6.1 and 6.2 are reminiscent of data from underwater explosions (Cole 1948). Indeed, the water layer between the free surface and the gaseous products of the explosion can be considered as an analogue of the vent fill. The shock wave generated by the explosion is the analogue of the upward compressional seismic wave. The interaction of the shock wave and the water surface forms the surface cavitation funnel (see Fig. 18). This funnel is the analogue of the volcano crater. The high-pressure product of the explosion is the analogue of the conduit magma.

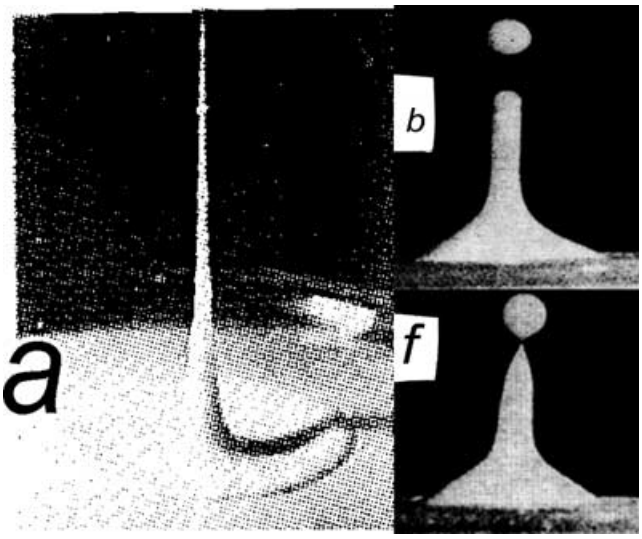

Figure 20. Jet formed by the liquid inrush focusing in the crater centre. [Similar to Worthington 1908 (a) and Hobbs & Kezweeny 1967 (b, f)].

In the case of a deep explosion the cavitation funnel does not propagate up to the gaseous product. A jet is generated on the funnel axis (see Plate XI from Cole 1948) due to the rush of the surface water. This process (see Figs 17 and 18) recalls the formation of the column of ejecta in the crater described in Section 6.1. In the case of a shallow explosion the cavitation funnel can be so deep that it connects the gaseous products with the atmosphere. As a result, these products, together with the water jet form a vertical column (see Plate XI from Cole 1948 and Fig. 109 from Lavrentev & Shabat 1977). The height of the column may be 600 m or more. This process recalls the dynamics of the large-scale eruption modelled in Section 6.2. Of course, the analogy between crater evolution (see Figs 17 and 19) and water surface dynamics occurs only for sufficiently large charges.

We considered how earthquake/volcano interaction explains Darwin's evidence in Sections 6.1 and 6.2. However, the models developed may be valid for other large earthquake-triggered eruptions. Indeed, all 20 of the single-day earthquake/eruption pairs listed by Linde & Sacks (1998) took place for cone-like volcanoes and large (magnitude ≥ 7) or very large (magnitude ≥ 8) earthquakes. Following Section 6.1, a column may be instantaneously generated in the craters of the conical volcanoes excited by the large earthquake. Of course, the effect depends on the form of the crater and the initial state of the volcano. For example at Ruapehu (Tongariro National Park, New Zealand), the boundary in magnitude of volcanic earthquakes, between those that accompany eruptions and those that do not, varies between about magnitude 2 under 'open-vent' conditions, and magnitude 3.4 under 'closed' conditions (Latter 1981). I think that the shape and the state of the four volcanoes during the 1835 Chilean earthquake were such that the vent fills were fragmented and the large-scale eruptions took place. The earthquake opened the conduits and the magma chambers and magma begun to erupt similarly to champagne from a bottle. The effect of the interaction of volcanoes (conduits) could take place and remind one of the tuning of resonant pipes in an organ.

It is interesting that the majority of the volcanoes presented in the list of earthquake-triggered eruption pairs (Linde & Sacks 1998) are truncated by large calderas. This observation agrees with Darwin's note (1839, p. 380) about 'great chimneys'.

6.4 Resonant capture of seismic waves by a ridge

Topographic relief can modify the velocity and path of a seismic wave. In particular, a ridge can form a waveguide. We consider this effect using the theory of Section 4.4.1. First, the expression for the velocity a_*, eq. (114) is treated. The velocity depends on the coordinates of the ridge and on time. The time dependence is determined by the vertical acceleration, so we have approximately $Z = Z(t)$, eq. (121). In this case, the expression for a_*^2, eq. (114) can be written as

$$a_*^2 = Z^*(x_1, x_2)/Z(t), \tag{217}$$

where $Z^*(x_1, x_2) = [h + 2E_1G_* + 4bh(1 - h_0^{-1}E_1G_*)G_*/3]$. For simplicity we ignore the weak dependence of Z^* on t. A ridge located on a shallow valley will be treated.

We assume that

$$Z^*(x_1, x_2) = H_0 + A_m \operatorname{sech}^2[e_m(x_1 + x_2)], \tag{218}$$

where $H_0 = h_0 + 2E_1G_* + 4b(h_0 - E_1G_*)G_*/3$. The function $A_m \operatorname{sech}^2[e_m(x_1 + x_2)]$ describes the ridge, and the constants A_m and e_m determine the height and form of the ridge. Now the resonance condition (166) yields

$$Z(t)k_{12}^2a_t^2 = \{H_0 + A_m \operatorname{sech}^2[e_m(x_1 + x_2)]\}[(k_{1,1} + K_{12,1})^2 + (k_{2,2} + K_{12,2})^2]. \tag{219}$$

Let us assume in eq. (219) that

$$a_t^2 = Z^{-1}(t), \quad k_{12} = 1, \quad k_1 = \xi_* x_1, \quad k_2 = 0, \quad K_{12} = a_m \tanh[e_m(x_1 + x_2)], \tag{220}$$

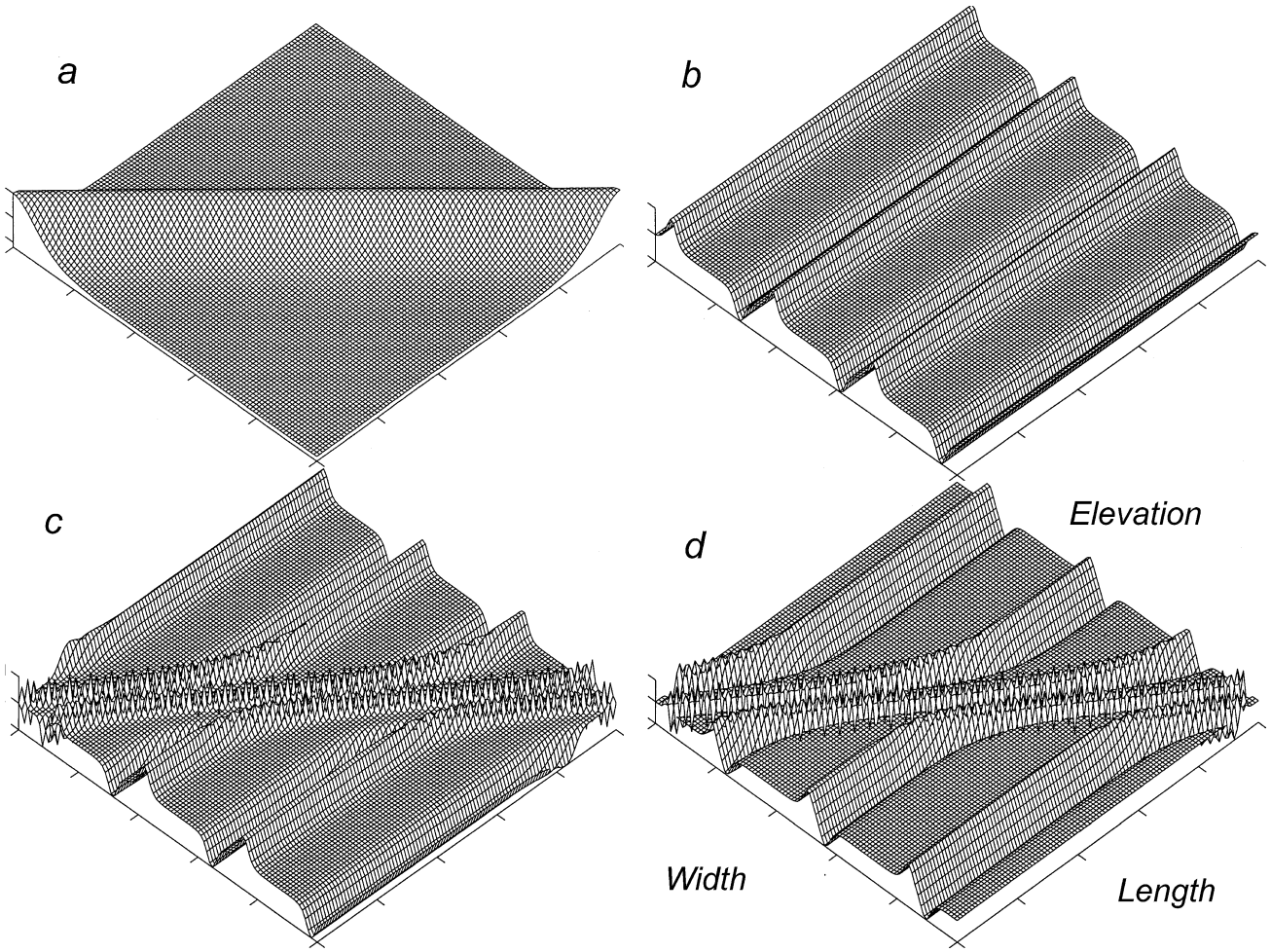

Figure 21. 2-D simulation of the capture of seismic waves by a ridge: the undisturbed surface of the valley (a), the resonant wave pattern calculated for the flat surface (b), the resonant wave patterns calculated for $a(t) = 0.5$ (c) and $a(t) = 1.3$ (d).

where ξ_* and a_m are constants. Expressions (220) are substituted into (219). We assumed that $\mathrm{sech}^2[e_m(x_1 + x_2)] \tanh^2[e_m(x_1 + x_2)] \approx 0$. Then, equating to zero the constants and terms containing $\mathrm{sech}^2[e_m(x_1 + x_2)]$, we obtain two algebraic equations:

$$\xi_*^2 = H_0^{-1}, \tag{221}$$

$$a_m^2 + \xi_* e_m^{-1} a_m + 0.5 A_m \xi_*^2 e_m^{-2} (A_m + H_0)^{-1} = 0. \tag{222}$$

Eq. (222) yields

$$a_m^{\pm} = 0.5\{-\xi_* e_m^{-1} \pm [\xi_*^2 e_m^{-2} - 2A_m \xi_*^2 e_m^{-2} (A_m + H_0)^{-1}]^{1/2}\}. \tag{223}$$

Now using eqs (220), (221) and (223), we have found expressions for r and s, eq. (160). Since $\varphi_{rs} \approx 0$, we have for φ that

$$\begin{aligned}\varphi = {} & J\{a(t) - H_0^{-0.5} x_1 - a_m \tanh[e_m(x_1 + x_2)]\} \\ & + J\{a(t) + H_0^{-0.5} x_1 + a_m \tanh[e_m(x_1 + x_2)]\}.\end{aligned} \tag{224}$$

Here J is an arbitrary function. Consider the resonant oscillations of the valley, when the driving frequency $\omega = N\pi a_*/L$. The resonant waves are determined by the expression (Galiev 1998, 1999; Galiev & Galiev 2001),

$$J(r) = A_i \,\mathrm{sech}^2(e_i \sin N\pi L^{-1} H_0^{1/2} r) \cos^2 N\pi L^{-1} H_0^{1/2} r, \tag{225}$$

where A_i and e_i are constants. These constants are determined by the non-linear and dissipative–dispersive characteristics of the system.

Now, using eqs (224) and (225), we can calculate the vertical displacement, since η is proportional to $\nabla^2\varphi$. Assuming that $a(t) = 0.5$ the 1-D wave resonant pattern calculated for the flat (without the ridge) surface of the valley is shown in Fig. 21(b). The influence of the ridge is shown in Fig. 21(c) ($a(t) = 0.5$) and Fig. 21(d) ($a(t) = 1.3$). The ridge traps the seismic waves. The 2-D patterns in Figs 21(c) and (d) demonstrate qualitatively the waveguide-like properties of the ridge.

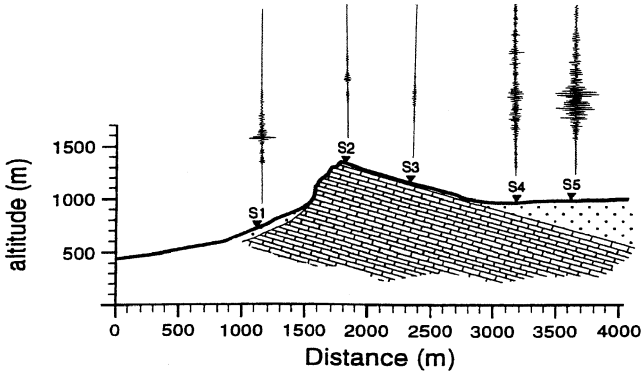

Figure 22. Amplification of seismic waves propagating in the sediment layer at the layer edge and within the slope of the ridge. From Pedersen *et al.* (1994). Used with permission.

7 SITE RESONANCE AND STRONGLY NONLINEAR SEISMIC PHENOMENA

The amplification of seismic waves due to resonant and topographic effects is a complex process, which is connected with site geology and the liquefaction. In particular, although earthquake-related damage tends to be more intense on ridge tops some observations suggest that the damage can concentrate on one side of a ridge. During the 1994 Northridge earthquake Ashford & Sitar (1997) observed damage to be concentrated on one slope of a coastal bluff in the Pacific Palisades, perpendicular to the wave travel path. The damage and the coastal amplification of seismic waves may be very strong (Davison 1936; Kramer 1996; O'Rourke & Pease 1997). Darwin (1839, p. 375), describing the 1835 Chilean earthquake, wrote that '*... the island of S. Maria.... raised to nearly three times the altitude of any other part of the coast*'. This type of amplification depends on the 3-D geology of the surface (O'Rourke & Pease 1997; Pease & O'Rourke 1997). A clear example of the influence of geology on seismic waves in a layer and site effects was found by Pedersen *et al.* (1994). A number of seismometers were placed across a 300 m high linear ridge in France (see Fig. 22 which was taken from Pedersen *et al.* 1994). Two of the stations (S2 and S3) were established on hard limestone, whereas the remaining three stations were placed on unconsolidated sediments. The greatest amplification took place at S5, near, but not very close to, the edge of the sediment layer. At this point there can be both amplification of waves travelling up slope and attenuation of waves travelling down slope. Thus, the concentration of seismic energy depends on the slope angle and occurs near the edge of the layer.

This amplification depends on the layer thickness variation, the spatial variation of motion (the horizontal motion transforms partly into vertical motion) and the impedance contrast between the downlying material and the sediments. Consider non-linear waves in a layer of marine deposits. Because of the earthquake-induced vibrations, the shear stress drops to zero and the layer material is practically transformed into a liquid. As a result, a strong analogy may be the amplification of earthquake-induced sediment waves and water waves (tsunami) at the coast line. For example, the Alaska 1899 earthquake raised the coast on Disenchantment Bay up to 14.5 m (Davison 1936). There were over 50 shocks on September 10. The first earthquake lasted 90 s. The main earthquake that caused great topographic changes occurred at 21:41 UTC (see http://neic.usgs.gov/neis/eqlists/USA/1899_09_10.html). I think they are a result of the resonance of seismic waves in a liquified coastal layer. It is known that the shear wave velocity can drop from 160 m s^{-1} to less than 10 m s^{-1} (up to 2–5 m s^{-1}) over a 16 s period as a result of earthquake-induced vibrations (Pease & O'Rourke 1997).

In this section we study the seismic wave evolution near the edge of the sediment layer and within the resonant band.

7.1 A new equation for edge waves

We shall describe 1-D seismic waves on a gentle slope using the equations of Section 2. In particular, for 1-D waves eq. (29) yields

$$(u_{1,tt} - X)(1 + u_{1,1}) + (2n+1)^{-1}\eta_{tt}\eta_1 + g(n+1)^{-1}(\eta_1 - \eta_1^+) + g\eta_1^- = -\rho^{-1}P_1$$
$$+ \frac{2}{3}\rho^{-1}G_*[(2u_{1,11} - h^{-1}\eta_1) - h^{-1}(\eta_1^+ - \eta_1^-) + 2u_{1,1}u_{1,11} + 2(2n+1)^{-1}\eta_1\eta_{11}]$$
$$- \frac{2}{3}h^{-2}\rho^{-1}n^2(2n-1)^{-1}G_*\eta\eta_1 + \rho_0^{-1}s_{11,1} + \rho^{-1}h^{-1}\tau_{31}. \qquad (226)$$

Thus, we have four equations (226), (23), (28) and (32), for four unknown values: u_1, P, ρ and η. Now, following Section 3, we can reduce this set of the equations to

$$u_{1,tt} - a_0^2 u_{1,11} + (2n+1)^{-1}(1 - a_1^{-1}\eta)\eta_1\left[\eta_{tt} - \frac{4}{3}\rho_0^{-1}G_*(1 + h^{-1}\eta + a_1^{-1}\eta)\eta_{11}\right]$$
$$= g[(n+1)^{-1}\eta_1^+ - \eta_1^-](1 - u_{1,1}) + \frac{2}{3}h^{-1}\rho_0^{-1}G_*(\eta_1^+ - \eta_1^-)(1 + h^{-1}a_1u_{1,1}) - X - gh_1$$
$$+ (\beta u_{1,1} + \beta_1 u_{1,1}^2)u_{1,11} + \mu u_{1,11t} - A_1^* h(n+2)^{-1}(u_{1,11tt} - \rho_0^{-1}G_*u_{1,1111}) + \rho_0^{-1}s_{11,1} + \rho_0^{-1}h^{-1}\tau_{31}, \qquad (227)$$

where $\eta = A_1^* u_{1,1} + A_2^* u_{1,1}^2 + A_3^* u_{1,1}^3$ and

$$a_0^2 = 2\rho_0^{-1} G_* + 2A_4^* \left(1 - \frac{2}{3} b G_*\right)(gh + \rho_0^{-1} G_*), \tag{228}$$

$$\beta = -\rho_0^{-1}\{(\chi g \rho_0 + 2h^{-1} G_*)[2A_2^* + h^{-1}(A_1^*)^2] + g\rho_0 (n+1)^{-1}(2A_2^* - A_1^*) - \frac{2}{3} G_* [2 - n^2 (2n-1)^{-1}(A_1^*)^2 h^{-2} + 3h^{-1} A_1^*]\}, \tag{229}$$

$$\begin{aligned}\beta_1 = -\rho_0^{-1} \Bigg\{ & \left(\chi g \rho_0 + \frac{4}{3} h^{-1} G_*\right)[3A_3^* + h^{-1}(A_1^*)^2 - 2h^{-1} A_1^* A_2^*] + g\rho_0 (n+1)^{-1}(3A_3^* - 2A_2^* + A_1^*) \\ & + \frac{2}{3} h^{-1} G_* (3A_3^* - 2A_2^* - 2A_1^* + 3h^{-1} A_1^* A_2^*) + \frac{2}{3} n^2 (2n-1)^{-1} h^{-2} G_* [3A_1^* A_2^* + h^{-1}(A_1^*)^3] \Bigg\},\end{aligned} \tag{230}$$

$$\chi = (2n+1)/(n+1), \tag{231}$$

$$A_1^* = -h\left(1 - \frac{2}{3} b G_*\right) A_4^*, \; A_2^* = h[1 + A_5^*(b + \phi_0 P_0^{-2} A_5^*)] A_4^*, \tag{232}$$

$$A_3^* = h\left[A_2^*\left(\chi g \rho_0 + \frac{4}{3} h^{-1} G_*\right)(2\phi_0 P_0^{-2} A_5^* + b) - 1 - \phi_0 P_0^{-3}(A_5^*)^2 (1 - A_5^*) - b A_5^*\right] A_4^*, \tag{233}$$

$$A_4^* = 1 \Big/ \left[1 + bh\left(\chi g \rho_0 + \frac{4}{3} h^{-1} G_*\right)\right], \qquad A_5^* = -\frac{2}{3} G_* + \left(\chi g \rho_0 + \frac{4}{3} h^{-1} G_*\right) A_1^*. \tag{234}$$

Eq. (227) corrects eq. (45) as it takes into account more accurately the vertical acceleration and the compressibility. As a result of this correction the wave velocity a_0 begins to depend on n. We recall that n determines the variation of the vertical displacement along the layer thickness, eq. (25). If $h \to \infty$ we have

$$a_0^2 = \frac{2}{3} \rho_0^{-1} \nu (1 - \alpha_s \phi_0)[2 - (2n+1)^{-1}] + 2(n+1)(2n+1)^{-1} \rho_0^{-1} [\lambda(1 - \phi_0) + \phi_0 P_0^{-1}]^{-1}. \tag{235}$$

It is seen that the effect of the vertical displacement may be important. If $\lambda \to \infty$ and $\phi_0 = 0$ in eq. (235), then $a_0^2 = \frac{2}{3}\rho_0^{-1}\nu[2 - (2n+1)^{-1}]$. In this case, if $n = 0.2$, we have the velocity of Rayleigh waves (Sheriff *et al.* 1995):

$$a_0 \approx 0.92(\rho_0^{-1}\nu)^{1/2}. \tag{236}$$

If $n = 0.5$, we have the velocity of shear waves $a_0 = (\rho_0^{-1}\nu)^{1/2}$.

According to eq. (227) perturbations having different speeds can be generated in the layer. The first speed is a_0, while the second speed is $\sqrt{4\rho_0^{-1}\nu(1 - \alpha_s\phi_0)/3}$. This result is valid only for weakly cohesive materials. Let us consider the vertical acceleration effect for liquified layers where $\lambda \to 0$. For simplicity we assume that $\nu \approx 0$ and $\phi_0 = 0$. In this case $a_0^2 = 2gh$, $\eta \approx -hu_{1,1}$, $\beta = -6gh$, $\beta_1 = 12gh$ and eq. (227) yields

$$\begin{aligned}u_{1,tt} - 2ghu_{1,11} - h(2n+1)^{-1} u_{1,11}\eta_{tt} = {} & g(n+1)^{-1}\eta_1^+ - X - gh_1 \\ & - 6gh(u_{1,1} - 2u_{1,1}^2)u_{1,11} + \mu u_{1,11t} + h^2 (n+2)^{-1} u_{1,11tt} + \rho_0^{-1} h_0^{-1} \tau_{31},\end{aligned} \tag{237}$$

where some small terms were neglected. It is seen that terms $2ghu_{1,11}$ and $6gh(u_{1,1} - 2u_{1,1}^2)u_{1,11}$ are different from the analogous terms in eqs (45) and (46). There is a term $h(2n+1)^{-1}u_{1,11}\eta_{tt}$ in eq. (237) that is absent in eq. (45). These differences are a result of the influence of vertical acceleration. Thus, although some terms of eq. (237) are similar to terms of eqs (45) and (46), we have derived here a new approximate equation for coastal waves. The terms of eq. (237) modify the linear, quadratic and cubic terms in Airy's equation (Airy 1845). Indeed, Airy (see eq. 46) did not consider coastal waves and had concluded $a_0^2 = gh$. However, it is known (Peregrine 1983) that near a beach the wave velocity a_0 is not well determined. The non-linear wave shape is usually unsteady and each point on the wave such as the highest point or point of maximum slope has a different, time-varying velocity. According to Peregrine (1983) it is realistic to expect a change of water wave velocity from gh to $2gh$ near a beach. The vertical component of the surface acceleration usually increases when the layer thickness reduces. For water waves this effect is seen well near the ocean coast. Thus, according to Airy's theory and eq. (237), when the water depth is reduced the water wave velocity varies from $a_0 = (gh)^{1/2}$ (far from the coast, Airy's model) to $a_0 = (2gh)^{1/2}$ (near the coast). Of course, this result is purely qualitative since near the coast assumptions (16), (26) and (27) should be corrected. However, eqs (227) and (237) properly describe the tendency for change in wave velocity. Indeed, according to Peregrine (1983) vertical accelerations greater than $5g$ can occur in natural breaking waves. Assume that the vertical acceleration η_{tt} in eq. (237) is $5g$. In this case, we have for water waves $a_0^2 = 2gh + 5gh/(n+1)$. If $n = 1$ in this expression (the linear law of the variation of the vertical acceleration along the layer thickness, eq. 25), then $a_0 = (3.666gh)^{1/2} \approx 2\sqrt{gh}$. If $n = 0.75$ (non-linear law of the variation of the vertical acceleration along the layer thickness, eq. 25), then $a_0 = 2\sqrt{gh}$. These results agree well with Peregrine's prediction (1983, p. 158). Thus, the speed of non-linear waves in liquified layers is strongly dependent on the vertical

acceleration near the layer edge. The influence of non-linearity on the wave velocity can be approximated by the formula $a_0 = 2\sqrt{g(h+\eta)}$ (Debnath 1994; Remoissenet 1996).

Of course, the preceding results are applicable only to large-amplitude surface waves. For moderate seismic waves in liquified layers we can use the expression $a_0 = \sqrt{gh}$. Let us consider, for example, a wave propagating in a layer with a thickness of 4.5 m. For this wave we have $a_0 \approx 6.5$ m s^{-1} in agreement with field data (Pease & O'Rourke 1997).

7.1.1 The transresonant evolution of the edge waves

Up to this point, we have not taken into account dispersive effects on wave velocity. This effect can be important for sufficiently thick layers. Let us consider a wave $u_1 = \cos \omega c_0^{-1}(c_0 t + x_1)$ propagating in a thick layer. In this case, eq. (39) yields

$$c_0^2 = a_0^2 - 0.333 A_* h^2 (1 - 0.666 b G_*)\omega^2 (1 - \rho_0^{-1} G_* a_0^{-2}). \tag{238}$$

In eq. (238) the most important terms for the analysis were preserved. It follows from eq. (238) that due to dispersion, waves of different wavelengths travel at different phase velocities c_0. According to eq. (238) the dispersion can change sign within the resonant band and every new Fourier component generated by non-linear modification of the initial wave shape has a different velocity. This effect prevents the formation of breaking or tsunami-like seismic waves on the surface of a thick layer.

If $h \to 0$ then the dispersive effect is reduced, the velocity of the wave $c_0 \to a_0$, eq. (238), and resonance occurs. Consider this resonance and the transresonant evolution of waves travelling along the layer slope (Fig. 22) using the results of Section 3.5. Eq. (87) yields $kJ''' + (c_0^2 - a_0^2)J' - \frac{1}{3}\beta_1 (J')^3 + 0.5 g\eta^+ = 0$. We assumed $\beta \approx \beta_2 \approx \beta_3 \approx 0$, $X = 0$, $h - h_0 \approx 0$ and $C_1 = 0$ in eq. (87). The preceding equation is rewritten so that

$$\eta^3 + 1.5 h^2 R\eta / 2^{2/3} + \Phi(c_0 t + x_1) = K_* \eta'', \tag{239}$$

where $\eta = hJ'$, $R = 2^{5/3}\beta_1^{-1}(a_0^2 - c_0^2)$, $K_* = 3kh^2\beta_1^{-1}$ and $\Phi\ (c_0 t + x_1) = -1.5 g h^3 \beta_1^{-1}\eta^+$. If $h \to 0$ then the difference $a_0^2 - c_0^2$ is small and depends on dispersion, non-linearity and vertical acceleration. We assume that the transresonant parameter R can vary near the layer edge from a positive to a negative value. Thus, the problem is reduced to the solution of equation (239). Using the analytical solutions of this equation we studied the non-linear transresonant evolution of harmonic (Figs 23 and 24) and solitary-type (Fig. 25E) waves near and at the edge of the layer (Fig. 22). Thin curves in Figs 23 and 24 show the variation of R.

First, we considered the case $\Phi(c_0 t + x) = Ah^2 \sin 0.5(c_0 t + x_1)$. Solutions of eq. (239) were constructed by the iterative method. We assumed approximately that $K_* \approx 0$. As a result algebraic solutions similar to (201)–(205) were found. Then the algebraic solution for the case $i = 2$ [see solutions (203)] was corrected. It was suggested that within the resonant band the dispersion is a function of the transresonant parameter R and $K_* = 0.024R + 0.1R^2$. The temporal and spatial evolution of the harmonic wave near the layer edge is shown in Fig. 23 for $L = 20$ m. $R = h/h_0 + 2(Ah_0/h)\,\mathrm{sech}[L\pi^{-1}(0.88h - 2A)]\cos[0.5(c_0 t + x)]$. $c_0 = (gh_0)^{0.5} h_0 = 1$ m, h varying from 1 m to 0, and $A = 0.1$ m. It is seen that the generation and evolution of the breaking wave are described by the analytical solution of eq. (239).

Reduction of the slope of the lower surface of the layer complicates the picture of coastal wave evolution (Fig. 24). The calculations were repeated for $L = 50$ m. Two breaking waves are shown in Fig. 24. Particles, voids and vortices can be generated due to the overturning of sediment (water) waves.

The transresonant evolution of the solitary-type wave near the layer edge is shown in Fig. 25. The case $\beta = -3gh_0$ was considered. The bottom slope $s = \frac{1}{15}$ (Figs 25A and C) or $\frac{1}{100}$ (Figs 25B, D and E). The initial waves are shown in Fig. 25(A)–(D) by dotted curves. Fig. 25 also simulates the coastal water waves. In particular, the profiles (A)–(D) show the evolution of solitary water waves on sloping plane beaches which was studied by Smith (1998). The quadratic non-linearity effect is taken into account. In this case eq. (87) yields that

$$(J')^2 + 0.666 RJ' - 0.333 h^{-1}\eta^+ = 0, \tag{240}$$

where $\eta^+ = l\,\mathrm{sech}^2 \alpha r$, $r = c_0 t - x_1$, $R = 1 - gh/(gh + g\eta^+)$ and

$$R \approx \eta^+ / h \approx l h^{-1}\,\mathrm{sech}^2 \alpha r. \tag{241}$$

The profiles A, B (Fig. 25) were calculated according to eq. (240). Taking into account eq. (241) we approximately assume that R varies near the front of the wave so that $R = -6.5(h_0 - h)^3\,\mathrm{sech}\{5(h_0 - h)[\alpha(r + h_0 - h)]\}$ and $\alpha = 0.5$. It is seen that the simple algebraic equation (240) describes qualitatively the wave evolution and results of numerical calculations (Smith 1998; Figs 7 and 8). Then effects of weak dissipation and weak dispersion on the wave evolution were studied. Using eq. (87) we derive the following equation for $c_0^2 = a_0^2$:

$$2kh\beta^{-1}\eta'' + 2\mu_* h c_0 \beta^{-1}\eta' - \eta^2 = glh^2\beta^{-1}\,\mathrm{sech}^2 \alpha r. \tag{242}$$

Following Sections 5.1 and 5.2 we construct an approximate solution of eq. (242),

$$\eta = \sqrt{\varepsilon}\{\tanh[-\beta\sqrt{\varepsilon}(\mu_* c_0 h\alpha)^{-1}\arctan(\exp \alpha r - C) + C_1] + \Phi_1\}\,\mathrm{sech}(\alpha r), \tag{243}$$

where $\varepsilon = -glh^2/\beta$,

$$\Phi_1 = k\beta\sqrt{\varepsilon}(\mu_*^2 c_0^2 h)^{-1}\exp(\alpha r)[1 + \exp(2\alpha r)]^{-1}\,\mathrm{sech}^2[-\beta\sqrt{\varepsilon}(\mu_* c_0 h\alpha)^{-1}\arctan(\exp \alpha r - C) + C_1]. \tag{244}$$

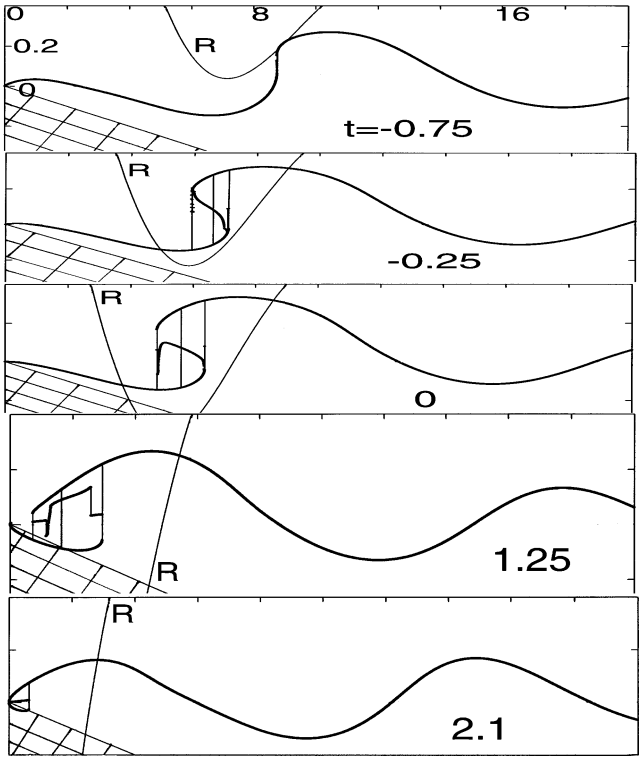

Figure 23. Dynamics of the intense periodic transresonant waves near the layer edge: the beginning of the overturning and the overturning of the breaker.

Profiles *C* and *D* (Fig. 25) were calculated according to solution (243) for $C_1 = 0$, $C = 1 - h/h_0$. Boundary friction was taken into account, therefore in eq. (242) $\mu_* = \mu_f/h_0\rho_0 = 1.15$ m^2 s^{-1}. We assume that the dispersive coefficient k depends on the slope and changes the sign at the resonance. Profiles *C* were calculated for $l = 0.3h_0$, $\alpha = 0.5$ m^{-1}, $k = -gh_0^3$ and profiles *D* for $l = 0.2h_0$, $\alpha = 0.25$ m^{-1}, $k = -1.38gh_0^3$. It is seen that the dissipative and dispersive effects are important for edge wave evolution. In particular, profiles *C* and *D* describe the data of Smith (1998, Figs 7 and 8) better than profiles *A* and *B*.

The transresonant evolution of the solitary wave into tsunami-like wave is shown in Fig. 25(E). Eq. (239) was used. We assumed that $K_* = 0$, $\Phi(c_0t + x_1) = -10h^2\,\mathrm{sech}^2 0.002(c_0\,t + x_1 - L/2)$, $L = 5000$ m, $R = -1.5 + 0.002x_1$, $c_0 = 15.5$ m s^{-1}, $h_0 = 25$ m and h varies from 50 to 0 m. The step in the vertical displacement is formed in front of the wave. The level of the ground surface is depressed ahead of this jump ($t =$ 175 s). As this reduction becomes deeper, a depression wave is formed near the edge of the layer ($t = 200$ s). At the same time the amplitude of the step increases. The solitary wave ($t = 0$ and 75 s) is transformed into a shock-like wave having ahead of it a deep depression (trough) ($t = 200$ s). According to the calculations the solitary wave can be amplified up to four to five times as a result of this transresonant evolution.

The results presented in Figs 23–25 qualitatively describe the wide range of phenomena which can take place due to the focusing of wave energy. In particular, Figs 23 and 24 qualitatively simulate the breaking of water waves on a beach. Thus, water breakers and coastal wave evolution, which are amongst the most common and most striking phenomena in Nature, are the result of a transresonant process. There is also an analogy between the focusing of seismic energy at the edge of a layer and acceleration of the end of the whip.

It is known that breakers can be excited in layers of weakly cohesive material (Jaeger *et al.* 1996). Sometimes shock-like waves having a deep depression ahead have been excited in granular layers under strong vertical excitation (Clément *et al.* 1996). Therefore, breaking waves might be expected to occur during large earthquakes. They rotate the ground surface in the x_1–x_3 plane. Indeed, Darwin (1839, p. 376) reports that '. . . *Some square ornaments on the coping of these same walls were moved by the earthquake into a diagonal position*. . .' and '. . . *the displacement at first appears to be owing to a vorticose movement*. . . '. Our calculations show that this 'vorticose movement' can be generated by earthquake-induced breaking waves propagating in liquified surface soil.

Darwin (1839, p. 377) also wrote that '. . . *the whole body of the sea retires from the coast, and then returns in great waves of overwhelming force*. . .'. Now this type of wave is called a tsunami. The tsunami may run ashore as a breaking wave, a wall of water or a tide-like flood. It is seen that the note qualitatively agrees with Fig. 25(E) where the appearance of the ebb and the formation of a non-linear wall of sediment are shown.

The evolution of surface waves near a coastline (transformation of the initially smooth waves into shock-like waves, breakers and vortices) is a long-standing problem. Here it has been shown that the problem can sometimes be simplified and solved analytically using the recently developed theory of transresonant wave processes (Galiev 1999a; 2000, 2003; Galiev & Galiev 2001). According to the analysis presented, amplification and the breaking of the seismic waves are possible in the liquified sediment layer if $h \to 0$. Perhaps, these effects explain the

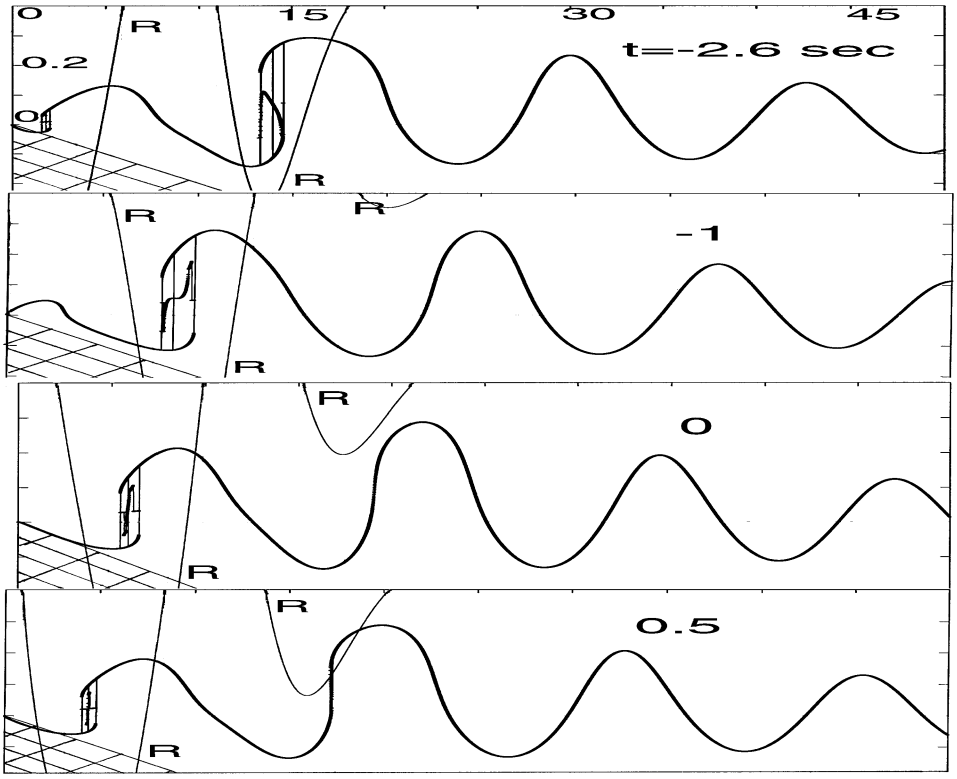

Figure 24. Dynamics of the intense periodic transresonant waves in the shallow layer edge: the growth and the curl of the waves and the breaking of the waves.

Alaska 1899 earthquake elevation of the coast up to 14.5 m (Davison 1936), the experimental data of Pedersen *et al.* (1994, see also Fig. 22) and the concentration of damage in marine deposits (O'Rourke & Pease 1997; Pease & O'Rourke 1997).

Thus the coastal evolution of waves is a site transresonant phenomenon (Mei & Liu 1993). A similar evolution can take place for any non-linear wave process if R is varied near $R = 0$.

7.2 Amplification, attenuation and evolution of transresonant waves

The width of the resonant frequency band depends on the amplitude of the excitation. For example, the width is determined by the equality $|R_*| = 1$ (see Section 5.1.2), therefore we have $(-4la_0^2/\beta L)^{1/2} = -\pi a_0^3(\omega_1 + \omega^*)/\beta L\omega^2$, which yields

$$\omega_1 + \omega^* = -2\beta\pi^{-1}\omega^2 a_0^{-2} L(-4l/\beta L)^{1/2}. \tag{245}$$

It follows from eq. (245) that $\omega_1 + \omega^* \to 0$ if $l \to 0$. As a result of the narrowing of the resonant band, weak waves cannot be amplified. Apparently, the wave is amplified in the resonators only if its amplitude exceeds some critical level. According to Beresnev & Wen (1996) this level for vertical earthquake-induced waves of acceleration may be near $0.1g_0$.

Let us consider the strong motion. We shall use eq. (87) assuming that $-\mu a_t J''' + gh_1 - X = 0$, $\beta_2 = \beta_3 = 0$, $0.5g\eta_1^+ = -A\cos\omega a_t^{-1} r$ and $a_t^2 - a_0^2 = -2^{-2/3} R\beta_1$. As a result, eq. (87) yields

$$k\beta_1^{-1} J'''' + [R/2^{2/3} - \beta\beta_1^{-1} J' + (J')^2]J'' - A\beta_1^{-1}\cos\omega a_t^{-1} r = 0. \tag{246}$$

First, the non-linear and dispersive effects are considered. The dispersive effect was connected with the transresonant parameter R. It was assumed that $k\beta_1^{-1} = K^* R^2$, where K^* is constant. Using the iterations (see Section 7.1) we constructed approximate analytical solutions of eq. (246) for the case $\beta = 0$. Results of these solutions are presented in Fig. 26 cases $K^* = 0$ (a) $K^* = 1$ (b) and $K^* = 5$ (c). The transresonant mushroom-like waves in Fig. 26 are reminiscent of waves generated due to instability of sinusoidal perturbations (Holmes *et al.* 1999; Sarpkaya 2002). Then the non-linear effect was treated.

If $A = \beta = k = 0$ equation (246) has solutions $J' =$ constant and $J' = \pm(-R)^{0.5}/2^{1/3}$ (see also eq. 86). The earthquake-induced wave $A\cos\omega a_t^{-1} r$ changes these solutions. Let

$$R/2^{2/3} - \beta\beta_1^{-1} J' + (J')^2 \neq 0. \tag{247}$$

In this case, eq. (246) describes shock- or mushroom-like waves. According to eqs (246) and (239) seismic waves of moderate amplitude can be amplified very strongly in natural resonators, while seismic waves of greater amplitude are weakly amplified. If the dimensionless amplitude of the driving oscillations is 0.001, then eq. (246) predicts the wave amplitude to be of the order of $(0.001)^{1/2}$ (if $\beta_1 = k = 0$, see also Sections 5.1 and 5.2) or 0.1 ($\beta = \mathrm{k} = 0$, see also Section 5.3). This result agrees qualitatively with data from the 1985 September

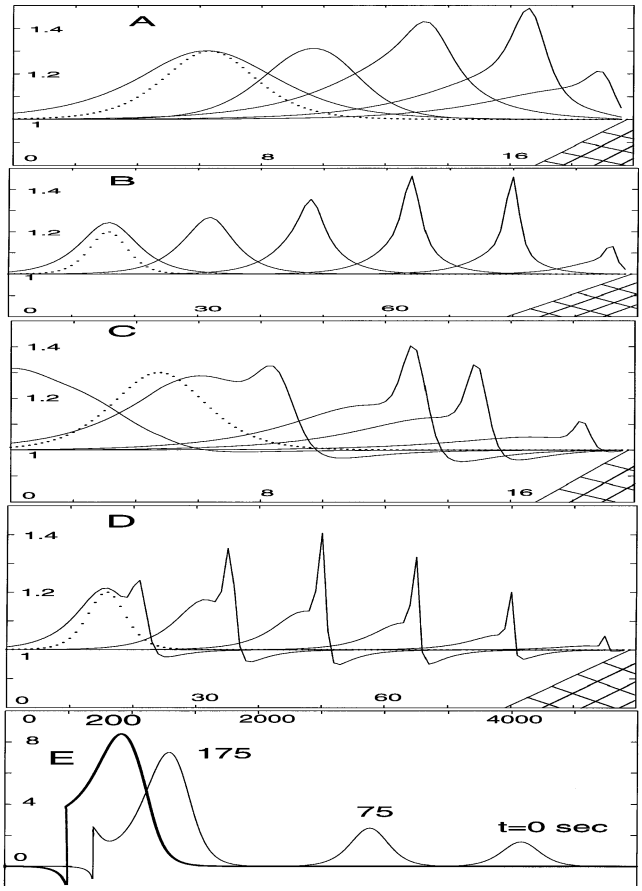

Figure 25. Generation, propagation, amplification and transformation of non-linear resonant edge waves. Profiles *A* and *C* simulate data of Smith (1998, Fig. 7) for the moderate slope of the layer bottom, profiles *B* and *D* simulate data of Smith (1998, Fig. 8) for the weak slope of the layer bottom. Profiles *E* show the evolution of a tsunami-like wave.

19 Michoacan earthquake and the Northridge 1994 Southern California earthquake, and other observations (Singh *et al.* 1988; Reiter 1990; Spudich *et al.* 1996; Su *et al.* 1998). At the same time, if the dimensionless amplitude of the seismic wave is greater than 1, then the amplitude of this wave is reduced by the resonator. Indeed, resonators that contain a clear fundamental resonance for moderate motion can exhibit a conspicuous absence of the peak in the strong motion (Field *et al.* 1997, 1998).

Let us additionally consider the vortex generation. We might expect that singularities of eq. (246) can transform the waves into vortices (Galiev & Galiev 2001; Galiev 2003). The singularities occur when

$$J' = 0.5[\beta\beta_1^{-1} + \sqrt{\beta^2\beta_1^{-2} - 4R/2^{2/3}}], \tag{248}$$

$$J' = 0.5[\beta\beta_1^{-1} - \sqrt{\beta^2\beta_1^{-2} - 4R/2^{2/3}}]. \tag{249}$$

For simplicity the case $\beta = 0$ will be considered. We expand eq. (246) for small displacements around eqs (248) and (249). In particular, let

$$J' = g \mp \sqrt{-2^{-2/3}R}, \quad r = r_0 + z, \tag{250}$$

where r_0 is some value of r in the neighbourhood of which we want to study the equation. Following Galiev (2003) a bilinear equation is found

$$g' = [\pm az + (b \mp D)g]/g, \tag{251}$$

where $a = 2^{-4/3}\omega a_0^{-1} A(-R)^{1/2}\cos\omega a_0^{-1} r_0$, $b = -2^{-4/3}\omega\beta_1 a_0^{-3} r_0 AR\cos\omega a_0^{-1} r_0$, $D \approx 2^{-4/3}(-R)^{-0.5}R'(r_0)$ and $r_0 \approx N\pi a_0\omega^{-1}$($N = 1, 2, 3, \ldots$). The solution is determined by eigenvalues λ,

$$\lambda_{1,2}^{-} = 0.5[(b - D) \pm \sqrt{(b - D)^2 + 4a}], \tag{252}$$

$$\lambda_{1,2}^{+} = 0.5[(b + D) \pm \sqrt{(b + D)^2 - 4a}]. \tag{253}$$

We emphasize that eigenvalues $\lambda_{1,2}^{-}$, eq. (252), correspond to the singular line, eq. (248), and $\lambda_{1,2}^{+}$ eq. (253), correspond to the singular line (249). The behaviour and the stability of solution curves in the J'–r plane depend on $\lambda_{1,2}^{\mp}$ and may be studied following Cunningham (1958). According to the theory the wave shape becomes distorted ($R \approx 0$) and triple-valued ($R < 0$).

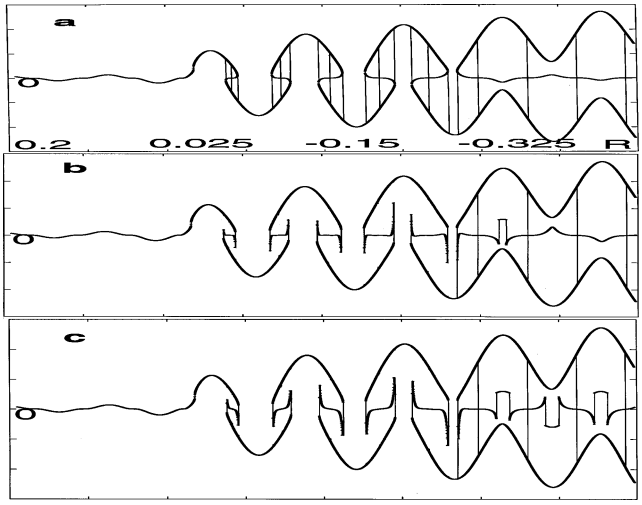

Figure 26. Transresonant evolution of the disturbances into mushroom-like waves. Non-linearity begins to form the mushroom when $R \approx 0$. Profiles (a) and (c) were calculated taking into account the dispersive effect [$K^* = 1$ (b) and $K^* = 5$(c)]. Due to this effect our analytic solutions describe qualitatively data generated by numerical calculations (Holmes *et al.* 1999; Sarpkaya 2002).

Unstable nodes and saddles are formed if both roots $\sqrt{(b-D)^2 \pm 4a}$ are real. When the roots become imaginary the unstable nodes can be transformed into spirals (focuses). These spirals are transformed into vortices if R reduces and $b - D \to 0$ (see fig. 4 from Galiev 2003). This evolution is determined by R and A (Galiev 2003). Thus, according to eq. (246) the transresonant amplification of seismic waves may be limited by the generation of vortices and the turbulent-like motion of the waves. It is known that in resonators, vortices and wave turbulence may be generated if an excitation is sufficiently strong (Merkli & Thomann 1975; Galiev & Galiev 2001; Galiev 2003).

8 DISCUSSION

Today, many scientists consider non-linear science as the most important frontier for gaining a fundamental understanding of Nature. Close to their critical point, greatly different systems exhibit strongly similar non-linear dynamics. Similar non-linear waves can be generated in various fields ranging from fluids, plasmas and the Bose–Einstein condensate to solid-state, chemical, biological, astrophysical and geological systems. Investigations of these waves over the last two centuries have been devoted to cnoidal, shock and soliton-like waves (Whitham 1974; Sagdeev *et al.* 1988; Debnath 1994; Jackson 1994; Scott 1999). Anomalous surface waves have been observed in recent decades (Chester & Bones 1968; Longuet-Higgins 1983; Lioubashevski *et al.* 1996, 1999; Umbanhowar *et al.* 1996; Cerda *et al.* 1997; Jiang *et al.* 1998; Zeff *et al.* 2000). It was found that these waves can be generated in different systems if relevant critical (resonant) conditions occur (Galiev 1997b, 1998, 1999, 2000a, 2003; Galiev & Galiev 1998a, 2001; Bhattacharyya *et al.* 2002). Near and at the resonance, various wave properties are determined by global parameters, such as non-linearity and diffusion (Sagdeev *et al.* 1988; Prigogine 1997).

In particular, there is a growing recognition of the importance of non-linear phenomena in many branches of geophysics, although linear models continue to be powerful tools for studying various geophysical processes. Non-linear amplification of seismic waves at sediment sites appears to be more pervasive than seismologists used to think (Aki 1993). Here we have considered non-linear seismic surface waves. Consideration of these waves is a complex problem that requires the derivation of new equations and the development of mathematical techniques. It is a new problem, although there are analogues between surface waves in liquified and water layers. We note that non-linear water waves have been studied over the last two centuries, but there are still unsolved problems in this field. The theory developed allows us to consider some of them.

There are two main goals of this research. The first is to develop the theory of non-linear transresonant waves and to study seismic surface waves in layers of soft, weakly cohesive and liquified materials. The second is to examine Charles Darwin's earthquake reports. Darwin himself did not personally observe all the phenomena which occurred over very large distances and have not been repeated since the 1835 Chilean earthquake. Therefore, I conclude that mathematical methods and recent experimental data allow us to appreciate the accuracy of Charles Darwin's evidence.

In this paper I have discussed in detail the most important aspects of the research. Here I want to consider additionally only issues which were discussed earlier in many papers and books so as to show more clearly some original aspects of the theory.

8.1 Some remarks on models of Sections 2–4

Our theory can, of course, be reduced to the elastic theory of classical linear seismology. Consider the linearized eqs (20), (23), (29), (30) and (32). In this case eqs (29) and (30) yield

$$u_{1,tt} = -\rho^{-1}P_1 + \rho^{-1}G_*\left(\nabla^2 u_1 + \frac{1}{3}\partial\Delta/\partial x_1\right) - \left[\frac{2}{3}\rho^{-1}h^{-1}G_* + g(n+1)^{-1}\right]\eta_1 + X + X_*, \tag{254}$$

$$u_{2,tt} = -\rho^{-1}P_2 + \rho^{-1}G_*\left(\nabla^2 u_2 + \frac{1}{3}\partial\Delta/\partial x_2\right) - \left[\frac{2}{3}\rho^{-1}h^{-1}G_* + g(n+1)^{-1}\right]\eta_2 + Y + Y_*, \tag{255}$$

where $X_* = \rho^{-1}h^{-1}\tau_{31} - g(n+1)^{-1}\eta_1^+ - g\eta_1^-$, $Y_* = \rho^{-1}h^{-1}\tau_{32} - g(n+1)^{-1}\eta_2^+ - g\eta_2^-$ and the dilatation $\Delta = u_{1,1} + u_{2,2}$. According to eqs (254) and (255) the influence of the vertical displacement can be important for thin layers ($h \to 0$). Then we find from the equation of state (23) and the equation of continuity (32) that

$$\nabla^2 P = -b^{-1}\nabla^2(\Delta + \eta/h). \tag{256}$$

This relation and expression (28) give the following:

$$\nabla^2\eta = -\left[g\rho_0(2n+1)/(n+1) + \frac{4}{3}h^{-1}G_* + b^{-1}h^{-1}\right]^{-1}\left(g\rho_0\nabla^2 h - \frac{2}{3}G_*\nabla^2\Delta + b^{-1}\nabla^2\Delta\right). \tag{257}$$

Now using eqs (254)–(257), after some algebra, we derive the equation for Δ

$$\partial^2\Delta/\partial t^2 - a_0^2\nabla^2\Delta = g^*\nabla^2 h + \partial(X + X_*)/\partial x_1 + \partial(Y + Y_*)/\partial x_2, \tag{258}$$

where

$$\begin{aligned} a_0^2 &= \rho_0^{-1}\left(b^{-1} + \frac{4}{3}G_*\right) + g^*\rho_0^{-1}\left(b^{-1} - \frac{2}{3}G_*\right), \\ g^* &= g\rho_0\left[g(n+1)^{-1} + \frac{2}{3}h^{-1}\rho_0^{-1}G_* - b^{-1}h^{-1}\rho_0^{-1}\right]\Big/\left[g\rho_0(2n+1)(n+1)^{-1} + \frac{4}{3}h^{-1}G_* + b^{-1}h^{-1}\right]. \end{aligned} \tag{259}$$

According to eq. (259) the speed of waves a_0 depends on the thickness, n and ϕ_0 since $b = \lambda\,(1 - \phi_0) + \phi_0 P_0^{-1}$ (see Section 3). If $h \to \infty$ we have the expression for the speed of elastic longitudinal body waves (see eq. 235). If additionally $\lambda = 0$, $\phi_0 = 0$ and $n \approx 0.2$, then a_0 coincides with the velocity of Rayleigh waves, eq. (236). If $g = 0$ then we have the expression for the velocity of longitudinal waves in plates, eq. (128).

The velocity of shear waves does not depend on the thickness. Indeed, eqs (254) and (255) yield

$$\partial^2(u_{1,2} - u_{2,1})/\partial t^2 - \rho_0^{-1}G_*\nabla^2(u_{1,2} - u_{2,1}) = \partial(X + X_1)/\partial x_2 - \partial(Y + Y_2)/\partial x_1. \tag{260}$$

Thus, it follows from eqs (258) and (260) that in the various cases the equations of Section 2 describe the propagation of the different waves: *P*-type waves, Rayleigh waves, the long longitudinal waves in plates and *SH* waves. These waves have a vertical component of the displacement (see eqs 257 and 25). Therefore, they also propagate 3-D shear and rotational motions.

In considering 2-D surface waves we assumed eq. (90). As a result, the rotation in the x_1–x_2 plane was eliminated. However, due to the vertical displacement the equations of Section 4 take into account the rotation in the x_1–x_3 and x_2–x_3 planes. In particular, according to eqs (19), (25) and (90) we have $s_{13}^* \approx -x_3^n h^{-n}\eta_1$ and $s_{23}^* \approx x_3^n h^{-n}\eta_2$. For the 1-D theory of Section 3 only s_{13}^* is conserved.

We have the classical equations for 2-D body waves in elastic media if $\eta = 0$, $\phi = 0$ and $h \to \infty$ in eq. (256). The main novelty of the linearized equations of Section 2 is determined by assumption (25). This assumption reminds us of Love's assumption (1906, p. 551), which improves the elementary theory of the longitudinal wave propagating in this bar. Love included in his consideration the lateral displacement (strain) of the bar $-\nu u_{1,1}$ (here ν is Poisson's ratio). We used assumption (25) to consider weakly cohesive media and the influence of the vertical displacement on the horizontal waves.

8.2 Transresonant evolution of a non-linear wave equation

We have shown that near some critical points the disturbed wave equations (45) and (113) transform into the non-linear diffusion equations (see eqs 138,163 and 164 and Sections 3.3, 3.4, 4.3 and 4.4.1). Let us consider this transformation for an arbitrary non-linear wave equation.

First, we consider Newton's second law for a mass m: $mu_{tt} = F$. If $F = ma_*^2 u_{11}$ we have the d'Alembert equation (1-D wave equation or string equation). If $F = ma_*^2(x_1, x_2, t)\nabla^2 u + mF_*(u) + mS(x_1, x_2, t)$, then Newton's second law yields

$$u_{tt} - a_*^2\nabla^2 u = F_*(u) + S(x_1, x_2, t), \tag{261}$$

where F_* is a non-linear function of u. It is emphasized that eqs (45) and (113) may be transformed into eq. (261). It is important that all equations noted contain a term u_{tt}. This term determines the motion of the wave far from a resonance.

Let us consider resonant bands where $u_{tt} \approx a_*^2\nabla^2 u$. For simplicity the 1-D version of eq. (261) is treated, where $S(x_1, t) = F_-(a_i t - x_1)$. We consider the resonance connected with the site effect (see Sections 6 and 7) and resonators located at $x_1 = x^i{}_1$, $i = 1, 2, 3, \ldots$. If $u_{tt} = a_*^2 u_{11}$ at points $x_1 = x^i{}_1$, singular solutions of the wave equations may be generated there (see Section 4.4). Near these points we assume $a_* = a_i + a_{1i}(x_1) + \cdots$. Here a_i is a constant, $a_i \gg a_{1i}(x_1)$ and $a_{1i}(x_1)$ is a slowly varying function. We shall consider the wave $u = J[a_i t - a_i f(x_1)]$, where $f(x_1) = \int_0^{x_1} a_*^{-1}\,dx_1 \approx a_i^{-1}x_1 - a_i^{-2}\int_0^{x_1} a_{1i}\,dx_1$. In this case near the critical points J may be expanded in a Taylor's series: $J[a_i t - a_i f(x_1)] = J - f_i J' + \cdots$, where $J = J(r) = J(a_i t - x_1)$, $f_i = -a_i^{-1}\int_0^{x_1} a_{1i}\,dx_1$. As a result, near the resonators eq. (261) approximately yields

$$a_i^2 f_{i,11}J' + (2a_{1i}^2 - a_i^2 f_i f_{i,11})J'' = F_*(J) + F_-(a_i t - x_1). \tag{262}$$

Eq. (262) is an analogue of a following non-linear diffusion-type equation:

$$a_i f_{i,11} u_t + (2a_{1i}^2 - a_i^2 f_i f_{i,11}) u_{11} = F_*(J) + F_-(a_i t - x_1), \tag{263}$$

because $u \approx J(a_i t - x_1)$. In contrast with eq. (261), eq. (263) contains a term u_t (instead u_{tt}). This term appears within the resonant bands and its generation lies beyond Newton's and d'Alembert's conception of the wave motion (Prigogine 1997). Thus, the wave diffusion may be generated near resonance independently on initial dissipation and dispersion (for example, even if $\mu^* = k^* = 0$ in eqs 45 and 113). In particular, the wave diffusion effect may be very important when resonators are located near to each other and the resonant bands intersect (Sagdeev *et al.* 1988).

Sometimes diffusive (parabolic) equations are used in water wave theory (Zakharov 1968; Mei & Liu 1993; Debnath 1994). In particular, the non-linear Schrödinger equation describes surface water waves. Equations for electromagnetic waves may also be approximated by the Schrödinger equation (Galiev & Galiev 2001).

Eqs (87), (181), (196) and (262) recall non-linear pendulum-type equations. However, in contrast with the pendulum equation, there are terms $(\cdots)''$ not connected with inertia in the Galilei and Newton conception of motion. These equations can have a chaotic solution (Grimshaw & Tian 1994; Soliman 1997; Thompson 1997; Nayfeh 2000). Thus resonances can destroy predictability. On the other hand, the chaotic dynamics may be determined by the wave diffusion and intersections of the resonant bands (Prigogine 1997; Sagdeev *et al.* 1988). According to eq. (262) non-linear resonant normal modes (eigenfunctions) do not depend on boundaries.

If $a_{1i} = 0$ (exact resonance) then eq. (262) can yield the algebraic equation (see Sections 3–5).

Eq. (262) has variable coefficients. The solutions presented in Sections 5–7 are valid for eq. (262) in the case of slowly varying coefficients. It is known that the non-linear diffusion equations can determine spiral waves. In particular, waves described by eq. (262) may be similar to non-linear diffusive curved waves (spiral waves) observed in different physical, chemical and biological systems (Cross & Hohenberg 1993; Scott 1999; Lin *et al.* 2000).

Thus the original non-linear wave equations can evolve within resonant bands into the non-linear diffusive equations (near the exact resonance) and then into algebraic equations (exact resonance). It is a result of the singular nature of the resonant problems. The bifurcation of the solutions, the secular terms in eqs (66) and (147) and the generation of new diffusion terms show that earthquake-induced wave motion may be not only predictable but also irregular and unpredictable. Any small differences in the parameters of non-linear problems could lead to great disparities at future times (usually initial conditions and the earthquake-educed excitation are not precisely known). Therefore, it is impossible to predict (Evans 1997; Geller 1997) with any degree of assurance the results of earthquake for natural resonators.

8.3 Conclusion

Non-linear, resonant and topographic effects are very important for vertically excited surface waves in granular layers (Pak & Behringer 1993; Jaeger *et al.* 1996; Umbanhowar *et al.* 1996). These effects may also be important for strong ground motions (see *Bull. Seism. Soc. Am.* **86**, No 1B, 1996 and **88**, No 6, 1998). A number of factors complicate the problem. First, since the amplitudes of seismic waves are usually small, non-linear effects are often also small. Thus, even strong earthquakes are studied in terms of linear elasticity. Secondly, topographic, resonant and non-linear effects are usually localized near the ground surface and depend on the orientation relative to the earthquake source. The shaking at any given site due to earthquakes may vary even when the intensities and the distances to the earthquake sources are similar. For trapped waves, this variation depends on the geometric and mechanical properties of the resonator, the frequency of excitation and the orientation of the earthquake-induced seismic wave. Thus, a moderate earthquake can generate in topography a more intensive shaking than a strong earthquake if the orientation and the natural frequency of the topography are favourable for the resonance. Thirdly, some geomaterials (for instance, those having a high water content) demonstrate linear behaviour up to very high strains (for example, Mexico City clay, Singh *et al.* 1988). Fourthly, it is difficult to simulate earthquake events with the help of experiments. Because of the above and other complexities (Evans 1997; Geller 1997, see also the paper), a non-linear theory of seismology valid for all situations has not been constructed.

In this paper I have considered non-linear surface waves propagating in weakly cohesive media where the non-linearity of the stress–strain relationships is small with respect to the non-linearity of the equations of deformable media and state, and the non-linearity of the boundary conditions. New approximate wave solutions of the equations of deformable media have been constructed by the perturbation method. A procedure is derived for the elimination of the secular terms in expressions for the displacement (66) and the displacement potential (147). Transresonant evolution of the perturbed wave equations are studied. At resonance, $u_{tt} \approx a_0^2 \nabla^2 u$ and these equations transform into non-linear diffusion equations, either to basic highly non-linear ordinary differential equation or to the basic algebraic equation for travelling waves. According to the theory presented mathematical singularities (resonances) reflect the generation of new strongly non-linear wave structures in natural and artificial systems which are needed for the new mathematical formulation of problems. Then the resonant conditions and the site resonance are considered. During an earthquake, travelling seismic waves may be trapped by topography. The non-linear theory predicts that unfamiliar resonant seismic waves of anomalous shape and steep fronts may be generated by topography. The evolution, form and amplitudes of these waves depend on competition between non-linear, dissipative, dispersive and spatial effects within resonant bands. At exact resonance, the first-order linear terms in the equations are eliminated and the problem is strictly non-linear. During the transresonant evolution, terrestrial moderate-amplitude waves can be transformed into shock-, jet- and breaking-like waves. Vortex-like structures may be generated. Strong ground motion is attenuated within the resonant band. Localized standing waves may be generated on the surface of the natural resonators.

The speed of waves in a layer of the weakly cohesive materials depends on the mechanical properties of the material, the geometry of the layer, and the vertical acceleration. In particular, the speed of some waves can be $\sqrt{2gh}$, and the breaker velocity can be up to $2\sqrt{gh}$. At the same time the speed of waves can depend on complex effects within the resonant band.

The non-linear theory presented herein qualitatively explains some reports of Charles Darwin (1839) regarding Quiriquina, the island of S. Maria and volcanoes, and supports his opinion that elevation of the land, fissures and columns of matter were parts of a single phenomenon. In particular, the theory explains qualitatively the same-day earthquake/large eruption events described by Darwin.

Following Galiev & Galiev (2001) I develop a theory of non-linear transresonant surface waves and study the evolution of singular wave phenomena within the resonant bands. It is shown that within the bands the equations of deformable media may be strictly simplified up to the basic non-linear algebraic equations for the travelling waves. It allows us to consider the wide spectrum of non-linear seismic problems for natural resonators.

The theory of non-linear transresonant waves was developed. Profile points of these waves occupy various positions within the resonant band. In other words, the wave profile is a function of the transresonant parameter R. On the other hand, the wave profile can depend strongly on non-linearity, the excitation, geometry of resonators and so on (Galiev 1999a, 2000a). Threrfore, an variety of unfamiliar transresonant waves may be excited within the resonant bands and the evolution of singular wave phenomena may be complex. When two or more resonances are simultaneously present in a system, they may result in the appearance of widespread chaotic wave phenomena (Sagdeev *et al.* 1988). Apparently, multi-resonant wave phenomena are the problem for the future.

It is possible to give a different interpretation of the paper results. I connected most of them with the seismic problems. However, the transition from the smooth waves to shock-, jet-, or mushroom-like waves and vortex-like structures have been observed in many natural and artificial (for example, the Bose–Einstein condensate) systems. The generation of wave turbulence may be connected with this transition. I have shown that this transition is determined by the strongly non-linear transresonant process. Usually, wave fields in classical and quantum systems are described with the help of the Fourier expansion. However, this expansion cannot simulate the formation of multi-valued wave fronts and the generation of particles, drops and bubbles in the wave front. The methods, which were used in this paper (Galiev & Galiyev 2001; Galiev 2003), allow us to study these complex transresonant wave phenomena. These phenomena may be described by ordinary differential equations or non-linear algebraic equations. Since these equations simulate the properties of many perturbed wave equations within the transresonant band, we think that similar evolution can take place in systems ranging from microresonators to the early Universe (Galiev & Galiyev 2001; Galiev 2003).

ACKNOWLEDGMENTS

The author thanks Dr R. Evans, Professors R. Geller, P. W. Brothers, D. Bhattacharyya, I. F. Collins, M. J. Pender, M. Campillio and Dr S. Hestholm for their help. The recommendations of Dr R. Evans and Professor R. Geller have improved and developed some important aspects of the theory presented.

REFERENCES

Aguirre, J. & Irikura, K., 1997. Nonlinearity, liquefaction, and velocity variation of soft soil layers in Port Island, Kobe, during the Hyogo-ken Nanbu earthquake, *Bull. seism. Soc. Am.,* **87,** 1244–1258.

Akhmediev, N.N. & Ankiewicz, A., 1997. *Solitons: Nonlinear Pulses and Beams,* Chapman and Hall, London.

Airy, G.B., 1845. Tides and waves, in *Encyclopaedia Metropolitana,* London, **5,** pp. 241–396.

Aki, K., 1993. Local site effects on weak and strong ground motion, *Tectonophysics,* **218,** 93–111.

Anilkumar, A.V., Sparks, R.S.J. & Sturtevant, B., 1993. Geological implications and applications of high-velocity two-phase flow experiments, *J. Volc. Geotherm. Res.,* **56,** 145–160.

Alidibirov, M. & Dingwell, D.B., 1996. Magma fragmentation by rapid decompression, *Nature,* **380,** 146–148.

Arnold, V.I., 1990. *Singularities of Caustics and Wave Fronts,* Kluwer, Dordrecht.

Ashford, S.A. & Sitar, N., 1997. Analysis of topographic amplification of inclined shear waves in a steep coastal bluff, *Bull. seism. Soc. Am.,* **87,** 692–700.

Bardet, J.P., 1990. Damage at a distance, *Nature,* **346,** 799.

Beji, S. & Nadaoka, K., 1997. A time-dependent nonlinear mild-slope equation for water waves, *Proc. R. Soc. Lond. A,* **453,** 319–332.

Beresnev, I.A. & Wen, K.-L., 1996a. The possibility of observing nonlinear path effect in earthquake-induced seismic wave propagation, *Bull. seism. Soc. Am.,* **86,** 1028–1041.

Beresnev, I.A. & Wen, K.-L., 1996b. Nonlinear soil response—a reality, *Bull. seism. Soc. Am.,* **86,** 1964–1978.

Bhattacharyya, D., Galiev, Sh.U. & Panova, O.P., 2002. Transresonant evolution of spherical waves governed by the perturbed wave equation, *Strength Mater.,* **N4,** 62–74.

Biot, M.A., 1973. Nonlinear and semilinear rheology of porous solids, *J. geophys. Res.,* **78,** 4924–4973.

Bouchon, M. & Barker, J.S., 1996. Seismic response of a hill: the example of Tarzana, California, *Bull. seism. Soc. Am.,* **86,** 66–72.

Bourne, N.K. & Field, J.E., 1992. Shock-induced collapse of single cavities in liquids, *J. Fluid Mech.,* **244,** 225–240.

Boussinesq, J., 1872. Théorie des ondes et remous qui se propagent le long d'un canal rectangulaire horizontal, en communiquant au liquide contenu dans ce canal des vitesses sensiblement pareilles de la surface au fond, *J. Math. Pures Appl. II*, **17,** 55–108.

Britan, A., Ben-Dor, G., Elperin, T., Igra, O. & Jiang, J.P., 1997. Gas filtration during the impact of weak shock waves on granular layers, *Int. J. Multiphase Flow,* **23,** 473–491.

Brodsky, E.E., Sturtevant, B. & Kanamori, H., 1998. Earthquakes, volcanoes, and rectified diffusion, *J. geophys. Res.,* **103,** 23 827–23 838.

Bühler, O. & Jacobson, T.E., 2001. Wave-driven currents and vortex dynamics on barred beaches, *J. Fluid Mech.,* **449,** 313–339.

Carcione, J.M. & Poletto, F., 2000. Sound velocity of drilling mud saturated with reservoir gas, *Geophysics,* **65,** 646–651.

Cerda, E., Melo, F. & Rica, S., 1997. Model for subharmonic waves in granular materials, *Phys. Rev. Lett.,* **79,** 4570–4573.

Chester, W., 1964. Resonant oscillations in closed tubes, *J. Fluid Mech.,* **18,** 44–64.

Chester, W. & Bones, J.A., 1968. Resonant oscillations of water waves. II. Experiment, *Proc. Roy. Soc. A,* **306,** 23–39.

Clarke, A.B., Voight, B., Neri, A. & Macedonio, G., 2002. Transient dynamics of vulcanian explosions and column collapse, *Nature,* **415,** 897–901.

Clément, E., Vanel, L., Rajchenbach, J. & Duran, J., 1996. Pattern formation in a vibrated granular layer, *Phys. Rev. E,* **53,** 2972–2975.

Cole, R.H., 1948. *Underwater Explosions,* Princeton University Press, Princeton.

Couch, S., Sparks, R.S.J. & Carroll, M.R., 2001. Mineral disequilibrium in lavas explained by convective self-mixing in open magma chambers, *Nature,* **411,** 1037–1039.

Cox, E. & Mortell, M.P., 1986. The evolution of resonant water-wave oscillations, *J. Fluid Mech.,* **162,** 99–116.

Cross, M.C. & Hohenberg, P.C., 1993. Pattern formation outside of equilibrium, *Rev. Mod. Phys.,* **65,** 851–1112.

Cunningham, W.J., 1958. *Introduction to Nonlinear Analysis,* McGraw-Hill, New York.

Darwin, C., 1839. *Journal of Researches into the Geology and Natural History of the Various Countries Visited by H.M.S. Beagle,* Henry Colburn, London.

Davies, G.F., 1999. *Dynamic Earth: Plate, Plumes and Mantle Convection,* Cambridge University Press, Cambridge.

Davison, C., 1936. *Great Earthquakes,* Murby, London.

Dean, R.G. & Dalrymple, R.A., 1991. *Water Wave Mechanics,* World Scientific, Singapore.

Debnath, L., 1994. *Nonlinear Water Waves,* Academic, New York.

Dobran, F., Neri, A. & Macedonio, G., 1993. Numerical simulations of collapsing volcanic columns, *J. geophys. Res.,* **98,** 4231–4259.

Dingemans, M.W., 1997. *Water Wave Propagation over Uneven Bottoms,* World Scientific, Singapore.

Dunn, D.C., McDonald, N.R. & Johnson, E.R., 2001. The motion of a singular vortex near an escarpment, *J. Fluid Mech.,* **448,** 335–365.

Evans, R., 1997. Assessment of schemes for earthquake prediction: editor's introduction, *Geophys. J. Int.* **131,** 413–420.

Field, E.H., Johnson, P.A., Beresnev, I.A. & Zeng, Y., 1997. Nonlinear ground-motion amplification by sediments during the 1994 Northridge earthquake, *Nature,* **390,** 599–604.

Field, E.H., Zeng, Y.H., Johnson, P.A. & Beresnev, I.A., 1998. Nonlinear sediment response during the 1994 Northridge earthquake: observations and finite source simulation, *J. geophys. Res.,* **103,** 26 869–26 883.

Fineberg, J., 1996. Physics in a jumping sandbox, *Nature,* **382,** 763–764.

Frohn, A. & Roth, N., 2000. *Dynamics of Droplets,* Springer, New York.

Fukushima, Y., Irikura, T.U. & Matsumoto, H., 2000. Characteristics of observed peak amplitude for strong ground motion from the 1995 Hyogoken Nanby (Kobe) earthquake, *Bull. seism. Soc. Am.,* **90,** 545–565.

Galiev, Sh.U., 1972a. Forced oscillations of a nonlinear elastic layer, *Izv. Acad. Nauk USSR, Mech. Solid Body,* **N1,** 58–63.

Galiev, Sh.U., 1972b. Forced longitudinal oscillations of a nonlinear elastic body, *Izv. Acad. Nauk USSR, Mech. Solid Body,* **N4,** 80–87.

Galiev, Sh.U., 1981. *Dynamics of Hydroelastoplastic Systems,* Naukova Dumka, Kiev (in Russian).

Galiev, Sh.U., 1988. *Nonlinear Waves in Bounded Continua,* Naukova Dumka, Kiev (in Russian).

Galiev, Sh.U., 1997a. The influence of cavitation upon anomalous behavior of a plate/liquid/underwater explosion system, *Int. J. Impact Eng.,* **19,** 345–359.

Galiev, Sh.U., 1997b. Resonant oscillations governed by the Boussinesq equation with damping, in *Proc. 5th Int. Congress on Sound and Vibration,* Adelaide, 1785–1796.

Galiev, Sh.U., 1998. *Is There Some New Kind of Nonlinear Surface Waves*?, Rep. 584, School of Engineering, The University of Auckland.

Galiev, Sh.U., 1999a. Topographic effect in a Faraday experiment, *J. Phys. A: Math. Gen.,* **32,** 6963–7000.

Galiev, Sh.U., 1999b. Passing through resonance of spherical waves, *Phys. Lett. A,* **260,** 225–233.

Galiev, Sh.U., 2000a. Unfamiliar vertically excited surface water waves, *Phys. Lett. A,* **266,** 41–52.

Galiev, Sh.U., 2000b. Simulation of Charles Darwin's evidence by new theory of nonlinear seismic waves, *Book of Abstracts II.* General Sessions, *4th Euromech Solid Mechanics Conf,* Univ. de Metz, Metz, France, p. 707.

Galiev, Sh.U., 2002. Trans-resonant evolution of wave equations, front singularities and vortices, *Phys. Lett. A,* (accepted).

Galiev, Sh. U., 2003. Trans-resonant evolution of wave singularities and vortices, *Phys. Lett. A,* **311,** 192–199.

Galiev, Sh.U. & Galiyev, T.Sh., 1994. Linear and discontinuous forced oscillations of flow of bubbly liquid in a deformable pipe (survey), *Strength Mater.,* **N9,** 633–654.

Galiev, Sh.U. & Panova, O.P., 1995. Periodical shock waves in spherical resonators (survey), *Strength Mater.,* **N10,** 602–620.

Galiev, Sh.U. & Galiev, T.Sh., 1998. Resonant travelling surface waves, *Phys. Lett. A,* **246,** 299–305.

Galiev, Sh.U. & Galiev, T.Sh., 2001. Nonlinear trans-resonant waves, vortices and patterns: from microresonators to the early Universe, *Chaos,* **11,** 686–704.

Galiev, Sh.U., Ilgamov, M.A. & Sadikov, A.V., 1970. Periodic shock waves in a gas, *Izv. Acad. Nauk USSR, Mech. Fluid Gas,* **N2,** 57–66.

Geller, R.J., 1997. Earthquake prediction: a critical review, *Geophys. J. Int.* **131,** 425–450.

Goodridge, C.L., Shi, W.T. & Lathrop, D.P., 1996. Threshold dynamics of singular gravity-capillary waves, *Phys. Rev. Lett.,* **76,** 1824–1827.

Goodridge, C.L., Shi, W.T., Hentschel, H.G.E. & Lathrop, D.P., 1997. Viscous effects in droplet-ejecting capillary waves, *Phys. Rev. E,* **56,** 472–475.

Grimshaw, R. & Tian, X., 1994. Periodic and chaotic behaviour in a reduction of the perturbed Korteweg–de Vries equation, *Proc. R. Soc. Lond. A,* **445,** 1–21.

Hill, D.P., Pollitz, F. & Newhall, C., 2002. Earthquake-volcano interaction, *Phys. Today,* **55,** N11, 41–47.

Hobbs, P.V. & Kezweeny, A.J., 1967. Splashing of a water drop, *Science,* **155,** 1112–1114.

Holmes, R.L. *et al.*, 1999. Richtmyer-Meshkov instability growth: experiment, simulation and theory, *J. Fluid Mech.,* **389,** 55–79.

Hunt, G.W., Mühlhaus, H.-B. & Whiting, A.I.M., 1997. Folding processes and solitary waves in structural geology, *Phil. Trans. R. Soc. Lond. A,* **355,** 2197–2213.

Ibrahim, R.A., Pilipchuk, V.N. & Ikeda, T., 2001. Recent advances in liquid sloshing dynamics, *Appl. Mech. Rev.,* **54,** 133–199.

Ilgamov, M.A., Zaripov, R.G., Galiullin, R.G. & Repin, V.B., 1996. Nonlinear oscillations of a gas in a tube, *Appl. Mech. Rev.,* **49,** 138–154.

Jackson, E.A., 1994. *Perspectives of Nonlinear Dynamics,* Cambridge University Press, New York.

Jaeger, H.M., Nagel, S.R. & Behringer, R.P., 1996. Granular solids, liquids, and gases, *Rev. Mod. Phys.,* **68,** 1259–1273.

James, A.J., Vukasinovich, B., Smith, M.K. & Glezer, A., 2003. Vibration-induced drop atomization and bursting, *J. Fluid Mech.,* **476,** 1–28.

Jiang, L., Perlin, M. & Schultz, W.W., 1998. Period tripling and energy dissipation of breaking standing waves, *J. Fluid Mech.,* **369,** 273–299.

Johnson, W., 1972. *Impact Strength of Materials,* Arnold, London.

Johnson, P.A., Zinszner, B. & Rasolofosaon, P.N.J., 1996. Resonance and elastic nonlinear phenomena in rock, *J. geophys. Res.,* **101,** 11 553–11 564.

Julien, S., Lasheras, J. & Chomaz, J.-M., 2003. Three-dimensional instability and vorticity patterns in the wake of a flat plate, *J. Fluid Mech.,* **479,** 155–189.

Karagiozova, D. & Jones, N., 2001. Influence of stress waves on the dynamic progressive and dynamic plastic buckling of cylindrical shells, *Int. J. Solids Struct.,* **38,** 6723–6749.

Kataoka, D.E. & Troian, S.M., 1999. Patterning liquid flow on the microscopic scale, *Nature,* **402,** 794–797.

Kieffer, S.W., 1977. Sound speed in liquid–gas mixtures: water–air and water–steam, *J. geophys. Res.,* **82,** 2895–2904.

Kientzler, C.F., Arons, A.B., Blanchard, D.C. & Woodcock, A.H., 1954. Photographic investigation of the projection of droplets by bubbles bursting at a water surface, *Tellus,* **6,** 1–7.

Kirby, J.T., 1997. Nonlinear, dispersive long waves in water of variable depth, in *Gravity Waves in Water of Finite Depth,* pp. 55–168, ed. Hunt, J.N., Computational Mech. Publications.

Koch, D.L. & Sangani, A.S., 1999. Particle pressure and marginal stability limits for a homogeneous monodisperse gas-fluidized bed: kinetic theory and numerical simulations, *J. Fluid Mech.,* **400,** 229–263.
Kolsky, H., 1953. *Stress Waves in Solids,* Clarendon Press, Oxford.
Kouznetsov, D. & Garcia-Valenzuela, A., 1999. Theory of the backscattering of sound by phase-matched nonlinear interaction, *J. Acoust. Soc. Am.,* **105,** 1584–1591.
Kramer, S.L., 1996. *Geotechnical Earthquake Engineering,* Prentice-Hall, Upper Saddle River.
Lamb, H., 1932. *Hydrodynamics,* 6th edn. Dover, New York.
Landau, L.D. & Lifshitz, E.M., 1987. *Fluid Mechanics,* Pergamon, New York.
Latter, J.H., 1981. Volcanic earthquakes, and their relationship to eruptions at Ruapehu and Ngauruhoe volcanoes, *J. Volc. Geotherm. Res.,* **9,** 293–309.
Lavrentev, M.A. & Shabat, B.V., 1977. *Hydrodynamic Problems and Their Mathematical Models,* Nauka, Moscow (in Russian).
Lin, A.L., Bertram, M., Martinez, K., Swinney, H.L., Ardelea, A. & Carey, G.F., 2000. Resonant phase patterns in a reaction–diffusion system, *Phys. Rev. Lett.,* **84,** 4240–4243.
Linde, A.T. & Sacks, I.S., 1998. Triggering of volcanic eruptions, *Nature,* **395,** 888–890.
Lioubashevski, O., Arbell, H. & Fineberg, J., 1996. Dissipative solitary states in driven surface waves, *Phys. Rev. Lett.,* **76,** 3959–3962.
Lioubashevski, O., Hamiel, Y., Agnon, A., Reches, Z. & Fineberg, J., 1999. Oscillons and propagating solitary waves in a vertically vibrated colloidal suspension, *Phys. Rev. Lett.,* **83,** 3190–3193.
Lohse, D., 2003. Bubble puzzles, *Phys. Today,* **56,** N2, 36–41.
Longuet-Higgins, M.S., 1983. Bubbles, breaking waves and hyperbolic jets at a free surface, *J. Fluid Mech.,* **127,** 103–121.
Love, A.E.H., 1906. *The Mathematical Theory of Elasticity,* Cambridge University Press, Cambridge.
Mader, H.M., 1998. Conduit flow and fragmentation, in *The Physics of Explosive Volcanic Eruptions,* Vol. 145, pp. 51–71, eds Gilbert, J.S. & Sparks, R.S.J., Geological Society, Special Publications.
Mei, C.C. & Liu, P.L.-F., 1993. Surface waves and coastal dynamics, *Annu. Rev. Fluid Mech.,* **25,** 215–240.
Melosh, H.J., 1996. Dynamical weakening of faults by acoustic fluidization, *Nature,* **379,** 601–606.
Mendelson, A., 1968. *Plasticity: Theory and Applications,* Macmillan, New York.
Merkli, P. & Thomann, H., 1975. Transition to turbulence in oscillating pipe flow, *J. Fluid Mech.,* **68,** 567–575.
Morrissey, M.M. & Mastin, L.G., 2000. Vulcanian eruption, in *Encyclopedia of Volcanoes,* pp. 463–475, ed. Sigurdsson, H., Academic, New York.
Mortell, M.P. & Seymour, B.R., 1981. A finite-rate theory of quadratic resonance in a closed tubes, *J. Fluid Mech.,* **112,** 411–431.
Mortell, M.P. & Varley, E., 1970. Finite amplitude waves in bounded media: nonlinear free vibrations of an elastic panel, *Proc. R. Soc. Land. A,* **318,** 169–196.
Mukerjee, M., 1996. Science with brass, *Sci. Am.,* **275,** 19–21.
Nakamura, K., 1975. Volcano structure and possible mechanical correlation between volcanic eruptions and earthquakes, *Bull. Volc. Soc. Jpn.,* **20,** 229–240.
Nikolaevskiy, V.N., 1996. *Geomechanics and Fluidodynamics,* Kluwer, Dordrecht.
Nakoryakov, V.E., Kuznetsov, V.V. & Dontsov, V.E., 1989. Pressure waves in saturated porous media, *Int. J. Multiphase Flow,* **15,** 857–875.
Nakoryakov, V.E., Dontsov, V.E. & Pokusaev, B.G., 1996. Pressure waves in a liquid suspension with solid particles and gas bubbles, *Int. J. Multiphase Flow,* **22,** 417–429.
Nayfeh, A.H., 2000. *Nonlinear Interactions,* Wiley, New York.
Nayfeh, A.H. & Mook, D.T., 1995. *Nonlinear Oscillations,* Wiley, New York.
Nigmatulin, R.I., 1991. *Dynamics of Multiphase Media,* Taylor & Francis, London.
Novozhilov, V.V., 1961. *Theory of Elasticity,* Pergamon, New York.
Nowacki, W., 1963. *Dynamics of Elastic Systems,* Chapman & Hall, London.
Ockendon, H., Ockendon, J.R. & Johnson, A.D., 1985. Resonant sloshing in shallow water, *J. Fluid Mech.,* **167,** 465–479.
O'Rourke, T.D. & Pease, J.W., 1997. Mapping liquefiable layer thickness for seismic hazard assessment, *J. Geotech. Engrg., ASCE,* **123,** 46–56.
Pak, H.K. & Behringer, R.P., 1993. Surface waves in vertically vibrated granular materials, *Phys. Rev. Lett.,* **71,** 1832–1835.
Pak, H.K. & Behringer, R.P., 1994. Bubbling in vertically vibrated granular materials, *Nature,* **371,** 231–233.
Pease, J.W. & O'Rourke, T.D., 1997. Seismic response of liquefaction sites, *J. Geotech. Engrg., ASCE,* **123,** 37–45.
Pedersen, H., Brun, B.L., Harzfeld, D., Campillo, M. & Bard, P.-Y., 1994. Ground motion amplitude across ridges, *Bull. seism. Soc. Am.,* **84,** 1786–1800.
Peregrine, D.H., 1983. Breaking waves on beaches, *Ann. Rev. Fluid Mech.,* **15,** 149–178.
Poincaré, H., 1892. *Les Methods Nouvelles de la Mechanique Celeste,* Gauthier-Villars, Paris.
Prigogine, I., 1997. *The End of Certainty,* Free Press, New York.
Puzyrev, N.N. & Kulikov, V.A., 1980. Experimental data on the propagation and excitation of transverse waves in water-saturated deposits, *Sov. Geol. Geophys.,* **21,** 71–77.
Rabotnov, Yu.N., 1969. *Creep Problems in Structural Members,* North-Holland, Amsterdam.
Reiter, L., 1990. *Earthquake Hazard Analysis,* Columbia University Press, New York.
Remoissenet, M., 1996. *Waves Called Solitons,* Springer-Verlag, Berlin.
Rial, J.A., Saltzman, N.G. & Ling, H., 1992. Earthquake-induced resonance in sedimentary basins, *Am. Sci.,* **80,** 566–578.
Rial, J.A., 1996. The anomalous seismic response of the ground at the Tarzana Hill site during the Northridge 1994 South California earthquake: a resonant, sliding block?, *Bull. seism. Soc. Am.,* **86,** 1714–1723.
Rinehart, J.S., 1960. The role of stress waves in the comminution of brittle, rocklike materials, in *Stress Wave Propagation in Materials,* pp. 247–269, ed. Davids, H., Interscience, New York.
Sagdeev, R.Z., Usikov, D.A. & Zaslavsky, G.M., 1988. *Nonlinear Physics,* Harwood, Chur.
Sarpkaya, T., 2002. Experiments on the stability of sinusoidal flow over a circular cylinder, *J. Fluid Mech.,* **457,** 157–180.
Scott, A., 1999. *Nonlinear Science,* Oxford University Press, New York.
Seed, H.B., Martin, P.P. & Lysmer, H., 1976. Pore water pressure changes during soil liquefaction, *J. Geotech. Engng., ASCE,* **102,** 323–346.
Sheriff, R.E. & Geldart, L.P., 1995. *Exploration Seismology,* Cambridge University Press, Cambridge.
Shima, S. & Oyane, M., 1976. Plasticity theory for porous metals, *Int. J. Mech.,* **18,** 285–291.
Sibgatullin, N.R., 1972. On nonlinear transverse resonant oscillations in an elastic layer and a layer of perfectly conducting fluid, *J. appl. Math.,* **36,** 70–78.
Singh, S.K., Mena, E. & Castro, R., 1988. Some aspects of source characteristics of the 19 September 1985 Michoacan earthquake and ground motion amplification in and near Mexico city from strong motion data, *Bull. seism. Soc. Am.,* **78,** 451–477.
Smith, R.A., 1998. An operator expansion formalism for nonlinear surface waves over variable depth, *J. Fluid Mech.,* **363,** 333–347.
Soliman, M.S., 1997. Nonlinear vibrations of hardening systems: chaotic dynamics and unpredictable jumps to and from resonance, *J. Sound Vibr.,* **207,** 383–392.
Sornette, D. & Sornette, A., 2000. Acoustic fluidization for earthquakes?, *Bull. seism. Soc. Am.,* **90,** 781–785.
Spudich, P., Hellweg, M. & Lee, W.H.K., 1996. Directional topographic site response at Tarzana observed in aftershocks of the 1994 Northridge, California, earthquake: implications for mainshock motions, *Bull. seism. Soc. Am.,* **86,** S193–S208.
Stoker, J.J., 1957. *Water Waves,* Interscience, New York.
Sturtevant, B., Kanamori, H. & Brodsky, E.E., 1996. Seismic triggering by rectified diffusion in geothermal systems, *J. geophys. Res.,* **101,** 25 269–25 282.

Su, F., Anderson, J.G. & Zend, Y., 1998. Study of weak and strong ground motion including nonlinearity from the Northridge, California, earthquake sequence, *Bull. seism. Soc. Am.,* **88,** 1411–1425.

Suplee, C., 1999. *Physics in the 20th Century,* Abrams, New York.

Tabor, M., 1989. *Chaos and Integrability in Nonlinear Dynamics,* Wiley, New York.

Taylor, G.I., 1953. An experimental study of standing waves, *Proc. R. Soc. Lond. A,* **218,** 44–59.

Taylor, G.I., 1969. Instability of jets, threads, and sheets of viscous fluid, in *Proc. 12th Int. Congress of Applied Mechanics,* Stanford, pp. 382–388, Springer-Verlag, Berlin.

Thompson, J.M.T., 1997. Designing against capsize in beam seas: Recent advances and new insights, *Appl. Mech. Rev.,* **50,** 307–324.

Umbanhowar, P.B., Melo, F. & Swinney, H.L., 1996. Localized excitations in a vertically vibrated granular layer, *Nature,* **382,** 793–796.

Van der Grinten, J.G.M., Van Dongen, M.E.H. & Van der Kogel, H., 1987. Strain and pore pressure propagation in a water-saturated porous medium, *J. Appl. Phys.,* **62,** 4682–4687.

van Wijngaarden, L., 1968. On the oscillations near and at resonace in open pipes, *J. Eng. Math.,* **2,** 225–240.

Verhagen, J.H.G. & Van Wijngaarden, L., 1965. Non-linear oscillations of fluid in a container, *J. Fluid Mech.,* **22,** 737–752.

Wassgren, C.R., Brennen, C.E. & Hunt, M.L., 1996. Vertical vibration of a deep bed of granular material in a container, *J. Appl. Mech.,* **63,** 712–719.

Whitham, G.B., 1974. *Linear and Nonlinear Waves,* Wiley, New York.

Worthington, A.M., 1908. *A Study of Splashes,* Longmans, London.

Wright, J., Yon, S. & Pozrikidiz, C., 2000. Numerical studies of two-dimensional Faraday oscillations of inviscid fluids, *J. Fluid Mech.,* **402,** 1–32.

Yeats, R.S., Sieh, K.E. & Allen, C.R., 1997. *The Geology of Earthquakes,* Oxford University Press, New York.

Yeh, C.-S., Teng, T.-J. & Chai, J.-F., 1998. On the resonance of a two-dimensional alluvial valley, *Geophys. J. Int.* **134,** 787–808.

Zakharov, V.E., 1968. Stability of periodic waves of finite amplitude on surface of a deep fluid, *J. Appl. Mech. Tech. Phys.,* **N2,** 190–194.

Zeff, B.W., Kleber, B., Fineberg, J. & Lathrop, D.L., 2000. Singularity dynamics in curvature collapse and jet eruption on a fluid surface, *Nature,* **403,** 401–404.